



US Army Corps  
of Engineers

DTIC FILE COPY

TECHNICAL REPORT GL-87-14

2

# SEISMIC STABILITY EVALUATION OF FOLSOM DAM AND RESERVOIR PROJECT

## Report 5 SEISMIC STABILITY EVALUATION OF DIKE 5

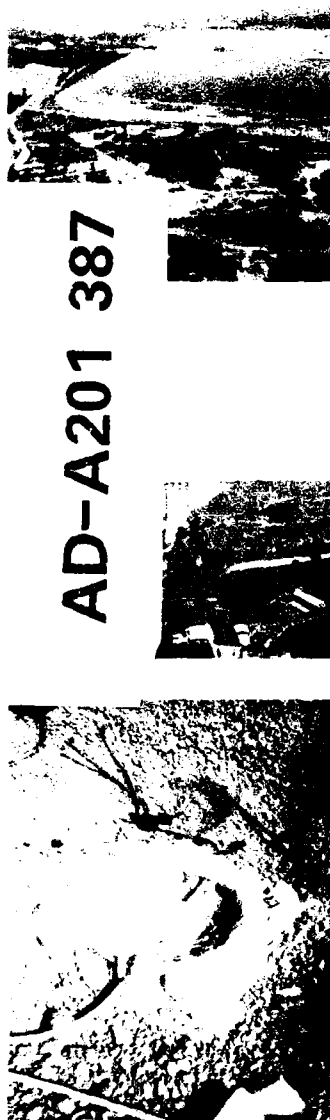
by

Ronald E. Wahl, Mary E. Hynes

Geotechnical Laboratory

DEPARTMENT OF THE ARMY  
Waterways Experiment Station, Corps of Engineers  
PO Box 631, Vicksburg, Mississippi 39181-0631

AD-A201 387



DTIC  
ELECTED  
NOV 21 1988  
S E D

November 1988

Report 5 of a Series

Approved For Public Release; Distribution Unlimited



Prepared for US Army Engineer District, Sacramento  
Sacramento, California 95814-4794

88 11 21 047

Unclassified

SECURITY CLASSIFICATION OF THIS PAGE

REPORT DOCUMENTATION PAGE				Form Approved OMB No. 0704-0188
1a. REPORT SECURITY CLASSIFICATION Unclassified		1b. RESTRICTIVE MARKINGS		
2a. SECURITY CLASSIFICATION AUTHORITY		3. DISTRIBUTION/AVAILABILITY OF REPORT Approved for public release; distribution unlimited.		
2b. DECLASSIFICATION/DOWNGRADING SCHEDULE				
4. PERFORMING ORGANIZATION REPORT NUMBER(S) Technical Report GL-87-14		5. MONITORING ORGANIZATION REPORT NUMBER(S)		
6a. NAME OF PERFORMING ORGANIZATION USAEWES Geotechnical Laboratory	6b. OFFICE SYMBOL (If applicable) WESGH	7a. NAME OF MONITORING ORGANIZATION		
6c. ADDRESS (City, State, and ZIP Code) PO Box 631 Vicksburg, MS 39181-0631		7b. ADDRESS (City, State, and ZIP Code)		
8a. NAME OF FUNDING/SPONSORING ORGANIZATION See reverse	8b. OFFICE SYMBOL (If applicable) SPKRD	9. PROCUREMENT INSTRUMENT IDENTIFICATION NUMBER		
8c. ADDRESS (City, State, and ZIP Code) 650 Capital Mall Sacramento, CA 95814		10. SOURCE OF FUNDING NUMBERS		
		PROGRAM ELEMENT NO.	PROJECT NO.	TASK NO.
		WORK UNIT ACCESSION NO.		
11. TITLE (Include Security Classification) Seismic Stability Evaluation of Folsom Dam and Reservoir Project; Report 5: Seismic Stability Evaluation of Dike 5				
12. PERSONAL AUTHOR(S) Wahl, Ronald E.; Hynes, Mary E.				
13a. TYPE OF REPORT Report 5 of a series	13b. TIME COVERED FROM 1982 TO 1988	14. DATE OF REPORT (Year, Month, Day) November 1988	15. PAGE COUNT 112	
16. SUPPLEMENTARY NOTATION Available from National Technical Information Service, 5285 Port Royal Road, Springfield, VA 22161.				
17. COSATI CODES		18. SUBJECT TERMS (Continue on reverse if necessary and identify by block number) Dam safety Earthquakes and hydraulic structures Folsom Dam safety, Geologic faults. (edc) ←		
FIELD	GROUP	SUB-GROUP		
19. ABSTRACT (Continue on reverse if necessary and identify by block number) The man-made water retaining structures at Folsom Dam and Reservoir Project, located on the American River about 20 miles upstream of the city of Sacramento, California, have been evaluated for their seismic safety in the event of a Magnitude 6.5 earthquake occurring on the East Branch of the Bear Mountains Fault Zone at a distance of about 15 km. This report documents the seismic stability study of Dike 5, one of the eight homogeneous saddle dikes at the Folsom Dam Project. The evaluation process involved extensive review of construction records, field and laboratory investigations, and analytical studies. Dike 5 is expected to perform well if subjected to the design earthquake motions. Due to similarities in the embankment cross sections and in foundation conditions with Dike 5, the other seven dikes at the Folsom Project are also expected to perform satisfactorily during the design earthquake. Key words: Earthquake resistant structures; ...				
20. DISTRIBUTION/AVAILABILITY OF ABSTRACT <input checked="" type="checkbox"/> UNCLASSIFIED/UNLIMITED <input type="checkbox"/> SAME AS RPT <input type="checkbox"/> DTIC USERS		21. ABSTRACT SECURITY CLASSIFICATION Unclassified		
22a. NAME OF RESPONSIBLE INDIVIDUAL		22b. TELEPHONE (Include Area Code)	22c. OFFICE SYMBOL	

Unclassified  
SECURITY CLASSIFICATION OF THIS PAGE

8a. NAME OF FUNDING/SPONSORING ORGANIZATION (Continued).

US Army Engineer District,  
Sacramento

Accession For	
NTIS	GRA&I
DTIC TAB	<input checked="" type="checkbox"/>
Unannounced	<input type="checkbox"/>
Justification	
By _____	
Distribution/ _____	
Availability Codes	
Dist	Avail and/or Special
A-1	



Unclassified  
SECURITY CLASSIFICATION OF THIS PAGE

## PREFACE

The US Army Engineer Waterways Experiment Station (WES) was authorized to conduct this study by the US Army Engineer District, Sacramento (SPK), by Intra-Army Order for Reimbursable Services Nos. SPKED-F-82-2, SPKED-F-82-11, SPKED-F-82-34, SPKED-F-83-15, SPKED-F-83-17, SPKED-F-84-14, and SPKED-D-85-12. This report is one in a series of reports which document the seismic stability evaluations of the man-made water retaining structures of the Folsom Dam and Reservoir Project, located on the American River in California. The Reports in this series are as follows:

- Report 1: Summary
- Report 2: Interface Zone
- Report 3: Concrete Gravity Dam
- Report 4: Mormon Island Auxiliary Dam - Phase I
- Report 5: Dike 5
- Report 6: Right and Left Wing Dams
- Report 7: Upstream Retaining Wall
- Report 8: Mormon Island Auxiliary Dam - Phase II

The work on these reports is a joint endeavor between SPK and WES. Messrs. John W. White and John S. Nickell, of Civil Design Section 'A,' Civil Design Branch, Engineering Division at SPK were the overall SPK project coordinators. Messrs. Gil Avila and Matthew G. Allen, of the Soil Design Section, Geotechnical Branch, Engineering Division at SPK, made critical geotechnical contributions to field and laboratory investigations. Support was also provided by the South Pacific Division Laboratory. The WES Principal Investigator and Research Team Leader was Dr. Mary Ellen Hynes, of the Earthquake Engineering and Geophysics Division (EEGD), Geotechnical Laboratory (GL), WES. The Primary Engineer on the WES team for the portion of the study documented in this report was Mr. Ronald E. Wahl, EEGD. Engineering support was also provided by Mr. Dave Sykora and Mike Sharp. Geophysical support was provided by Mr. Jose Llopis, EEGD.

Professors H. Bolton Seed, Anil K. Chopra and Bruce A. Bolt of the University of California, Berkeley; Professor Clarence R. Allen of the California Institute of Technology; and Professor Ralph B. Peck, Professor Emeritus of

the University of Illinois, Urbana, served as Technical Specialists and provided valuable guidance during the course of the investigation.

Overall direction at WES was provided by Dr. A. G. Franklin, Chief, EEGD, and Dr. W. F. Marcuson III, Chief, GL.

COL Dwayne G. Lee, EN, is Commander and Director of WES. Dr. Robert W. Whalin is Technical Director.

## CONTENTS

	<u>Page</u>
PREFACE.....	1
PART I: INTRODUCTION.....	5
General.....	5
Project History.....	6
Hydrology and Pool Levels.....	6
Site Geology.....	7
Description of the Eight Saddle Dikes.....	8
Seismic Hazard Assessment.....	9
Seismological and geological investigations.....	9
Selection and design ground motions.....	10
PART II: REVIEW OF CONSTRUCTION RECORDS.....	12
General.....	12
Foundation Conditions.....	12
Dike 5.....	12
Dikes 1, 2, 3, 4, 6, 7, and 8.....	13
Embankment Materials.....	14
PART III: FIELD INVESTIGATIONS CONDUCTED FOR THIS STUDY.....	17
General.....	17
Undisturbed Samples.....	17
Standard Penetration Tests.....	17
Geophysical Testing.....	19
Surface vibratory tests.....	19
Crosshole testing.....	20
PART IV: LABORATORY TESTING OF COMPACTED DECOMPOSED GRANITE PERFORMED FOR THIS STUDY.....	22
General.....	22
Index Tests.....	22
Triaxial Tests.....	22
PART V: ONE-DIMENSIONAL DYNAMIC RESPONSE ANALYSIS AND EVALUATION OF LIQUEFACTION POTENTIAL OF DIKE 5.....	24
General.....	24
Dynamic Response Analysis and Liquefaction Analysis of Centerline Profile.....	24
Description of SHAKE.....	24
Inputs to dynamic response of centerline profile.....	24
Results of SHAKE analysis.....	25
Evaluation of liquefaction potential of centerline profile...	26
Dynamic Response Analysis and Liquefaction Evaluation of Upstream Slope Profile.....	27
Inputs to SHAKE.....	27
Results of SHAKE analysis.....	28
Evaluation of the liquefaction potential of the upstream slope profile.....	28
Summary of Liquefaction Evaluation.....	29

	<u>Page</u>
<b>PART VI: PERMANENT DISPLACEMENT ANALYSIS OF DIKE 5.....</b>	<b>30</b>
General.....	30
Computation of Yield Accelerations.....	30
Inputs to ARCEQS.....	30
Yield accelerations computed with ARCEQS.....	31
Makdisi-Seed Method.....	31
Computation of fundamental period and maximum crest acceleration.....	32
Permanent displacements.....	33
Sarma-Ambrayseys Method.....	35
Newmark sliding block analysis.....	35
Dynamic response analysis using SEISCOE.....	35
Permanent displacements.....	36
<b>PART VII: SUMMARY AND CONCLUSIONS.....</b>	<b>39</b>
<b>REFERENCES.....</b>	<b>41</b>
<b>TABLES 1-17</b>	
<b>FIGURES 1-45</b>	
<b>APPENDIX A: COMPUTATIONS USING THE MAKDISI-SEED SIMPLIFIED PROCEDURE FOR ESTIMATING THE CREST ACCELERATION AND FUNDAMENTAL PERIOD OF DIKE 5.....</b>	<b>A1</b>

SEISMIC STABILITY EVALUATION OF FOLSOM DAM AND RESERVOIR PROJECT

Report 5: Seismic Stability Evaluation of Dike 5

PART I: INTRODUCTION

General

1. This report is one of a series of reports that document the investigation and results of a seismic stability evaluation of the man-made water retaining structures at the Folsom Dam and Reservoir Project, located on the American River in Sacramento, Placer, and El Dorado Counties, California, about 20 airline miles northeast of the City of Sacramento. This seismic safety evaluation was performed as a cooperative effort between the US Army Engineer Waterways Experiment Station (WES) and the US Engineer District Sacramento (SPK). Professors H. Bolton Seed, Anil K. Chopra, and Bruce A. Bolt of the University of California, Berkeley, Professor Clarence A. Allen of California Institute of Technology, and Professor Ralph B. Peck, Professor Emeritus of the University of Illinois, Urbana, served as Technical Specialists for the study. This report documents the seismic stability studies of Dike 5, one of eight earthfill saddle dikes at the Folsom Project. A location map and plan of the project are shown in Figures 1 and 2.

2. Figure 2 shows the location of each of the eight saddle dikes. Their total crest length is 10,887 ft. Each has an essentially homogeneous cross section constructed of compacted saprolite and is founded on weathered bedrock. Dike 5 is the largest of the eight dikes and has a crest length of 1,920 ft and a maximum height of approximately 110 ft. As the largest, Dike 5 is most likely to have water on the upstream slope and have saturated zones within its interior. Consequently, Dike 5 was determined to be the most critical dike and was selected for detailed analysis. Plan and cross sectional views of Dike 5 are shown in Figures 3 and 4.

3. The seismic stability investigation of Dike 5 includes a review of construction records, field and laboratory investigations, and analytical studies which evaluate the potential for liquefaction of the compacted soils and permanent displacements within the embankment due to the design earthquake

motions. These studies and the conclusions drawn concerning the seismic stability of Dike 5 are documented in this report.

4. Based on these studies it has been concluded that Dike 5 will remain stable if subjected to the motions of the design earthquake. An analysis of the liquefaction potential of the embankment soils showed that liquefaction will not occur. A Newmark-type permanent displacement analysis indicated that the maximum potential displacements will be less than about 0.8 m (2.5 ft). The conclusions also hold for the other seven dikes at the project which were constructed of similar materials and have cross-sections and foundation conditions which are similar to Dike 5.

#### Project History

5. The Folsom project was designed and built by the Corps of Engineers in the period 1948 to 1956, as authorized by the Flood Control Act of 1944 and the American River Basin Development Act of 1949. Upon completion of the project in May 1956, ownership of the Folsom Dam and Reservoir was transferred to the US Bureau of Reclamation for operation and maintenance. As an integral part of the Central Valley Project, the Folsom Project provides water supplies as well as flood protection for the Sacramento Metropolitan area and extensive water related recreational facilities. Releases from the Folsom Reservoir are also used to provide water quality control for project diversions from the Sacramento-San Joaquin Delta, to maintain fish-runs in the American River below the dam, and to help maintain navigation along the lower reaches of the Sacramento River.

#### Hydrology and Pool Levels

6. Folsom Lake impounds the runoff from 1,875 square miles of rugged mountainous terrain. The reservoir has a storage capacity of 1 million acre-feet at gross pool and is contained by approximately 4.8 miles of man-made water-retaining structures that have a crest Elevation of 480.5 ft above sea level. These structures are the Right and Left Wing Dams, the Concrete Gravity Dam, Mormon Island Auxiliary Dam, and eight Saddle Dikes. At gross pool, Elevation 466, there are 14.5 ft of freeboard. This pool level was selected for the safety evaluation, based on a review of current operational procedures

and hydrologic records (obtained for a 29-year period, from 1956 to 1984) for the reservoir which shows that the pool typically reaches Elevation 466 ft about 10 percent of the time during the month of June, and considerably less than 10 percent of the time during the other months of the year. Under normal operating conditions, the pool is not allowed to exceed Elevation 466 ft. Hydrologic records show that situations which would cause the pool to exceed Elevation 466 are rare events.

#### Site Geology

7. At the time of construction, the geology and engineering geology concerns at the site were carefully detailed in the foundation report by US Army Engineer District, Sacramento (1953). This foundation report from construction records and a later paper by Keirsch and Treasher (1955) are the sources for the summary of site geology provided in this section.

8. The Folsom Dam and Reservoir Project is located in the low, western-most foothills of the Sierra Nevada in central California, at the confluence of the North and South Forks of the American River. Topographic relief ranges from a maximum of 1,242 ft near Flagstaff Hill located between the upper arms of the reservoir, to 150 ft near the town of Folsom just downstream of the Concrete Gravity Dam. The North and South Forks once entered the confluence in mature valleys up to 3 miles wide, but further downcutting of the river channel resulted in a V-shaped inner valley 20 to 185 ft deep. Below the confluence, the inner canyon was flanked by a gently sloping mature valley approximately 1.5 miles wide bounded on the west and southeast by a series of low hills. The upper arms of the reservoir, the North and South Forks, are bounded on the north and east by low foothills.

9. A late Pliocene-Pleistocene course of the American River flowed through the Blue Ravine and joined the present American River channel downstream of the town of Folsom. The Blue Ravine was filled with late Pliocene-Pleistocene gravels, but with subsequent downcutting and headward erosion, the Blue Ravine was eventually isolated and drainage was diverted to the present American River Channel.

10. The important formations at the dam site are: a quartz diorite granite which forms the foundation at the Concrete Gravity Dam, Wing Dams, and Saddle Dikes 1 through 7; metamorphic rocks of the Amador group which underlie

Saddle Dike 8 and the foundation at Mormon Island Auxiliary Dam; the Mehrten formation, a deposit of cobbles and gravels in a somewhat cemented clay matrix which caps the low hills that separate the saddle dikes and is part of the foundation at Dike 5; and the alluvium that fills the Blue Ravine at Mormon Island Auxiliary Dam.

11. Weathered granitic or metamorphic rock is present throughout the area. Figure 2 shows a geologic map of the project area. The Concrete Gravity Dam, the Wing Dams, the retaining walls, and Dikes 1 through 7 are founded on weathered quartz diorite granite. Between Dikes 7 and 8 there is a change in the bedrock. Dike 8 and Mormon Island Auxiliary Dam are underlain by metamorphic rocks of the Amador group. The Amador group consists predominately of schists with numerous dioritic and diabasic dikes.

#### Description of the Eight Saddle Dikes

12. Figure 2 shows a plan of the 8 dikes, which have a total length of 10,887 ft. Each of the eight saddle dikes spans topographic saddles. A summary of the crest lengths and maximum height of each dike is listed in Table 1. Dike 5 is the largest of these compacted earthfill saddle dikes, all founded on weathered rock. As the largest, Dike 5 is more likely to have water against its upstream slope and have saturated zones than the other dikes, which are typically dry. Since all the dikes are essentially homogeneous in section, composed of compacted saprolite, Dike 5 is typical of the sections for all the other dikes. Consequently, Dike 5 was selected for study to represent the most critical case for all the dikes. Plan and cross-sectional views of Dike 5 are shown in Figures 3 and 4, respectively.

13. Dike 5 has a crest length of 1,920 ft and a maximum height of 110 ft near Station 180+00. The embankment is located in a relatively steep-walled topographic saddle. Two basic types of foundation conditions are present beneath the embankment. The portion of the embankment whose foundation is above elevation 450 is founded on the Mehrten formation, which is composed of cobbles and gravels in a cemented clayey matrix. The remainder of the embankment is founded upon a weathered quartz diorite granite. The embankment is essentially homogenous and is constructed of compacted decomposed granite scraped from the weathered granite in borrow areas located in what is now the reservoir. The compacted decomposed granite, a saprolite, classifies as Silty

Sand (SM) according to the Unified Soil Classification System (USCS). The construction specifications required that the central portion of the embankment, Zone C, receive a higher compactive effort than Zone D located in areas directly under the upstream and downstream slopes. Seepage is controlled by a downstream gravel drainage blanket. The upstream side of the embankment has slopes of 3.25 horizontal to 1 vertical below Elevation 466 ft and 2.25 to 1 between Elevation 466 and 480.5 ft (crest elevation). The downstream side has one continuous slope of 2.25 horizontal to 1.0 vertical.

14. Dikes 1, 2, 3, 4, 6, 7, and 8 span low topographic saddles and are much lower in height than Dike 5. Dikes 1, 2, 3, 4, 6 and 7 are located on the western boundary of the project. These six dikes all have foundations conditions similar to those at Dike 5 in that they are founded directly on granite which is intensely to moderately weathered. Dike 8 is founded directly on metamorphic rocks over its entire length. Each of the saddle dikes is essentially homogeneous and constructed of compacted decomposed granite similar to that of Dike 5.

#### Seismic Hazard Assessment

##### Seismological and geological investigations

15. Detailed geological and seismological investigations in the immediate vicinity of Folsom Reservoir were performed by Tierra Engineering, Incorporated to assess the potential for earthquakes in the vicinity, to estimate the magnitudes these earthquakes might have, and to assess the potential for ground rupture at any of the water-retaining structures (see Tierra Engineering, Inc., 1983 for a comprehensive report). A 12-mile wide by 35-mile long study area centered on the Folsom Reservoir was extensively investigated using techniques such as areal imagery analysis, ground reconnaissance, geologic mapping, and detailed fault capability assessment. In addition, studies by others relevant to the geology and seismicity of the area around Folsom were also compiled. These additional literature sources include numerous geologic and seismologic studies published through the years, beginning with the "Gold Folios" published by the US Geologic Survey in the 1890's, the engineering geology investigations for New Melones and the proposed Marysville and Auburn Dams, studies performed for the Rancho Seco Nuclear Power Plant as well as unpublished student theses and county planning studies. It was determined

that no capable faults underlie any of the water-retaining structures or the main body of the reservoir at the Folsom Project. The tectonic and seismicity studies also indicated that it is unlikely that the Folsom Lake can induce major seismicity. Since the faults that underlie the water retaining structures at the Folsom Project were found to be noncapable, seismic fault displacement in the foundations of the water retaining structures is judged to be highly unlikely.

16. The closest capable fault is the East Branch of the Bear Mountains fault zone which has been found to be capable of generating a maximum magnitude  $M = 6.5$  earthquake. The return period for this maximum earthquake is estimated to exceed 400 years (Tierra Engineering Inc. 1983). Determination that the East Branch of the Bear Mountains Fault Zone is a capable fault came from the Auburn Dam earthquake evaluation studies. The minimum distance between the East Branch of the Bear Mountains Fault Zone and Mormon Island Auxiliary Dam is 8 miles, the Gravity Dam is 9.5 miles, and Dike 5 is 9 miles. The focal depth of the earthquake is estimated to be 6 miles. This hypothetical maximum magnitude earthquake would cause more severe shaking at the project than earthquakes originating from other known potential sources.

#### Selection of design ground motions

17. The seismological and geological investigations summarized in the Tierra report were provided to Professors Bruce A. Bolt and H. B. Seed to determine appropriate ground motions for the seismic safety evaluation of the Folsom Dam Project. The fault zone has an extensional tectonic setting and a seismic source mechanism that is normal dip-slip. The slip rate from historic geomorphic and geological evidence is very small, less than  $10^{-3}$  centimeters per year with the most recent known displacement occurring between 10,000 and 500,000 years ago in the late Pleistocene period.

18. Based on their studies of the horizontal ground accelerations recorded during the Imperial Valley earthquake of 1979, as well as recent studies of a large body of additional strong ground motion recordings, Bolt and Seed (1983) recommend the following design ground motions:

Peak horizontal ground acceleration	= 0.35 g
Peak horizontal ground velocity	= 20 cm/sec
Bracketed duration ( $\alpha \geq 0.05$ g)	= 16 sec

Because of the presence of granitic plutons at the site, it is expected that the earthquake accelerations might be relatively rich in high frequencies. Bolt and Seed (1983) provided 2 accelerograms that are representative of the design ground motions expected at the site as a result of a maximum magnitude  $M = 6.5$  occurring on the East Branch of the Bear Mountains Fault Zone. The accelerograms are designated as follows (Bolt and Seed 1983):

M6.5 - 15k - 83A. This accelerogram is representative of the 84-percentile level of ground motions that could be expected to occur at a rock outcrop as a result of a Magnitude 6-1/2 earthquake occurring 15 km from the site. It has the following characteristics:

Peak accelerations = 0.35 g  
Peak velocity = 25 cm/sec  
Duration = 16 sec

M6.5 - 15k - 83B. This accelerogram is representative of the 84-percentile level of ground motions that could be expected to occur as a result of a Magnitude 6-1/2 earthquake occurring 15 km from the site. It has the following characteristics:

Peak acceleration = 0.35 g  
Peak velocity = 19.5 cm/sec  
Duration = 15 sec

Figure 5 shows plots of acceleration as a function of time for the two design accelerograms and Figure 6 show response spectra of the motions for damping ratios of 0, 2, 5, 10, and 20 percent damping.

PART II: REVIEW OF CONSTRUCTION RECORDS

General

19. Detailed construction records were kept to document the initial site reconnaissance, selection of borrow areas, foundation preparation and construction sequence for the eight dikes. Pertinent information from these construction records are summarized in this chapter. This information provides key background data used in development of an idealized section for analysis and detailed descriptions for the foundation and embankment materials. The information gathered was also used to demonstrate the similarity in embankment and foundation conditions for each of the eight dikes on the Folsom project.

Foundation Conditions

20. The discussion of foundation conditions in the following paragraphs are based upon the foundation reports of each of the eight dikes (US Army Engineer District, Sacramento 1953, 1954, and 1955). The foundation conditions and site geology noted in the foundation reports were based on study of samples taken from numerous drill holes and test pits made prior to construction, as well as from observations made from the shallow cutoff trenches excavated along the centerlines of the dikes during construction.

Dike 5

21. Dike 5 spans a relatively steep walled saddle as shown in the plan view of Figure 3. The dike, which is 1,920 ft long at the crest, has two basic types of foundation conditions. At the higher elevations, Above Elevation 450 ft, the embankment is founded on the Mehrten Formation at both the left abutment (between Station 174+00 and Station 175+20) and right abutment (between Station 186+20 and Station 193+00). At the lower elevations of the saddle, between Station 175+20 and Station 186+20, the embankment is founded on weathered granite.

22. The Miocene-Pliocene Mehrten formation was deposited under fluvial-tile conditions upon the underlying granite surface. This formation consists of well sorted and rounded cobbles, gravel and sand which are tightly cemented by clay. The minerals are predominately andesitic.

23. The granite foundation is characterized by two major sets of closely spaced structural joints. The first set trends N 60° E to S 70° E and dips between 52° and 65° SE to SW. These joints trend in a direction which is parallel to the lineation of the minerals of the rock and were considered to be shrinkage joints. They were filled with the products of the weathering process. The joints of the second set trend from N 32° E to N 58° E and dip from 50° to 89° NW. Many individual joints of this group were open by a fraction of an inch. In the lowest portion of the saddle, near Station 181+40, the joints trend N 60° E to N 80° E and dip 51° to 68° NW. All of these were open and were receptive to the flow of ground water. The open joints appear to have controlled the geomorphic development of the saddle. Ground water transportation of weathering agents through the joints has had a profound effect in the upper 30 to 80 ft of the foundation granite where the degree of weathering varies from moderate to intense. Thus, almost all of the surface rock is intensely weathered to irregular depths.

24. A cutoff and grout curtain were installed along the centerline of Dike 5 to cutoff seepage through the foundation. As per specification, in the granite foundation, the core trench was excavated to firm weathered material using ordinary excavating equipment. At Dike 5 a Lorain L-50k power backhoe was used to excavate the core trench. The depths of the core trench increases toward the ends of the dike. A maximum depth of 15 ft was reached near the top of the right abutment. The grout curtain was installed in drill holes which were up to 100 ft deep.

25. Outside the cutoff trench at the lower elevations of the topographic saddle the foundation was stripped of vegetation and loose soil to expose a firm weathered granitic surface. Stripping was achieved using DW-20 and twin engine 20 yd Euclid power scrapers. The thickness of the stripped material was typically between 6 in. and 2 ft.

#### Dikes 1, 2, 3, 4, 6, 7, and 8

26. Dikes 1, 2, 3, 4, 6, 7, and 8 have foundation conditions which are similar to Dike 5 in that they are all founded directly upon weathered rock. Dikes 1, 2, 3, 4, 6, and 7 are constructed upon weathered granite for their entire lengths. Like Dike 5, the weathered granite beneath these dikes was observed to be jointed and moderately to intensely weathered. The foundation report indicated that grout curtains were constructed only beneath Dikes 1, 4, 6, and 7. The contact between the granite and the metamorphic series of rocks

(Amador) is located at a point approximately 100 ft east of the left abutment of Dike 7. The entire length of Dike 8 is founded directly on these metamorphic rocks which are composed of amphibolitic schists. The foundation report indicated that the foundation is firm and impervious and that bonding between the foundation rock and the embankment materials was very good. No grout curtain was installed beneath Dike 8.

#### Embankment Materials

27. Basic data on the embankment materials of Dike 5 and the other 7 saddle dikes were obtained from record samples recovered during construction and from disturbed and undisturbed samples recovered during the field investigations performed by WES and SPK for the seismic stability study. Discussions of the recent field investigations associated with this study are provided in the next chapter of this report.

28. The eight saddle dikes have essentially homogeneous sections constructed of compacted decomposed granite obtained from Borrow Areas 1, 2, and 4 which were located in the reservoir near the axis of the dam. Figure 4 shows typical cross sections of Dikes 1, 4, 5, 6, 7, and 8.

29. The central impervious core and the shells of Dike 5 are constructed of Zone C and D material, respectively. Both zones are compacted decomposed granite, a saprolite, excavated from Borrow Area 2 (see Figure 2). The material from Borrow Area 2 classifies as Silty Sand (SM) according to the Unified Soil Classification System. The average gravel, sand, and fines contents are 7, 65, and 28 percent, respectively. The fines are nonplastic and have a liquid limit of approximately 25 percent and a plasticity index of about 3 percent. The basic difference between the two zones is that Zone C was placed with a slightly higher compactive effort than Zone D. Details of the placement requirements used for the different zones are given in Table 2. Table 2 also lists the material source and placement requirements for the downstream blanket drain in Dike 5.

30. Zones G and H, the materials of Dikes 7 and 8, are compacted decomposed granite obtained from Borrow Area 1. Construction records show that the material in Borrow Area 1 is very similar to that in Borrow Area 2. This material classifies as Silty Sand (SM). The gradation of Borrow Area 1 materials indicates that the average gravel, sand, and fines contents are about

10, 60, and 30 percent, respectively. The fines are nonplastic and have a liquid limit of 25 percent and an average plasticity index less than 5 percent. Zone G was placed with more compactive effort than Zone H as shown in Table 2.

31. Dikes 1, 2, 3, and 4, were constructed of compacted decomposed granite (SM) obtained from Borrow Area 4. Borrow Area 4 not shown in Figure 2, is located in the reservoir adjacent to Dikes 1, 2, and 3. Construction records show that the materials in Borrow Area 4 are similar to those in Borrow Areas 1 and 2. The gradation of this material indicates average gravel, sand, and fines contents of 10, 65, and 25 percent, respectively. The fines are nonplastic.

32. A summary of the gradations expressed in terms of the gravel, sand, and fines contents and the Atterberg limits for the materials in each of the borrow areas used in constructing the dikes is listed in Table 3. Table 3 shows that the materials from each of the borrow pits are similar having approximately the same amounts of gravel, sand, and fines and similar plasticity characteristics. In general, the decomposed granite has approximately 10 percent gravel, 65 percent sand, and 28 percent fines (percent passing the No. 200 sieve). The fines content has a liquid limit of about 25 percent and a plasticity index of about 4 percent. The material classifies as Silty Sand (SM) according to the USCS. Analysis of data given in Table 2 indicates that the compaction requirements for the compacted decomposed granite of Zones C and G and Zones D and H of Dikes 5, 7, and 8 are similar. The material from Borrow Area No. 4 used to construct Dikes 1, 2, 3, 4, and 6 required greater compactive effort and thinner lift thickness to achieve the desired degree of compaction than did the materials from Borrow Areas 1 and 2 used to construct Dikes 5, 7, and 8.

33. Record samples were obtained from each embankment during construction as a quality control measure. A summary of the densities obtained from record samples taken during construction for each of the eight dikes are given in Table 3. The dry densities range from 122 pcf to 136 pcf. The average dry density of Dike 5 based on seven samples was estimated to be 127 pcf. A plot of the gradation of the Dike 5 record samples is shown in Figure 7. The gradations, Atterberg limits, and USCS soil classification (SM) for these samples match those given for Borrow Area 2 which are listed in Table 4.

34. Based on examination of the data pertaining to gradation, Atterburg limits, densities, and compaction requirements of the compacted decomposed granite it is concluded that each of the eight dikes are essentially homogeneous and that the compacted decomposed granite in each is essentially the same.

35. The properties of the compacted decomposed granite selected for use in the initial design of the dikes were based on laboratory tests performed prior to construction. The design dry density was 123.4pcf based on 95 percent Modified AASHO density. The saturated unit weight was 140pcf. The effective shear strength parameters of cohesion and tangent of the friction angle were 0 and 0.70 ( $\phi' = 35^\circ$ ), respectively.

### PART III: FIELD INVESTIGATIONS CONDUCTED FOR THIS STUDY

#### General

36. As part of the seismic stability study, field investigations were conducted at Dike 5. The field investigations included Standard Penetration Test (SPT) soundings, disturbed and undisturbed soil sampling, and geophysical testing. The field tests were conducted on or downstream of the dam centerline. In view of the symmetry indicated in construction drawings, this information is assumed to be representative of the materials located upstream of the centerline as well. A plan view of the borehole locations is shown in Figure 3. A plan view of the geophysical test locations is shown in Figure 8.

#### Undisturbed Samples

37. Undisturbed samples of the embankment and foundation were retrieved from borings US-1 and US-10 at Dike 5. Boring US-1 was located near Station 180+00 at the centerline and drilled to a depth of 120 ft. The top of US-1 was at the crest elevation of 480.5 ft. Boring US-10 was located near Station 180+00 on the downstream slope and drilled to a depth of 90 ft. The elevation of the top of US-10 was approximately 423 ft.

38. Two sampling techniques were used in each boring. In the compacted decomposed granite of the embankment, 5-in. diameter undisturbed samples were obtained using a modified Denison sampler. The weathered granite in the foundation was sampled using a rock core barrel. In US-1, the foundation was encountered at a depth of 97 ft and in US-10 the foundation was encountered at a depth of 42 ft. After drilling, the holes were cased with 4 in. polyvinyl-chloride (PVC) pipe and subsequently used for crosshole testing. Undisturbed samples recovered from the embankment were subsequently used in laboratory testing.

#### Standard Penetration Tests

39. Standard Penetration Tests (SPT) were performed in borings SS-1 on the centerline and SS-10 on the downstream slope. Both borings were located near Station 180+00. The top of Boring SS-1 was located on the crest

(Elevation 480.5 ft) approximately 10 ft south of US-1. Boring SS-1 was drilled to a depth of 120 ft. The SPT soundings were performed in the compacted decomposed granite, the upper 97 ft of the boring. Between depths of 97 and 120 ft the foundation granite was sampled using a rock core barrel. The top of Boring SS-10 was on the downstream slope at approximately Elevation 423 ft about 10 ft south of US-10. SS-10 was approximately 60 ft deep. The SPT soundings were performed in the embankment soils, the upper 42 ft of the boring. The weathered granite foundation between 42 and 60 ft was sampled using a rock core barrel.

40. The SPT soundings in Borings SS-1 and SS-10 were performed using a WES trip hammer and a 2-in. split spoon sampler. The SPT measurements were made at 5-ft depth intervals in holes stabilized with drilling mud. Jar samples retrieved from the SPT holes were saved for laboratory classification by the SPD laboratory. After the drilling was completed, the holes were cased with 4-in. PVC pipe and the casing was grouted in place with a grout that sets up with a consistency similar to that of soil. These borings were later used for geophysical testing.

41. Energy-corrected blowcounts,  $N_{60}$ , were determined from the blowcounts measured in Boreholes SS-1 and SS-10. Experience with the WES trip hammer shows that it provides 1.3 times more energy than the recommended standard energy level of 60 percent of the theoretical free fall (Seed 1986). Therefore, all field blowcounts were multiplied by 1.3 to adjust the trip hammer blowcounts to their standard energy level equivalent,  $N_{60}$ .

42. A second adjustment was made to correct the  $N_{60}$  blowcounts to their equivalent at an effective overburden stress of 1 tsf. The resulting energy and overburden-corrected blowcount is designated  $(N_1)_{60}$ . The  $(N_1)_{60}$  blowcount was computed with Equation 1:

$$(N_1)_{60} = C_n \times N_{60} \quad (1)$$

where  $C_n$  is the overburden correction factor. The relationship between  $C_n$  and effective overburden stress is shown in Figure 9. Figures 10 and 11 are plots of  $N_{60}$  and  $(N_1)_{60}$  versus depth for Borings SS-1 and SS-10. The mean  $(N_1)_{60}$  values obtained from Borings SS-1 and SS-10 are 64 and 48 blows per foot, respectively. (The combined average  $(N_1)_{60}$  value for the compacted decomposed granite is 60.) The  $N_{60}$  and  $(N_1)_{60}$  values are used to determine

the cyclic strength of the compacted decomposed granite in the liquefaction analysis discussed in Part V.

#### Geophysical Testing

43. The geophysical investigation conducted at Dike 5 consisted of surface refraction seismic, surface vibratory, and crosshole tests. The objective of these tests was to determine the in-situ variation of compression wave (p-wave) and shear wave (s-wave) velocities with depth for the embankment and the foundation. This information was used in developing idealized soil profiles and determining soil moduli for input to the dynamic analysis discussed in Part V. The layout of the geophysical tests is shown in Figure 8. The geophysical tests were reported by Llopis 1983 and 1984.

##### Surface vibratory tests

44. The surface vibratory test is used to measure the surface Rayleigh-wave velocity which is typically about 10 percent (or less) slower than the shear wave velocity. Rayleigh waves are generated by a surface vibrator which is swept through a range of discrete frequencies and arrival times are measured by geophones placed at selected intervals along a straight line on the surface of the ground. Wave velocities are approximately average values for an effective depth of one-half the wave length corresponding to the vibrator frequency (Ballard 1964). The locations of the surface vibratory tests are shown on Figure 8.

45. Rayleigh-wave velocities along the crest of the dam were determined, by means of four 200 ft long surface vibratory lines V-5 through V-8, as functions of depth and to search for anomalous zones. Lines V-5 and V-6 were conducted with the vibrator positioned at the highest section of the dam, Station 180+50. The R-wave velocities measured for both lines are shown in Figure 12. The velocities measured by the two lines are similar and both range from about 800 fps near the surface to about 925 fps at a depth of about 60 ft which was the maximum depth of R-wave penetration. The velocities over the depth range of 0 to 60 ft, were influenced entirely by the compacted decomposed granite. No anomalous velocity zones were detected over the area covered by lines V-5 and V-6.

46. Surface vibratory lines V-7 and V-8 were investigated with the vibrator in position at about Station 190+00. These lines were located along

the portion of the dike founded on the Mehrten formation. The average embankment height in this area is about 15 ft. The R-wave velocities measured by V-7 and V-8 are shown in Figure 13. The velocities increase from about 800 fps at 10 ft to about 1,050 fps at 20 ft in depth and remain essentially constant from 20 ft to about 60 ft, which was the maximum depth of R-wave penetration. The R-wave velocities measured by lines V-7 and V-8 were influenced by the relatively shallow depth to the Mehrten foundation in this location. The results indicate that the Mehrten formation has a higher R-wave velocity than the overlying embankment and is therefore a stiffer material. No anomalous zones were detected by lines V-7 and V-8.

#### Crosshole testing

47. Two sets of crosshole tests were conducted in pairs of boreholes on the crest of the dam and on the downslope near Station 180+50. Boreholes SS-1 and US-1, each 120 ft deep and spaced 10 ft apart on the centerline, were used for the crosshole tests labeled C1A and C1B in Figure 8, and Boreholes SS-10 and US-10, each 60 ft deep and spaced 10 ft apart on the downstream slope, were used for the crosshole tests labeled S1A and S1B. Both P- and S-wave velocities were measured in each crosshole set. In both cases the boreholes extended through the embankment and into the underlying weathered granite foundation.

48. Crosshole S-wave velocity tests were conducted with a downhole vibrator inserted at a given depth into the source borehole. The vibrator was then swept through a range of frequencies (50 to 500 hz) to find one that propagated well through the soil and which transmitted the highest amplitude signal to the receiver. Borehole deviation surveys were performed to minimize the source to receiver distance errors in the reduction of the data. Exploding bridge-wire detonators were used as the source for the P-wave crosshole tests. Measurements were made at 5 ft depth intervals for each type of test.

49. Figure 14 shows the P-wave velocity zones interpreted from both crosshole sets superimposed on the section of Dike 5 at Station 180+50. The interpretation indicates that the velocity of the compacted decomposed granite in the embankment ranges from 1,650 fps to 4,550 fps. Zones with velocities approaching 4,800 fps are saturated or nearly saturated. The results indicate that at the time of testing probably only the portions of the embankment just above the foundation upstream of the centerline had high degrees of

saturation. The p-wave velocity of the weathered granite foundation was measured to be about 10,000 fps.

50. The shear wave velocity zones interpreted from the crosshole sets are shown in Figure 15. In the compacted decomposed granite of the embankment, the shear wave velocities generally increased with depth. The measured velocities ranged from 950 fps to 1,600 fps. The s-wave velocities measured in the weathered granite foundation were 2,300 fps at the centerline and 2,900 fps under the slope. A measure of shear modulus, independent of confining stress, is the value of  $K_2$ . It is computed as follows:

$$K_2 = \frac{G}{1,000(\sigma'_m)^{0.5}} \quad (2)$$

where

$G$  = the shear modulus in psf

$\sigma'_m$  = the effective mean normal pressure in psf

At low shear strain levels,  $G$  and  $K_2$  can be estimated from the shear wave velocity measurements,  $V_s$ , as follows:

$$G = V_s^2 \times \rho \quad (3)$$

$$K_2 = \frac{V_s^2 \times \rho}{1,000(\sigma'_m)^{0.5}} \quad (4)$$

where  $\rho$  is the mass density. Any consistent units can be used in Equation 3, but in Equation 2 the units must be feet, pounds, and seconds. From the field measured shear-wave velocities in Dike 5 and the Wing Dams (where compacted decomposed granite formed the impervious core), it was estimated that a representative average value of  $K_2$  for the compacted decomposed granite was 120.

PART IV: LABORATORY TESTING OF COMPACTED DECOMPOSED GRANITE  
PERFORMED FOR THIS STUDY

General

51. A laboratory testing program was conducted using disturbed and undisturbed samples of the compacted decomposed granite to determine characteristics and properties required for the liquefaction and seismic stability analyses. Index tests were performed on samples to determine soil classifications, Atterberg limits, and gradations of the embankment soils. Additionally, undrained triaxial compression tests with pore pressure measurements ( $\bar{R}$  tests) were conducted on undisturbed samples to determine representative shear strength parameters for use in the stability analysis. The test results reported in this chapter were performed by SPD Laboratory and are reported in US Army Engineer Laboratory, South Pacific Division (1986).

Index Tests

52. Gradation and index tests were performed on samples recovered from the borings located at the centerline and downstream slope. Basic information acquired from the laboratory tests is summarized in Tables 5 and 6 for the samples from the centerline and downstream slope, respectively. Gradation ranges obtained from mechanical sieve analysis for the centerline and downstream slope samples are shown in Figure 16. As expected, the gradation range of these samples matches the data obtained from the record samples presented in Figure 7. The mean grain size is about 0.50 mm, the fines content is about 15 percent, the liquid limit is about 25 percent, and the plasticity index is about 4 percent. Most of the samples classified as Silty Sands (SM) according to the USCS, which matches the construction data.

Triaxial Tests

53. Shear strength parameters for the compacted decomposed granite were determined from a series of anisotropically consolidated undrained triaxial tests with pore pressure measurements ( $\bar{R}$  tests). The tests were performed on undisturbed samples acquired from Dike 5 and the impervious cores of the Left

and Right Wing Dams which were also constructed of decomposed granite compacted to the same specifications as Dike 5. Each sample tested had a nominal 4-in. diameter and 9-in. height. The failure envelopes for total (R) and effective stress ( $\bar{R}$ ) conditions are shown in Figures 17 and 18. Also shown on each figure are the consolidation stress ratios,  $K_c$ , and the post-consolidation dry densities. The failure envelopes were determined by favoring the tests which had a dry density of approximately 127pcf which was the average dry density of Dike 5 as determined from record samples taken during construction. Figure 17 shows that the consolidated-undrained shear strength envelope has a cohesion intercept of about 4 tsf and a friction angle of  $30.6^\circ$ . Figure 19 shows that the compacted decomposed granite has a cohesion intercept of zero and a friction angle of  $38^\circ$ . These results are also listed in Table 7.

PART V: ONE-DIMENSIONAL DYNAMIC RESPONSE ANALYSIS AND  
EVALUATION OF LIQUEFACTION POTENTIAL OF DIKE 5

General

54. A dynamic response analysis and an evaluation of the liquefaction potential were performed on two idealized one-dimensional soil profiles. The two profiles are representative of conditions at the centerline and upstream slope near Station 180+50. The locations of the two profiles in relation to Dike 5's cross section are shown in Figure 19. The dynamic response of each profile to the design ground motions was computed using the computer program SHAKE. The liquefaction evaluation was performed using the field-performance based techniques developed by Seed et al. (1984) in which the cyclic strengths are estimated from the SPT blowcounts. Safety factors against liquefaction were then computed by dividing the cyclic strength by the dynamic shear stresses determined with SHAKE.

Dynamic Response Analysis and Liquefaction  
Analysis of Centerline Profile

Description of SHAKE

55. SHAKE is a one-dimensional wave propagation code developed at the University of California, Berkley by Schnabel, Lysmer, and Seed (1972). SHAKE uses a total stress approach to calculate the dynamic response of a soil column and solves the wave equation through use of the Fast Fourier Transform (FFT). The equivalent linear constitutive model is used to handle the nonlinear stress-strain characteristics of soil behavior. As a one-dimensional model, it is assumed that the ground surface is level and that all soil layers in the profile are horizontal and infinite in lateral extent. Each soil layer is assigned a total unit weight and the strain-dependent shear modulus (or shear wave velocity) and damping. The dynamic shear stresses and peak accelerations for each soil layer are the key output sought from SHAKE in the analysis of each soil profile.

Inputs to dynamic  
response of centerline profile

56. The idealized centerline profile used for the SHAKE analysis is shown in Figure 19. The profile was subdivided into 17 layers. The top

16 layers represent the compacted decomposed granite embankment soil whose combined thicknesses total 97 ft. The unit weight for each of these layers was assumed to be 127 pcf in the computations. The low strain amplitude shear wave velocities input to SHAKE are listed for each layer and were determined from the geophysical tests. Other information in Figure 20 includes SPT blowcounts and data from the index tests performed in the laboratory. The strain dependent modulus degradation and damping curves used for each of the top sixteen layers are those recommended by Seed (1970) for sands and are shown in Figure 21. The weathered granite foundation baserock is represented by layer 17.

57. The centerline profile was excited by both Accelerograms A and B to determine which caused the stronger response. The accelerograms are shown in Figure 5. The design accelerograms were input to SHAKE as rock outcrop motions with a peak acceleration of 0.35 g.

#### Results of SHAKE analysis

58. Peak accelerations of selected layers and dynamic stresses were the key values sought from the SHAKE calculations. Figure 22 shows the peak accelerations in the centerline profile in response to Record A. The plot shows that the peak baserock acceleration of 0.24 g is amplified by a factor of 1.63 at the ground surface where the peak acceleration is 0.39 g. Figure 23 shows the peak accelerations in the centerline profile in response to Record B. In this case, the peak baserock acceleration of 0.31 g is magnified by a factor of 1.48 at the ground surface where the maximum acceleration was 0.46 g.

59. The effective dynamic shear stresses induced by Records A and B are compared in Figure 24. The effective dynamic shear stress represents the average dynamic shear stress acting over eight equivalent cycles (the recommended number of equivalent cycles for a Magnitude 6.5 event). The effective dynamic shear stress is 65 percent of the peak dynamic shear stress in the dynamic shear stress history of a soil layer. The plot shows that the dynamic shear stresses induced in the centerline profile by Record A are typically slightly larger than those by Record B; therefore the stresses of Record A were used in the liquefaction potential analysis.

Evaluation of liquefaction potential of centerline profile

60. The liquefaction potential of the embankment soils was evaluated using the field-performance-based technique developed by Seed et al. (1984). Liquefaction potential is determined by comparing the dynamic stresses induced by the earthquake with the cyclic strength of the soil. The dynamic shear stresses were computed with SHAKE and the cyclic shear strengths were determined from SPT blowcounts.

61. The cyclic strengths of the compacted decomposed granite were determined using Seed's chart in Figure 25 and the SPT blowcounts obtained in the field. This chart relates measured  $(N_1)_{60}$  values to estimated cyclic stress ratios at several sites which have been subjected to earthquake shaking from a  $M = 7.5$  seismic event. The lines on the chart distinguish safe combinations of  $(N_1)_{60}$  from unsafe combinations based on whether or not surface evidence of liquefaction was observed in the field. This chart is interpreted to relate  $(N_1)_{60}$  to the cyclic stress ratio required to generate 100 percent residual excess pore pressure. The chart provides data for clean and silty fines contents, expressing the cyclic stress ratio for a confining pressure of about 1 tsf and level ground conditions and for earthquakes with  $M = 7.5$ , as a function of the  $N_1$  value of a soil corrected to a 60 percent energy level,  $(N_1)_{60}$ . Seed's work (Seed et al. 1983, and Seed et al. 1984a) shows that for  $M = 6.5$  events, the cyclic strength is about 20 percent higher, for any value of  $(N_1)_{60}$ , than for  $M = 7.5$  earthquakes. Figure 26 is a chart showing the cyclic strengths versus  $(N_1)_{60}$  for soils with varying fines contents for Magnitude 6.5 earthquakes. This chart was used in this study.

62. As discussed in Part III, the average  $(N_1)_{60}$  values obtained from the SPT measurements performed in the field in the compacted decomposed granite were 48 blows/ft in the downstream slope and 64 blows/ft at the centerline. Entering the chart on Figure 26 at a value of 48 and using the curve for 15 percent fines content indicates that the cyclic strength of the soil is indeterminately high since this curve approaches an  $(N_1)_{60}$  value of about 25 as an asymptote. Since the strengths were indeterminate it was not possible to compute safety factors against liquefaction. Hence, the liquefaction potential of the embankment soils was evaluated using an alternate approach. In this study, liquefaction potential was evaluated by comparing field measured  $N_{60}$  blowcounts with the  $N_{60}$  blowcounts required for a safety factor

against liquefaction of one. For a safety factor of one the earthquake induced stresses are equal to the cyclic strength of the soil. The required values of  $N_{60}$  for a safety factor of one were computed from the SHAKE stresses and the magnitude-adjusted chart in Figure 25 with the curve for a fines content of 15 percent. Since the chart was developed for a vertical stress of 1 tsf, and because the increase of cyclic strength with confining pressure is nonlinear, the SHAKE stress ratios were adjusted using Equation 5:

$$\left(\frac{\tau/\sigma'}{\sigma'_v}\right)_{\sigma'_v = 1 \text{ tsf}} = K_g \times \left(\frac{\tau/\sigma'}{\sigma'_v}\right)_{\sigma'_v = 1 \text{ tsf}} \quad (5)$$

$K_g$  was determined from the vertical stress and the chart developed by Harder and Seed (1985) shown in Figure 27. The 15 percent fines content curve on Figure 25 was then entered at the ordinate for the earthquake induced stress ratio computed from Equation 4 to determine the  $(N_1)_{60}$  value required for a safety factor of one. The  $(N_1)_{60}$  value was then corrected to field overburden conditions using the relationship:

$$N_{60} = (N_1)_{60}/C_n \quad (6)$$

In Equation 6, the  $C_n$  factor introduced earlier was determined from the vertical effective stress and from the chart in Figure 9.

63. Figure 28 shows a comparison of the field-measured  $N_{60}$  blowcounts from Boring SS-1 (from Figure 10) and the required  $N_{60}$  blowcounts for a safety factor against liquefaction of one. The required  $N_{60}$  blowcounts were calculated using the effective shear stresses induced from Record A shown in Figure 24. Figure 28 shows that all measured  $N_{60}$  blowcounts are much larger than the value required to give a safety factor of one, typically by a factor of two or greater.

#### Dynamic Response Analysis and Liquefaction Evaluation of Upstream Slope Profile

##### Inputs to SHAKE

64. The idealized profile used for the SHAKE analysis of the upstream slope is shown in Figure 29. The top nine layers in the profile represent the

compacted decomposed granite embankment and have a combined thickness of 42 ft. The low strain amplitude velocities measured in the geophysical testing program are also listed. All layers were submerged and assigned a saturated unit weight of 142pcf. Other information shown in Figure 29 includes SPT blowcounts (not energy corrected) and data from the index tests performed in the laboratory from samples obtained from US-10 and SS-10. The weathered granite foundation is represented by layer 10.

65. As with the centerline profile, the upstream slope profile was excited by both Accelerograms A and B to determine which induced the stronger response. The design accelerograms were input to SHAKE as rock outcrop motions with a peak acceleration of 0.35 g.

#### Results of SHAKE analysis

66. Figure 30 shows the peak accelerations in the upstream slope profile in response to Record A. The peak base rock acceleration of 0.32 g was amplified to 0.52 g at the surface. This results in a magnification factor of 1.62. Figure 31 shows the peak accelerations induced by Record B. At base-rock the peak acceleration was 0.31 g which was amplified to 0.48 g at the surface for a magnification ratio of 1.55.

67. The effective dynamic shear stresses induced by Records A and B are shown in Figure 32. The plot shows that the stresses induced by both records increase with depth. The stresses induced by Record A are slightly larger than those induced by Record B, therefore the stresses induced by Record A were used in the analysis of liquefaction potential.

#### Evaluation of the liquefaction potential of the upstream slope profile

68. The evaluation of liquefaction potential of the materials in the upstream slope profile was performed in the same way as for the centerline profile. The measured  $N_{60}$  blowcounts from Boring SS-10 (see Figure 11) are compared with the calculated blowcounts required for a safety factor of one in Figure 33. The required  $N_{60}$  blowcounts were computed using the effective dynamic shear stresses induced by Record A in Figure 32. The plot shows that all measured  $N_{60}$  blowcounts from Boring SS-10 are greater than the value required to give a safety factor of one, typically by a factor of about two.

Summary of Liquefaction Evaluation

69. Based on the evaluation of the dynamic response of the center-line and upstream slope profiles and the high penetration resistance of the soil, with average  $(N_{1,60})$  values of 48 to 64 blows/ft, it was concluded that liquefaction of the compacted decomposed granite can not occur. Furthermore, since the field-measured blow counts are much larger than the values required to give a safety factor of one, no significant excess pore-pressures are expected to develop in the embankment if it is subjected to the design ground motions.

## PART VI: PERMANENT DISPLACEMENT ANALYSIS OF DIKE 5

### General

70. A permanent displacement analysis was performed to estimate the displacements that might be expected to occur along potential sliding surfaces during the design earthquake and to determine whether such movements would threaten the integrity of the embankment. The downstream slope, though not submerged, was evaluated as well as the upstream slope because it has steeper slopes than the upstream side. The deformations were determined from yield accelerations, the dynamic response accelerations at different levels in the embankment, and a Newmark sliding block analysis. In the yield accelerations calculations, it was assumed that no significant excess pore pressures would develop in the embankment as a result of the earthquake shaking. Two similar analytical techniques were used to estimate the permanent displacements. These were the Makdisi-Seed and Sarma-Ambrayseys methods. The yield accelerations were calculated using ARCEQS, a slope stability computer program developed by Sarma (1979).

### Computation of Yield Accelerations

#### Inputs to ARCEQS

71. The yield accelerations,  $k_y$ , were calculated using ARCEQS, a slope stability computer program written by Sarma (1979). The yield acceleration is the pseudo-static acceleration applied at the center of gravity of a sliding mass which will reduce the safety factor against sliding to one. The yield accelerations for potential sliding masses at Dike 5 were calculated with the assumption that no significant excess pore pressures would develop as a result of the earthquake shaking. This assumption follows from the results of the liquefaction analysis discussed in Part V.

72. The cross section selected for the ARCEQS calculations is shown in Figure 34. The cross section shows the embankment geometry, the pool level, and the phreatic surface. Dike 5 was modeled as a homogeneous embankment 97 ft high founded on rock. The embankment soil was assigned a unit weight of 127 pcf above and below the phreatic surface. A bilinear failure envelope was used for the shear strength of the compacted decomposed granite as shown in

Figure 35. It was constructed from the envelopes for drained and undrained conditions shown in Figures 17 and 18. The ordinates of the drained and undrained envelopes were reduced by 20 percent to account for any minor pore pressure build-up or reduction of shear strength which might result from the earthquake shaking. However, since the intersection between the reduced drained and undrained envelope is at 20 tsf and since the confining stresses in the 97 ft high embankment are much less than 20 tsf the drained shear strength parameters only were employed in the calculations. The shear strength parameters used for the compacted decomposed granite in the ARCEQS analysis were a cohesion of zero and a friction angle of 32°.

Yield accelerations computed by ARCEQS

73. The critical yield accelerations were determined using a search technique for failure circles tangent to Elevations 460.5, 441.2, 421.8, 402.4, and 383 ft which correspond to dimensionless depth ratios,  $y/h$ , of 20, 40, 60, 80, and 100 percent. Critical yield accelerations and slip circles for each elevation for both the downstream and upstream slopes are shown in Figure 36. All upstream circles emerged from the slope downstream of the centerline and all downstream circles emerged upstream of the centerline. Figure 36 shows that the yield accelerations on the upstream slope decrease with depth and range from 0.287 g to 0.152 g. The downstream slip circles have higher yield accelerations than the corresponding upstream circles. Their values range from 0.326 g to 0.153 g.

Makdisi-Seed Method

74. The Makdisi-Seed technique was used to estimate the amount of Newmark-type sliding that might occur along potential slip surfaces in the embankment. The technique was developed for dams founded directly on rock and is based on the analysis of many dynamic finite element solutions. Permanent displacements are estimated from charts and a knowledge of the embankment's crest acceleration, fundamental period at earthquake induced strain levels, and yield accelerations. The crest acceleration and fundamental period were approximated using a procedure developed by Makdisi-Seed (1979).

Computation of fundamental period and maximum crest acceleration

75. The simplified procedure for computing the fundamental period and maximum crest acceleration can be carried out by hand with an iterative technique in which the solution depends upon the strain dependent soil properties (modulus degradation and damping) and the acceleration response spectra of the input accelerogram (Makdisi and Seed 1979). Figure 37 shows the primary components involved in the procedure.

76. The fundamental period and peak crest acceleration were computed for both accelerograms A and B. The computations are given in Appendix A. The results for the Record A are given below:

Fundamental period:	$T_o = 0.34 \text{ sec}$
Peak crest acceleration:	$\ddot{u}_{\max} = 1.27 \text{ g}$
Effective strain level:	$\gamma = 0.051 \text{ percent}$

The results of the Record B calculations are listed below:

Fundamental period:	$T_o = 0.32 \text{ sec}$
Peak crest acceleration:	$\ddot{u}_{\max} = 1.11 \text{ g}$
Effective strain level:	$\gamma = 0.051 \text{ percent}$

The results show that the effective fundamental periods and peak crest accelerations induced by both records give similar values. The results indicate that Record A will induce a slightly stronger response in the embankment than Record B. These results are consistent with the SHAKE calculations discussed previously in which the dynamic responses of both the centerline and upstream slope profiles were similar for both records.

77. The fundamental period at earthquake induced strain levels obtained by the Makdisi-Seed calculations was checked with the formula for homogeneous embankments founded on rock from Sarma (1979):

$$T_o = 2.61 \times H/V_s \quad (7)$$

where

$H$  = embankment height

$V_s$  = shear wave velocity

According to Figure 21, at the effective shear strain level of about 0.05 percent predicted by the Makdisi-Seed procedure the shear modulus will degrade to about 43 percent of its low strain amplitude value (the modulus before shaking starts). The shear wave velocity degradation factor is equal to the square root of the modulus degradation factor which for Dike 5 is  $(0.43)^{1/2}$  or 0.65. Based on the geophysical tests the average low strain amplitude shear wave velocity in the embankment is 1,225 fps. Therefore the shear wave velocity effective at the earthquake-induced strain levels is about

$$V_s = 0.65 \times 1,225 \text{ fps} = 796 \text{ fps}$$

Substituting  $H = 97 \text{ ft}$  and  $V_s = 796 \text{ fps}$  into Equation 7 gives

$$T_o = 2.61 \times 97 \text{ ft} / 796 \text{ fps} = 0.32 \text{ sec}$$

which is in very good agreement with the values of fundamental period computed with the Makdisi-Seed method.

#### Permanent displacements

78. The Makdisi-Seed method was used to estimate the permanent displacements for the failure masses identified in the analysis of yield accelerations,  $k_y$ , shown in Figure 36. Displacements along upstream and downstream slip circles were calculated for the motions of both accelerograms. Charts used in the displacement analysis are shown in Figure 38. Figure 38a shows a range of normalized maximum accelerations,  $k_{max}/u_{max}$ , versus the normalized depth,  $y/h$ . The average curve was used to determine the relationship between these two normalized parameters. At each of the depths investigated, the earthquake-induced acceleration of the sliding mass,  $k_{max}$ , was determined by multiplying the maximum acceleration ratio obtained from the chart by the peak crest acceleration,  $u_{max}$ . For the calculations involving Record A,  $u_{max}$  was 1.27 g and for Record B,  $u_{max}$  was 1.11 g as determined from the previous section. The permanent displacements for each circle were determined from Figure 38b. This chart displays the variation of displacement,  $U$ , (divided by  $k_{max}$ , the acceleration of gravity g, and the fundamental period

$T_o$ ) versus yield acceleration,  $k_y$  (normalized with respect to  $k_{max}$ ). The ratio  $k_y/k_{max}$  was computed for each sliding mass and the chart was entered on the abscissa at that point. The corresponding displacement term was obtained from the ordinate axis using the curve for Magnitude 6.5 events. The displacement,  $U$  in ft, was calculated by multiplying the chart displacement term by  $k_{max}$ ,  $g$  in  $ft/sec^2$ , and  $T_o$  in seconds. This displacement in turn was multiplied by a factor,  $\alpha$ , of 1.22 which accounts for the direction of the resultant shearing force which comes from the solution of the equation of motion for a sliding block on a plane (Hynes-Griffin and Franklin 1984). The term  $\alpha$  was computed from Equation 7:

$$\alpha = \cos(\beta - \theta - \phi)/\cos \phi \quad (8)$$

where

$\beta$  = angle between the horizontal and the direction of the resultant shear force

$\theta$  = direction of the acceleration, measured from the horizontal

$\phi$  = friction angle between the block and the plane

The  $\beta$  was assigned a value of  $25^\circ$  based on the average direction of shearing resistance of the circles from the ARCEQS computations;  $\theta$  was set to zero since the applied accelerations are horizontal; and  $\phi$  was set to  $37^\circ$  which is the effective friction angle of the compacted decomposed granite.

79. The Makdisi-Seed computations for the upstream slip circles are summarized on Tables 8 and 9 for Records A and B, respectively. Plots of displacement versus elevation are plotted in Figure 39. The plot shows that the displacements associated with Record A are greater than those of Record B at all elevations and that generally the displacement decreases with depth. The maximum potential displacement for upstream circles is 1.76 ft for the slip circle tangent to Elevation 441 ft ( $y/h = 40$  percent).

80. The computations for the set of downstream slip circles are summarized on Tables 10 and 11 for Records A and B, respectively. A plot of displacement versus elevation for both accelerograms is shown in Figure 40. The plot shows that the displacements induced by Record A are greater than those of Record B at all elevations and that the displacements generally decrease with depth. The maximum potential displacement expected for the downstream set of circles is 1.11 ft for the circle tangent to Elevation 461 ft ( $y/h = 20$  percent).

81. Comparison of the data in Figures 39 and 40 shows that the Makdisi-Seed method predicts that the displacements along potential failure circles will be larger on the upstream side than on the downstream side. This result was to be expected since the yield accelerations on the upstream side are lower than those at corresponding elevations on the downstream side. The overall results indicate that the displacements will be less than 2 ft, and that the amount of displacement of deep-seated potential failure surfaces will be less than 0.4 ft.

#### Sarma-Ambrayseys Method

82. The second method used to estimate the displacements along potential failure surfaces in Dike 5 was the Sarma-Ambrayseys technique. The results of yield acceleration, sliding block, and dynamic response analyses are required inputs to this method. The yield accelerations and slip circles used in the analysis were computed with ARCEQS as discussed earlier and presented in Figure 36.

#### Newmark sliding block analysis

83. Newmark sliding block displacements computed for various values of N/A for Accelerograms A and B are shown in Figure 41. The term N/A is the ratio of yield acceleration,  $k_y$ , to the acceleration of the sliding mass,  $k_{max}$ . The curves for each accelerogram were obtained by computing the displacements for various values of N/A by numerical integration of the equations of motion for a block sliding on an inclined plane. The displacement curves were computed for a magnification factor of one. The results show that Accelerogram A will give higher displacements for all values of N/A than will Accelerogram B.

#### Dynamic response analysis using SEISCOE

84. The computer program SEISCOE, developed by Sarma (1979), was used to calculate the dynamic response for the Sarma-Ambrayseys displacement analysis of Dike 5. The dynamic response was needed to estimate the seismic coefficients or ground motion amplification factors for potential failure masses within the embankment. The program SEISCOE solves the equations of motion (wave equation) using a one-dimensional shear beam approach. Embankment and foundation soils are treated as linear elastic materials possessing viscous

damping. In SEISCOE, Dike 5 was modeled as a triangular-shaped homogeneous wedged founded directly on rock as shown in Figure 42. The embankment material was assigned a shear wave velocity of 1,225 fps, a density of 127 pcf, and a damping ratio of 9 percent. The velocity reflects the average of the measurements made in the geophysical investigation and the damping ratio was selected based on the strain compatible damping computed with SHAKE.

85. The results of the SEISCOE calculations are shown in Figure 43. Amplification factors are plotted versus a range of fundamental periods for failure wedges tangent to depth ratios,  $y/h$ , of 20, 40, 60, 80, and 100 percent. The amplification factors for Records A and B are given by the plots on the upper and lower portions of Figure 43, respectively. The proper amplification factors for potential failure wedges at various levels in the embankment are dependent upon the embankment's fundamental period. The fundamental period of the embankment was determined to be about 0.33 sec for either accelerogram based on the Makdisi-Seed calculations. The amplification factors for Records A and B were determined by entering the respective charts on Figure 43 at 0.33 sec. The amplification factors pertaining to each Record are listed in Table 12. The tabulated values show that the amplifications decrease with depth for both Records A and B. The table also indicates that Record A induces a slightly stronger response since its amplifications are slightly greater than those of Record B.

#### Permanent displacements

86. The displacements were computed using the results of the yield accelerations, sliding block, and the dynamic response analyses. The same slip circles were analyzed as in the Makdisi-Seed analysis at  $y/h$  levels of 20, 40, 60, 80, and 100 percent. The displacement for each was calculated using the following procedure. The earthquake-induced acceleration of the sliding mass,  $k_{max}$ , was estimated as the product of the base motion, taken to be 0.35 g, and the SEISCOE magnification factor listed in Table 9. The Newmark sliding block displacement for a magnification factor of one is determined by entering Figure 41 at the appropriate value of N/A. The ratio N/A is the ratio of yield acceleration,  $k_y$ , to  $k_{max}$ . This displacement is then multiplied by the SEISCOE magnification factor to account for the increased displacement resulting from the amplified ground motion. This displacement is in turn multiplied by a (defined in Equation 7) to determine the field displacement. As discussed earlier in the section on the Makdisi-Seed

calculations, the factor  $\alpha$  accounts for the direction of the resultant of the shearing resistance acting on the surface of sliding. As before  $\alpha$  was set equal to 1.22.

87. The Sarma-Ambrayseys calculations for the slip circles on the upstream slope are summarized in Tables 13 and 14 for Records A and B. The displacements are also plotted in Figure 44. The figure shows that the displacements for Record A are larger than those for Record B for all circles at corresponding tangent elevations. The maximum computed potential displacement was 2.31 ft. This displacement occurs at a  $y/h$  level of 40 percent which is for the failure surface tangent to Elevation 456 ft.

88. The calculations for the downstream set of circles are summarized in Tables 15 and 16 for Records A and B, respectively. The displacements for both accelerograms are plotted in Figure 45. Again, the displacements for Record A are larger than those for Record B along all corresponding failure surfaces. The maximum displacement was computed to be 1.25 ft and occurs at a  $y/h$  of 20 percent which is for the failure circle tangent to Elevation 468 ft. Generally, the displacements decrease with increasing depth within the embankment.

89. Due to the lower yield accelerations of the upstream failure masses, comparison of the results of the analysis on Figures 44 and 45 indicates that the potential displacements on the upstream side are somewhat greater than those on the downstream side. The maximum estimated displacement of 2.31 ft predicted by the Sarma-Ambrayseys is in fairly good agreement with the displacement of 1.76 ft predicted by the Makdisi-Seed method.

90. The displacements computed by the Makdisi-Seed and Sarma-Ambrayseys methods represent very conservative estimates of the displacements expected in a well compacted embankment such as Dike 5. These estimates are the outcome of the conservatively selected shear strength parameters ( $c = 0$ ,  $\phi = 32^\circ$ ) used in the stability analysis for determining the yield accelerations. Since earthquake induced excess pore pressures are not expected to occur, the use of drained shear strengths and their reduction by 20 percent are very conservative choices which lead to low estimates of yield acceleration and large permanent displacements. Thus, a second set of Makdisi-Seed calculations were performed to provide a more realistic and less conservative estimate of the permanent displacements. Displacements were determined for circles tangent to the 40 and 100 percent (base) levels in the upstream portion of the

embankment. Yield accelerations were determined using a shear strength envelope situated approximately midway between the drained and undrained strength envelopes shown on Figures 17 and 18. This resulted in shear strength parameters with a cohesion intercept of 2.0 tsf and a friction angle of 31°. Yield accelerations were computed to be 1.88 g and 0.97 g at the 40 and 100 percent levels, respectively. The calculations are summarized in Table 17. The calculations result in no displacement for both circles. Since Dike 5 is a very well constructed embankment very small displacements are considered to be a realistic prediction of its field performance due to the design ground motions.

## PART VII: SUMMARY AND CONCLUSIONS

91. This report documents the seismic stability evaluation of Dike 5 and the other seven saddle dikes at the Folsom Project. The investigation included a detailed review of construction records, field investigations, laboratory testing, and analytical studies aimed at evaluating the potential for liquefaction in the embankment soils and permanent displacements in the embankment. The design earthquake selected for the site was a Magnitude 6.5 event with a peak acceleration of 0.35 g, a peak velocity of 20 cm/sec and a bracketed duration of about 16 sec.

92. Review of construction records revealed that the total crest length of the eight saddle dikes is 10,887 ft. Each embankment is founded directly on bedrock, is essentially homogeneous in cross section, and is constructed of a compacted decomposed-granite saprolite. The material classifies as a Silty Sand (SM), and has a gravel content of about 10 percent, a sand content of 65 percent, and a fines content of about 25 percent. Compaction requirements were similar for each of the eight embankments. Dike 5 was determined to be the most critical dike, and was selected for detailed analysis because it is the tallest (maximum height of about 110 ft) and the most likely to have water on the upstream slope and saturated zones within its interior. Dike 5 is typical of the sections for all the dikes.

93. Field investigations were performed at Dike 5 to obtain data relevant to the seismic analysis. The field investigations included Standard Penetration Tests (SPT), undisturbed soil sampling, and geophysical testing. The SPT measurements and undisturbed sampling were performed at the centerline and on the downstream slope of the embankment near Station 180+50. The average of the  $(N_1)_{60}$  blowcounts from the SPT measurements performed in the compacted decomposed granite was about 64 blows/ft at the centerline and 48 blows/ft in the downstream slope. These blowcounts were used to determine the cyclic strength of the embankment soil. Undisturbed samples were tested in the laboratory to determine the drained and undrained shear strength parameters for the permanent displacement analysis. Geophysical studies were used to measure the shear wave velocities in the foundation and embankment for the dynamic response analysis.

94. An evaluation of the liquefaction potential of the embankment soils was performed using the Seed-Idriss field-performance-based procedure which

relates SPT blowcounts to the cyclic strength the soil. The dynamic response of the embankment was evaluated using two one-dimensional soil profiles and the wave propagation code, SHAKE. The results indicate that the embankment has sufficient cyclic strength to preclude any possibility of liquefaction. Typically, the blowcounts measured in the field exceeded by a factor of two the values needed for a safety factor against liquefaction of unity. Also, due to its high penetration resistance, no significant excess pore pressures are expected to develop in the compacted decomposed granite embankment as a result of the design earthquake.

95. A permanent displacement analysis was performed to evaluate the seismic stability of Dike 5. Two similar approaches based on the Newmark sliding block approach were used to estimate the displacements along potential sliding masses in the upstream and downstream portions of the embankment as a consequence of the earthquake shaking. The approaches selected were the Makdisi-Seed and the Sarma-Ambrayseys methods. The results obtained from both were in good agreement. The maximum potential displacements are expected on the upstream side and will be less than 2.5 ft in magnitude. This estimate is conservative since it was made using conservatively selected shear strength parameters. Even so, this amount of displacement is not considered excessive and should not effect the embankments ability to impound the pool. Since the embankment is constructed of well compacted material the expected field displacements will probably be very small and will not exceed more than a few inches.

96. Based on the foregoing analysis, Dike 5 is expected to perform well during and after the design earthquake. This conclusion also applies for the other seven dikes of the Folsom Project since they are lower than Dike 5, and since their embankment materials and foundation conditions are similar to those of Dike 5, and since they are typically dry and are not likely to have saturated zones during the design earthquake. Remedial measures are not recommended for any of the eight dikes at the Folsom Project.

## REFERENCES

Ballard, R. F., Jr. 1964. "Determination of Soil Shear Moduli at Depths by In Situ Vibratory Techniques," Miscellaneous Paper No. 4-691, US Army Engineer Waterways Experiment Station, CE, Vicksburg, MS.

Bolt, B. A. and Seed, H. B. 1983. "Accelerogram Selection Report for Folsom Dam Project, California." Contract Report DACW 05-83-Q-0205, US Army Engineer District, Sacramento, CA.

Hynes-Griffin, M. E. 1979. "Dynamic Analyses of Earth Embankments for Richard B. Russell Dam and Lake Project," Final report prepared for US Army Engineer District, Savannah, GA.

Hynes-Griffin, M. E. and Franklin, A. G. 1984. "Rationalizing the Seismic Coefficient," Miscellaneous Paper GL-84-13, US Army Engineer Waterways Experiment Station, Vicksburg, MS.

Kiersch, G. A., and Treasher, R. C. 1955. "Investigations, Areal and Engineering Geology - Folsom Dam Project, Central California," Economic Geology, Vol 50, No. 3, pp 271-310.

Llopis, J. L. 1983. "Preliminary Results of an In-Situ Seismic Investigation of Folsom Dam, California." Draft Letter Report to US Army Engineer District (CESPK-ED-F), Sacramento, California, from US Army Engineer Waterways Experiment station (CEWES-GH-I), Vicksburg, MS.

. 1984. "Preliminary Results of In Situ Surface Vibratory Tests of Folsom Dam, California." Letter Report to Commander, US Army Engineer District (CESPK-ED-F), Sacramento, California, from US Army Engineer Waterways Experiment Station (CEWES-GH-I), Vicksburg, MS.

Makdisi, F. I., and Seed, H. B. 1979. "A Simplified Procedure for Computing Maximum Crest Acceleration and Natural Period for Embankments," Journal of the Geotechnical Engineering Division, American Society of Civil Engineers, Vol 104, NS-T7.

. 1979. "Simplified Procedure for Estimating Dam and Embankment Deformations," Journal of the Geotechnical Engineering Division, American Society of Civil Engineers, Vol 104, No. GT7, pp 849-867.

Newmark, N. M. 1965. "Effects of Earthquakes on Dams and Embankments," Geotechnique, Vol 15, No. 2, pp 139-160.

Sarma, S. K. 1979. "Response and Stability of Earth Dams During Strong Earthquakes." Miscellaneous Paper GL-79-13, US Army Engineer Waterways Experiment Station, CE, Vicksburg, MS.

Schnabel, P. B., Lysmer, J., and Seed, H. B. 1972. "SHAKE, A Computer Program for Earthquake Response Analysis of Horizontally Layered Sites," Report No. EERC 72-12, Earthquake Engineering Research Center, College of Engineering, University of California, Berkeley, CA.

Seed, H. B. 1979. "19th Rankine Lecture: Considerations in the Earthquake Resistant Design of Earth and Rockfill Dams," Geotechnique, Vol 29, No. 3, pp 215-263.

Seed, H. B., and Idriss, I. M., 1970. "Soil Moduli and Damping Factors for Dynamic Response Analyses." Report No. EERC 70-10. Earthquake Engineering Research Center, University of California, Berkeley, CA.

Seed, H. B., Idriss, I. M., and Arango, I. 1983. "Evaluation of Liquefaction Potential Using Field Performance Data," Journal of the Geotechnical Engineering Division, American Society of Civil Engineers, Vol 109, No. GT3, pp 458-482.

Seed, H. B. and Peacock, W. H. 1971. "Test Procedures for Measuring Soil Liquefaction Characteristics," Journal of the Soil Mechanics and Foundations Division, American Society of Civil Engineers, Vol 97, No. SM8, pp 1099-1119.

Seed, H. B., Tokimatsu, K., Harder, L. F., and Chung, R. M. 1984. "The Influence of SPT Procedures in Soil Liquefaction Resistance Evaluations," UCB/EERC Report No. 84/15, University of California, Berkeley, CA.

Seed, H. B., Wong, R. T., Idriss, I. M., and Tokimatsu, K. 1984. "Moduli and Damping Factors for Dynamic Analyses of Cohesionless Soils." Report No. EERC 84-14. Earthquake Engineering Research Center, University of California, Berkeley, CA.

Tierra Engineering Consultants, Inc. 1983. "Geologic and Seismologic Investigations of the Folsom, California Area." Contract Report DACW 05-82-C-0042, US Army Engineer District, Sacramento, CA.

US Army Engineer District, Sacramento. 1950. "Part IV: Dam and Appurte-  
nances, Appendix C, Soils Date and Embankment Design," American River,  
California Folsom Project, Vols 1 and 2, Sacramento, CA.

\_\_\_\_\_. 1953. "Foundation Report, Dike 5, American River, California,  
Folsom Project," Sacramento, CA.

\_\_\_\_\_. 1954. "Foundation Report, Dikes 1, 2, 3, 4, and 6, American  
River, California, Folsom Project," Sacramento, CA.

\_\_\_\_\_. 1955. "Foundation Report, Dike 7, American River California,  
Folsom Project," Sacramento, CA.

US Army Engineer Laboratory, South Pacific Division. 1986. "Report of Soil  
tests, Folsom Dam Laboratory Program," Sausalito, CA.

Table 1  
Crest Lengths and Maximum Heights of the Eight Saddle  
 Dikes on the Folsom Project

<u>Dike</u>	<u>Crest Length, ft</u>	<u>Maximum Height, ft</u>
1	1,980	26.5
2	1,765	17.5
3	1,100	14.5
4	1,325	20.5
5	1,920	110.0
6	1,418	48.5
7	740	55.0
8	<u>639</u>	18.5
<b>Total</b>	<b>10,887</b>	

Table 2  
Placement Requirements for Embankment Materials of  
Dikes 1, 2, 3, 4, 5, 6, 7, and 8

<u>Zones</u>	<u>Source</u>	<u>Equipment</u>	<u>No. of Passes or Coverages</u>	<u>Maximum Lift Thickness</u>
C	Borrow area No. 2	Sheepsfoot roller	12	12
		Pneumatic-tired roller	6	18
D	Borrow area No. 2	Sheepsfoot roller	8	12
		Pneumatic-tired roller	4	18
G	Borrow area No. 1	Sheepsfoot roller	12	12
		Pneumatic-tired roller	6	18
H	Borrow area No. 1	Sheepsfoot roller	8	12
		Pneumatic-tired roller	4	18
Dikes 1, 2, 3, 4, and 6	Borrow area No. 4	42-kip sheepsfoot roller	In core trench	
			15	8
			Outside core trench	
			10	8
Minus 2 in. sand and gravel drain	5A	D-8 Caterpillar	12*	12

\* Specification requires 3 complete coverages. It was assumed that 3 complete coverages correspond to 12 passes with a D-8 caterpillar tractor.

**Table 3**  
**Dry Densities Obtained During Construction from Record**  
**Samples of the Eight Dikes at the Folsom Project**

Dike No.	Average Dry Density (pcf)			Remarks
	Inside Core Trench	Outside Core Trench	Other Zones	
1	125	123	--	--
2	124	124	--	--
3	125	123	--	--
4	122	123	--	--
5	--	--	130	Zone C (3 samples)
5	--	--	125	Zone D (4 samples)
6	124	122	--	--
7	--	--	130	Zone G (3 samples)
7	--	--	--	Zone H (no samples)
8	--	--	136	Zone H (1 sample)

Note: Densities for Dikes 1, 2, 3, 4, and 6 were obtained from Condition Report for these dikes.  
 Densities for Dikes 5, 7, and 8 were obtained from Report of Soil Tests or Record Samples.

**Table 4**  
**Gradation and Atterberg Limits of Decomposed Granite in**  
**Borrow Areas 1, 2, and 4 Used in Construction of**  
**the Eight Dikes at the Folsom Project**

Borrow Area	Dike	Gradation			Atterburg Limits	
		% Gravel	% Sand	% Fines	LL	PI
1	7,8	10	60	30	25	5
2	5	7	65	28	25	3
4	1,2,3,4,5	10	65	25	--	NP

Table 5  
Summary of Classification Tests Performed on Samples Taken  
from Borings on Centerline (US-1 and SS-1)

<u>Hole</u>	<u>Depth ft</u>	<u>Description</u>	<u>Classification</u>	<u>D<sub>50</sub> mm</u>	<u>Percent Passing No. 200</u>	<u>LL Percent</u>	<u>PI Percent</u>
SS-1	6.0	Silty clayey sand	SP-SC	0.25	12	32	10
SS-1	16.0	Clayey sand	SM-SC	0.60	17	26	6
SS-1	25.5	Silty sand	SM	0.60	13	22	2
SS-1	35.0	Silty sand	SM	0.75	15	20	1
SS-1	46.0	Silty sand	SM	0.48	20	23	2
SS-1	56.0	Silty sand	SM	0.48	24	24	2
SS-1	65.0	Silty sand	SM	0.62	15	22	1
SS-1	76.0	Silty sand	SM	0.38	27	20	1
SS-1	85.0	Clayey sand	SM-SC	0.40	21	24	4
SS-1	96.0	Silty sand	SM	0.42	21	23	1
US-1	51.0	Clayey sand	SC	0.55	19	35	14
				0.50	18	25	4

**Table 6**  
**Summary of Classification Tests Performed on Samples Taken**  
**From Downstream Slope Borings (US-10)**

<u>Hole</u>	<u>Depth ft</u>	<u>Description</u>	<u>Classification</u>	<u>D<sub>50</sub> mm</u>	<u>Percent Passing No. 200</u>	<u>LL Percent</u>	<u>PI Percent</u>
US-10	7.0	Silty sand	SM	0.44	21	19	1
US-10	10.0	Clayey sand	SC	0.75	12	29	9
US-10	11.0	Clayey sand	SC	0.33	25	29	9
US-10	12.3	Silty sand	SM	0.75	15	22	1
US-10	16.7	Silty sand	SM	0.65	16	23	2
US-10	22.1	Silty sand	SM	0.61	13	22	2
US-10	27.1	Silty sand	SM	0.74	12	23	2
US-10	36.1	Clayey sand	SM-SC	0.65	12	25	4
US-10	32.0	--	--	<u>1.1</u>	<u>11</u>	--	--
			<b>Averages</b>	<b>0.67</b>	<b>15</b>	<b>24</b>	<b>4</b>

**Table 7**  
**Shear Strength Parameters for Compacted**  
**Decomposed Granite**

<u>Drainage Conditions</u>	<u>Cohesion Intercept tsf</u>	<u>Friction Angle ϕ°</u>
Undrained	4.06	30.6
Drained	0.0	38.0

Table 8  
Makdisi-Seed Method Dike 5 Permanent Displacement Analysis  
Upstream Slip Circles Record A

Y/H	$\ddot{u}_{\text{max}}$	Crest	$k_y$	$k_{\text{max}} /$	$k_{\text{max}}$	$k_y /$	$U/k_{\text{max}}$	U	$\alpha$	$U \times \alpha$
	g			$\ddot{u}_{\text{max}}$		g	$\times g \times T_o$			
20.00	1.27	0.287	0.88	1.12	0.26	0.09	0.09	1.09	1.22	1.33
40.00	1.27	0.191	0.70	0.89	0.21	0.15	0.15	1.44	1.22	1.76
60.00	1.27	0.176	0.52	0.66	0.27	0.08	0.08	0.57	1.22	0.70
80.00	1.27	0.162	0.41	0.52	0.31	0.07	0.07	0.37	1.22	0.45
100.00	1.27	0.152	0.34	0.43	0.35	0.06	0.06	0.26	1.22	0.31

$T_o = 0.336 \text{ sec.}$

$\ddot{u}_{\text{max}} = 1.27 \text{ g.}$

Table 9  
Makdisi-Seed Method Dike 5F Upstream Slip Circles Record B

Y/H	$\ddot{u}_{\text{max}}$	Crest	$k_y$	$k_{\text{max}} /$	$k_{\text{max}}$	$k_y /$	$U/k_{\text{max}}$	U	$\alpha$	$U \times \alpha$
	g			$\ddot{u}_{\text{max}}$		g	$\times g \times T_o$			
20.00	1.11	0.287	0.88	0.98	0.29	0.08	0.08	0.82	1.22	1.00
40.00	1.11	0.191	0.70	0.78	0.25	0.19	0.19	0.73	1.22	0.88
60.00	1.11	0.176	0.52	0.58	0.30	0.07	0.07	0.42	1.22	0.51
80.00	1.11	0.162	0.41	0.46	0.36	0.05	0.05	0.25	1.22	0.30
100.00	1.11	0.152	0.34	0.38	0.40	0.04	0.04	0.16	1.22	0.19

$T_o = 0.322 \text{ sec.}$

$\ddot{u}_{\text{max}} \text{ crest} = 1.11 \text{ g.}$

Table 10  
Makdisi-Seed Method Dike 5 Permanent Displacement Analysis  
Downstream Slip Circles Record A

$\frac{Y}{H}$	$\frac{\ddot{u}_{max}}{g}$ Crest	$\frac{k_y}{g}$	$\frac{k_{max}}{\ddot{u}_{max}}$	$\frac{k_{max}}{g}$	$\frac{k_y}{k_{max}}$	$\frac{U/k_{max}}{\times g \times T_o}$ sec	$U$ ft	$\alpha$	$U \times \alpha$ ft
20.00	1.27	0.326	0.88	1.12	0.29	0.08	0.91	1.22	1.11
40.00	1.27	0.245	0.70	0.89	0.28	0.08	0.77	1.22	0.94
60.00	1.27	0.215	0.52	0.66	0.33	0.06	0.43	1.22	0.52
80.00	1.27	0.192	0.41	0.52	0.37	0.05	0.27	1.22	0.45
100.00	1.27	0.153	0.34	0.43	0.35	0.06	0.26	1.22	0.31

$T_o = 0.366$  sec.

$\ddot{u}_{max}$  crest = 1.77 g.

Table 11  
Makdisi-Seed Method Dike 5 Downstream Slip Circles Record B

$\frac{Y}{H}$	$\frac{\ddot{u}_{max}}{g}$ Crest	$\frac{k_y}{g}$	$\frac{k_{max}}{\ddot{u}_{max}}$	$\frac{k_{max}}{g}$	$\frac{k_y}{k_{max}}$	$\frac{U/k_{max}}{\times g \times T_o}$ sec	$U$ ft	$\alpha$	$U \times \alpha$ ft
20.00	1.11	0.326	0.88	0.98	0.33	0.06	0.61	1.22	0.74
40.00	1.11	0.245	0.70	0.78	0.32	0.07	0.52	1.22	0.64
60.00	1.11	0.215	0.52	0.58	0.37	0.05	0.29	1.22	0.35
80.00	1.11	0.192	0.41	0.46	0.42	0.04	0.17	1.22	0.21
100.00	1.11	0.153	0.34	0.38	0.41	0.04	0.15	1.22	0.18

$T_o = 0.322$  sec.

$\ddot{u}_{max}$  crest = 1.11 g.

Table 12  
Amplification Factors Computed with SEISCOE from  
Records A and B for Dike 5

Y/H <u>Percent</u>	Amplification Factors For	
	Record <u>A</u>	Record <u>B</u>
20	3.9	3.6
40	3.2	3.0
60	2.7	2.3
80	2.4	2.4
100	1.9	1.8

Table 13  
 Permanent Displacements Computed with Sarma-Ambrayseys  
 Method for Dike 5, Upstream Slopes, Record A

Elevation ft	Y/H	a (rock) g	Magnifi- cation factor, M	A( $k_{max}$ ) g	N( $k_y$ ) N/A	Chart		Computed Field Displacement	
						U cm	U x (m) cm	U x a x M cm	U x a x M ft
468.00	20	0.35	3.90	1.37	0.287	0.21	10.00	39.00	1.22
456.00	40	0.35	3.20	1.12	0.191	0.17	18.00	57.60	1.22
444.00	60	0.35	2.70	0.95	0.176	0.19	16.00	43.20	1.22
432.00	80	0.35	2.40	0.84	0.162	0.19	12.00	28.80	1.22
420.00	100	0.35	1.90	0.67	0.152	0.23	9.00	17.20	1.22
								20.86	0.68

\* Obtained from chart in Figure 41.

Table 14

Permanent Displacements Computed with Sarma-Ambreysey's  
Methods for Dike 5, Upstream Slopes, Record B

Elevation ft	Y/H	a (rock) g	Magnifi- cation factor, M	A (k <sub>max</sub> ) g	N (k <sub>y</sub> )	N/A	U cm	U x (m) cm	a cm	Computed Field Displacements	
										U x a x M	U x a x M
468.00	20	0.35	3.60	1.26	0.287	0.23	4.60	16.56	1.22	20.20	0.66
456.00	40	0.35	3.00	1.05	0.191	0.18	6.60	19.80	1.22	24.16	0.79
444.00	60	0.35	2.30	0.81	0.176	0.22	4.80	11.04	1.22	13.47	0.44
432.00	80	0.35	2.40	0.84	0.162	0.19	6.40	15.36	1.22	18.74	0.61
420.00	100	0.35	1.80	0.63	0.152	0.24	4.00	7.20	1.22	8.86	0.66

Table 15

Permanent Displacements Computed with Sarma-Ambrayses  
Method for Dike 5, Downstream Slopes, Record A

Elevation ft	$\frac{Y/H}{g}$	$\frac{a}{(rock)}$	Magnifi- cation factor, $M$	$A(k_{max})$	$\frac{N(k_y)}{g}$	$\frac{N/A}{cm}$	$U$ $\frac{cm}{cm}$	$U \times (m)$ $\frac{cm}{cm}$	$\frac{\alpha}{cm}$	Computed Field Displacements	
										$\frac{U \times \alpha \times M}{cm}$	$\frac{U \times \alpha \times M}{ft}$
468.00	20	0.35	3.90	1.37	0.326	0.24	8.00	31.20	1.22	38.06	1.25
456.00	40	0.35	3.20	1.12	0.245	0.22	8.80	28.16	1.22	34.36	1.13
444.00	60	0.35	2.70	0.95	0.215	0.23	8.60	23.22	1.22	28.33	0.93
432.00	80	0.35	2.40	0.84	0.192	0.23	8.60	20.64	1.22	25.18	0.83
420.00	100	0.35	1.90	0.67	0.153	0.23	8.60	16.34	1.22	19.93	0.65

Table 16

Permanent Displacements Computed with Sarma-Ambrayses  
Method for Dike 5, Downstream Slope, Record B

Elevation ft	$\frac{Y}{H}$	$\frac{a \text{ (rock)}}{g}$	Magnifi- cation factor, M	$\frac{A(k_{\max})}{g}$	$\frac{N(k_y)}{N/A}$	Computed Field Displacements		
						$\frac{U}{cm}$	$\frac{U \times (m)}{cm}$	$\frac{a}{ft}$
468.00	20	0.35	3.60	1.26	0.326	0.26	3.70	13.32
456.00	40	0.35	3.00	1.05	0.245	0.23	4.40	13.20
444.00	60	0.35	2.30	0.81	0.215	0.27	3.20	7.36
432.00	80	0.35	2.40	0.84	0.192	0.23	4.40	10.56
420.00	100	0.35	1.80	0.63	0.153	0.24	4.00	7.20

Table 17

Makdisi-Seed Method Dike 5 Permanent Displacement Analysis for  
Upstream Slip Circles Computed Using Record A and Shear  
Strengths Midway Between the Drained and Undrained  
Envelopes for Compacted Decomposed Granite

Y/H	$\frac{\dot{u}_{max}}{g}$		$\frac{k_{max}}{\dot{u}_{max}}$		$\frac{k_y}{g}$		$\frac{U/k_{max}}{g \times T_o}$		U ft	$\alpha$	$U \times \alpha$ ft
	Crest	g	g	$\dot{u}_{max}$	g	$k_{max}$	sec				
40.00	1.27	1.88	0.70	0.89	2.11	~ 0	~ 0	0	1.22	0	0
100.00	1.27	0.97	0.34	0.43	2.25	~ 0	~ 0	0	1.22	0	0

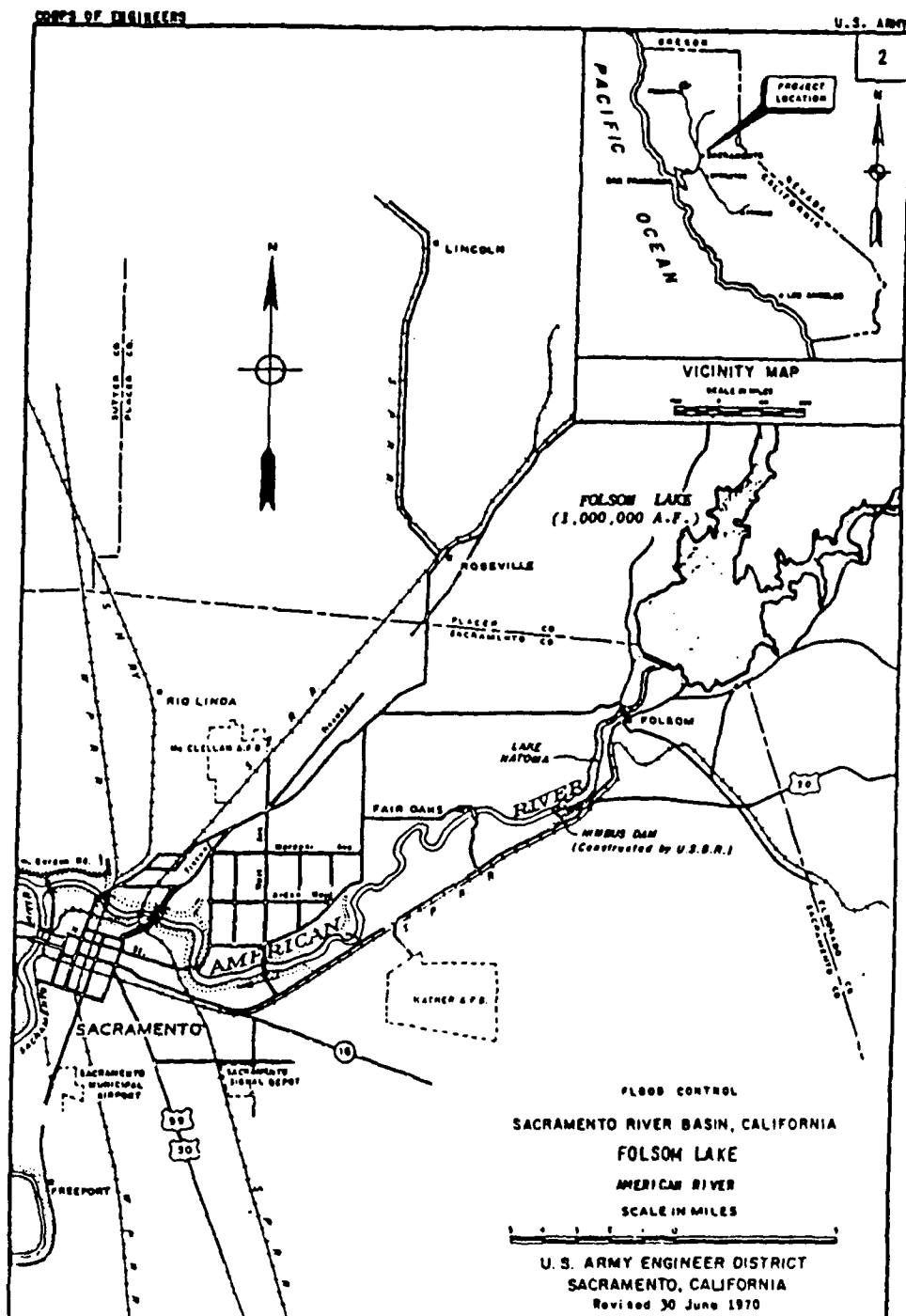
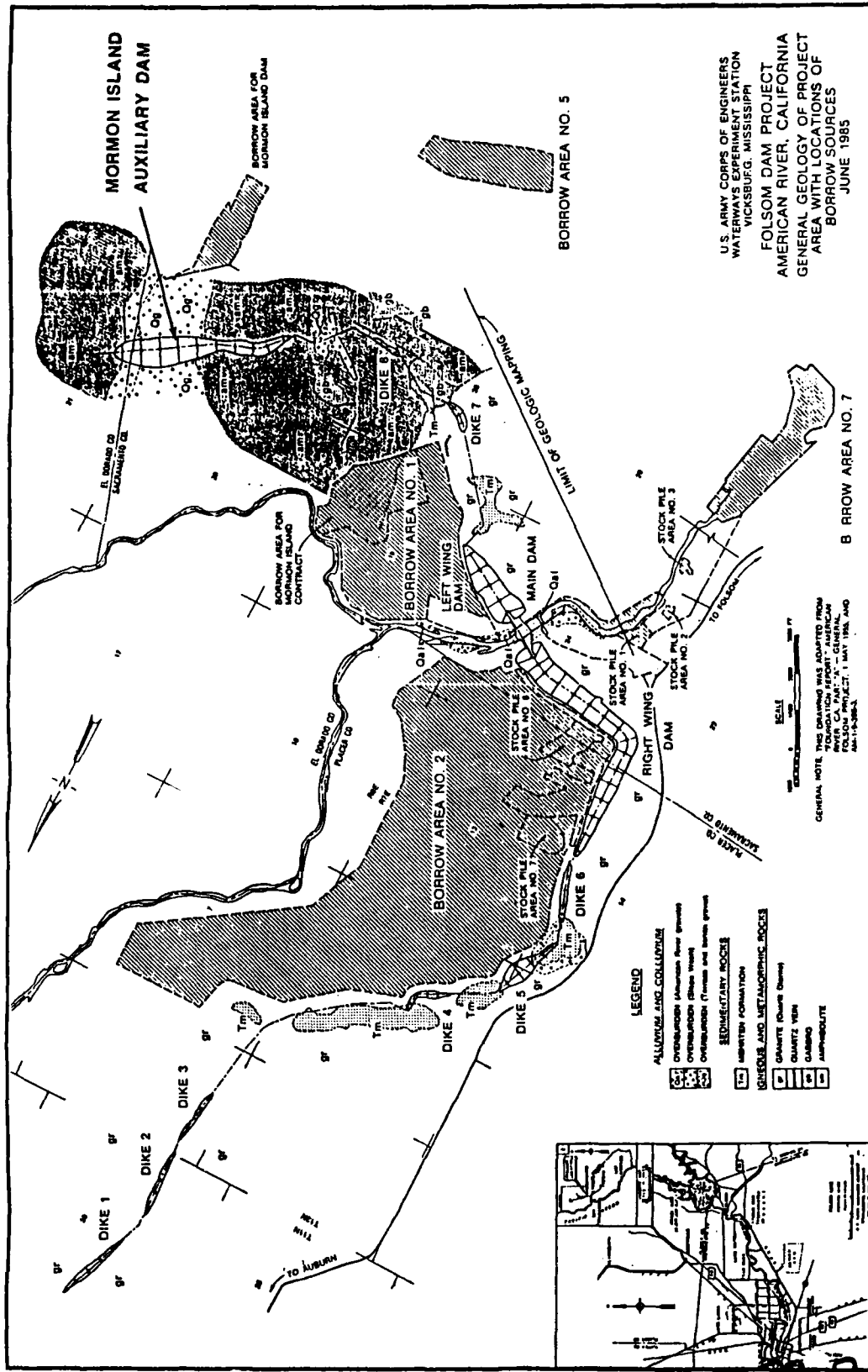


Figure 1. Location of the Folsom Dam and Reservoir Project.



**Figure 2. Plan of the man-made water retaining structures at the Folsom Dam Project.**

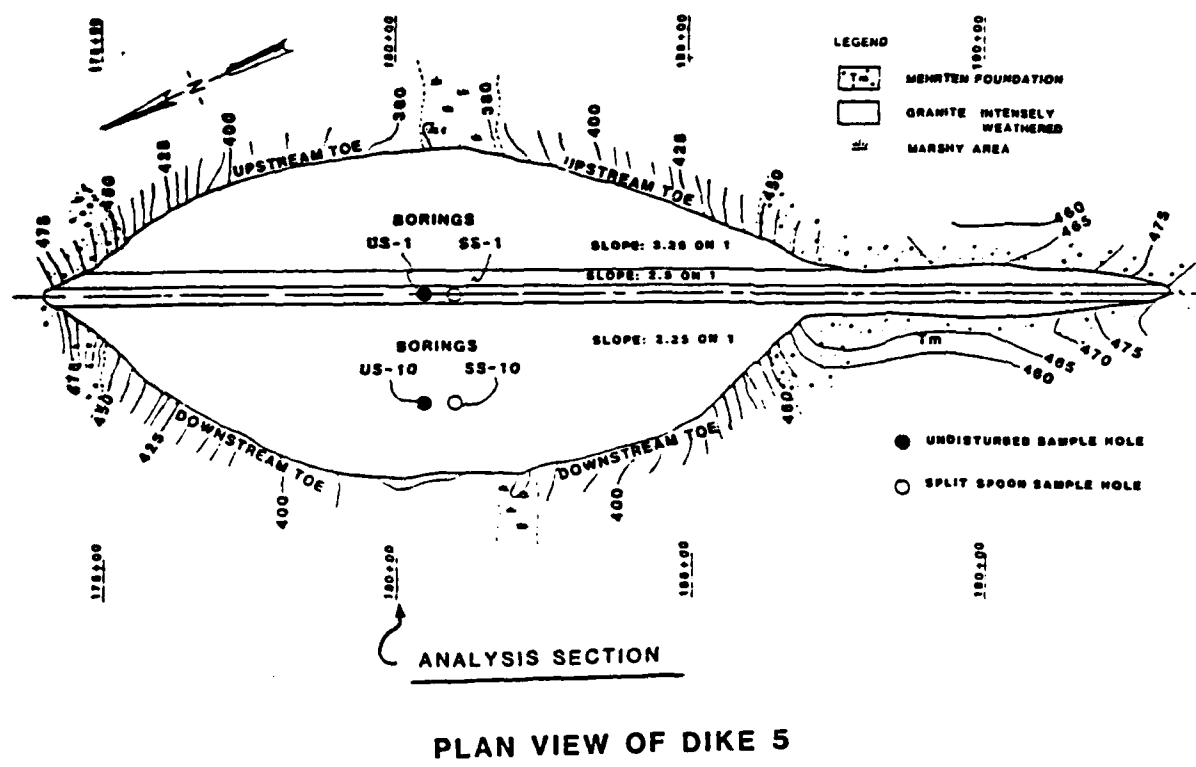
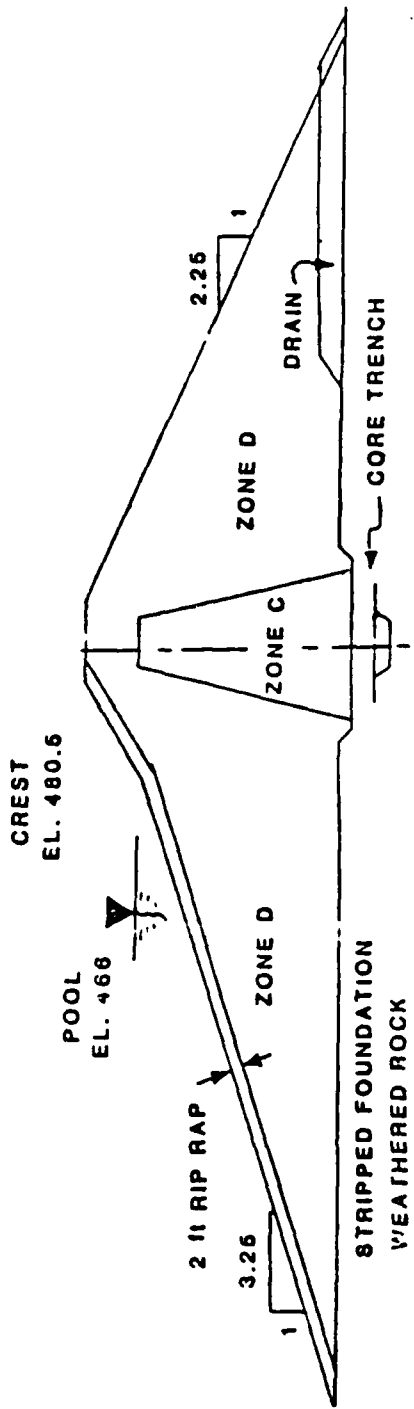


Figure 3. Plan view of Dike 5.



DIKE 5 - TYPICAL SECTION

Material descriptions

Zone C - Decomposed granite from Borrow Area No. 2 and suitable fine-grained material from American river channel

Zone D - Decomposed granite from Borrow Area No. 2 - practically the same as material in Zone C.

Figure 4a. Cross-sectional view of Dike 5.

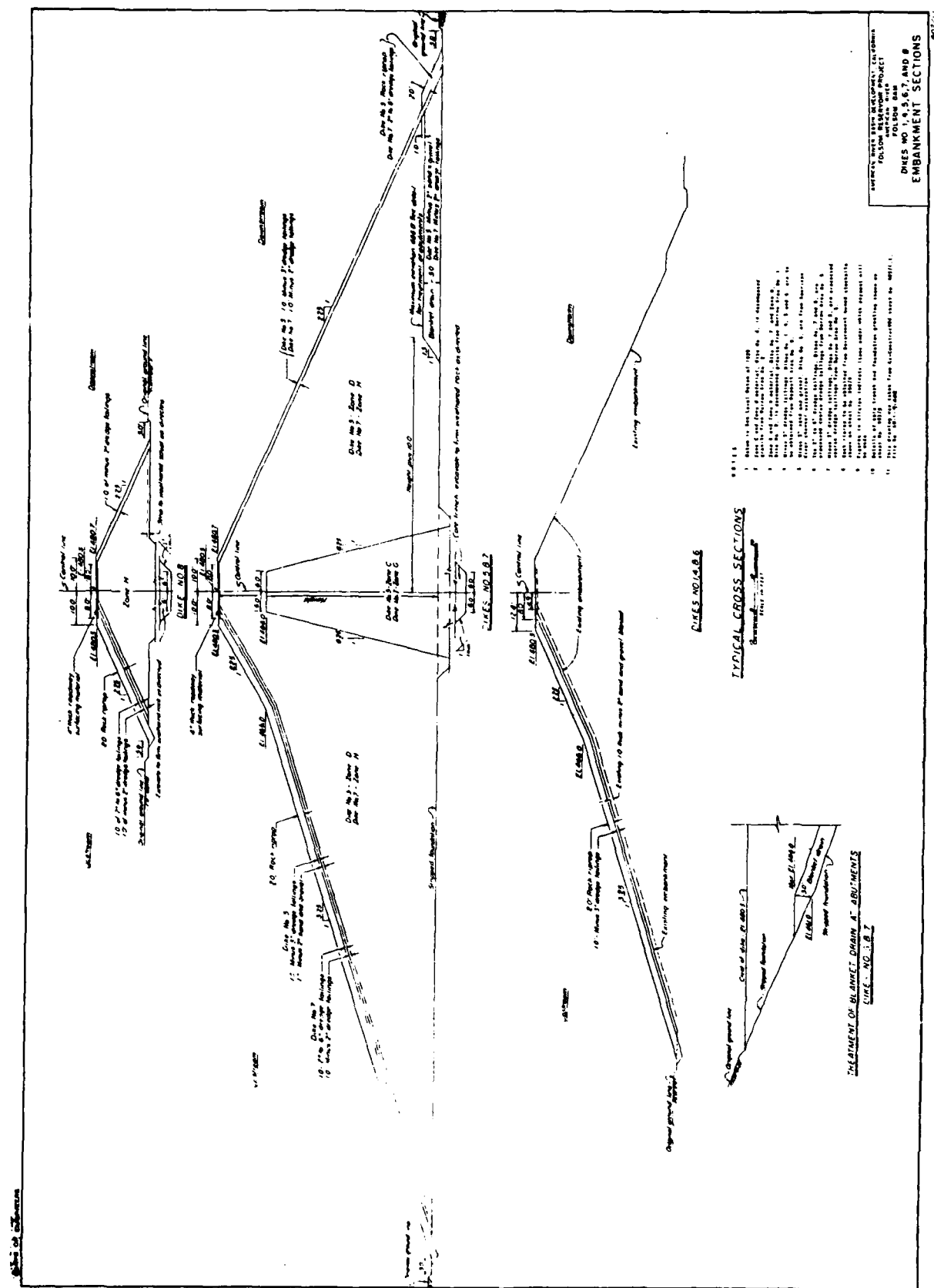


Figure 4b. Typical crosssections of Dikes 1, 4, 5, 6, 7, and 8.

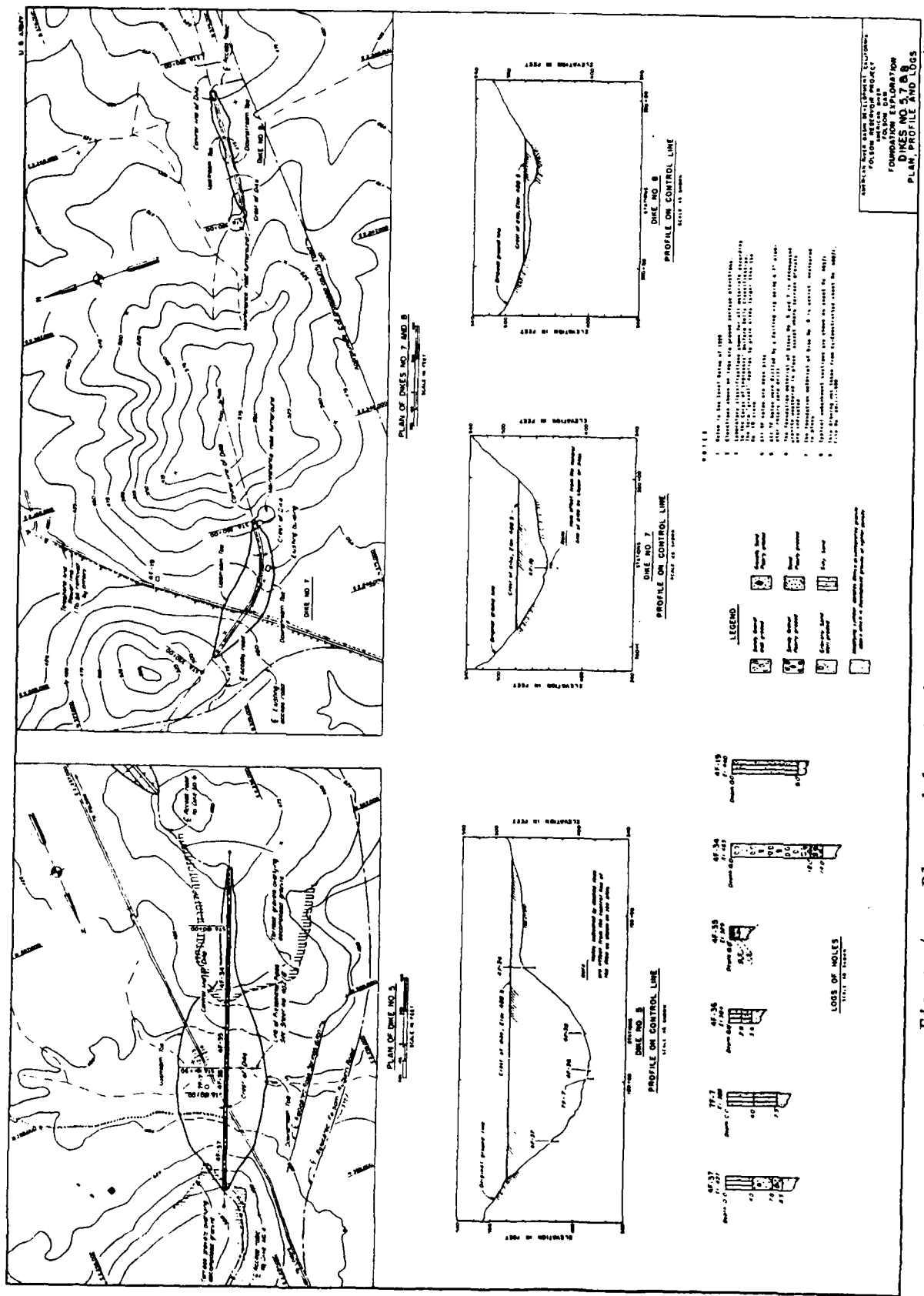
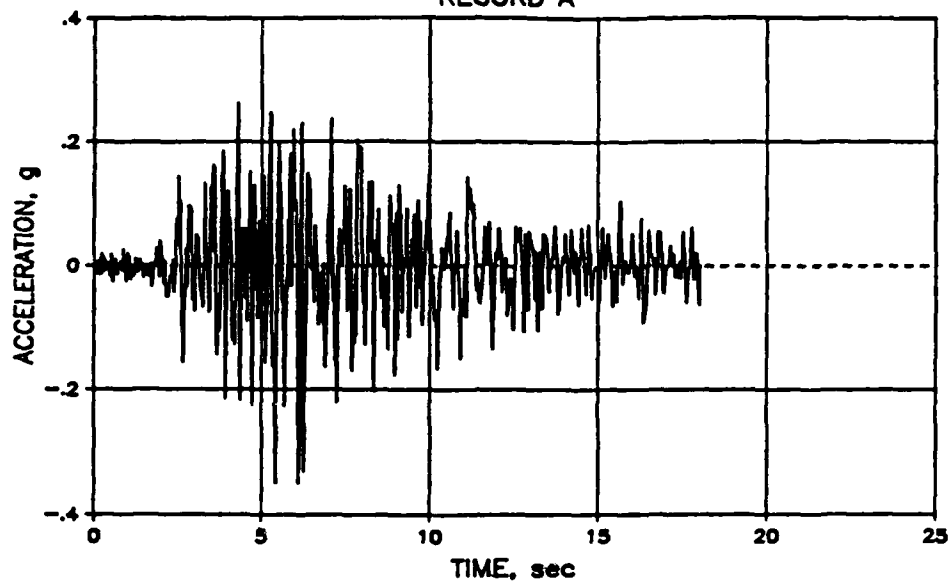


Figure 4c. Plan and longitudinal views of Dikes 5, 7, and 8.

FOLSOM DAM PROJECT  
RECORD A



RECORD B

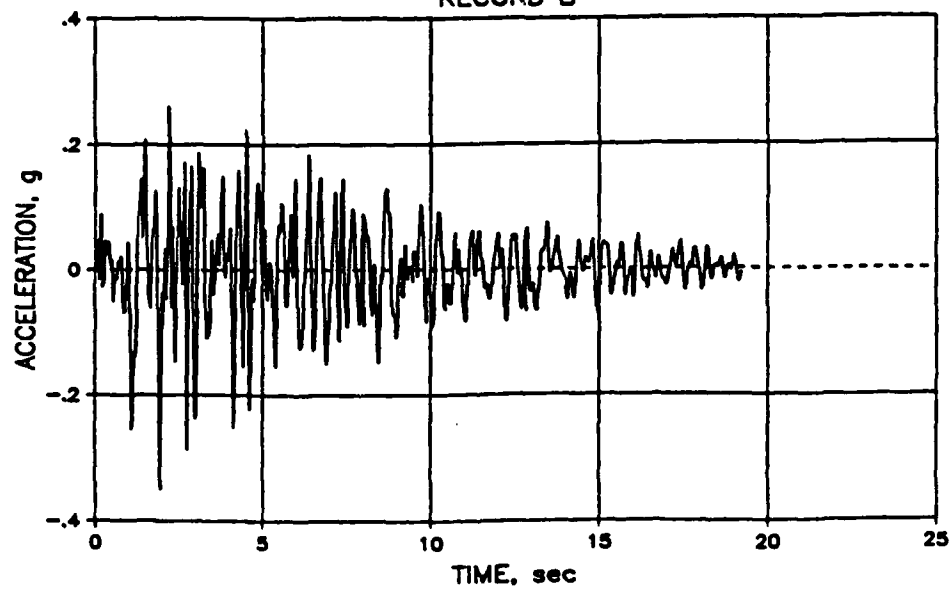


Figure 5. Acceleration histories used in the analysis.

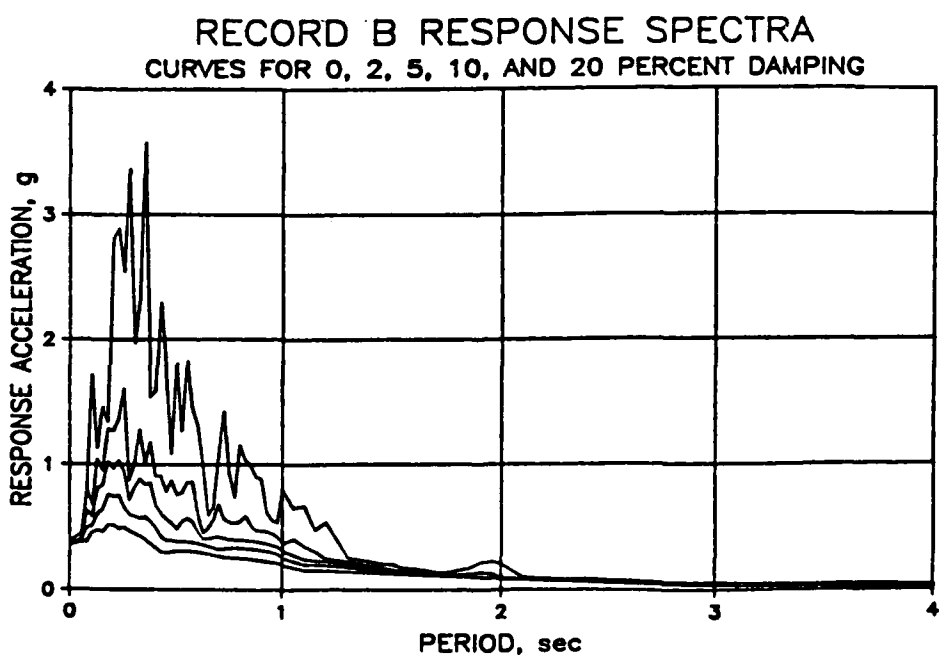
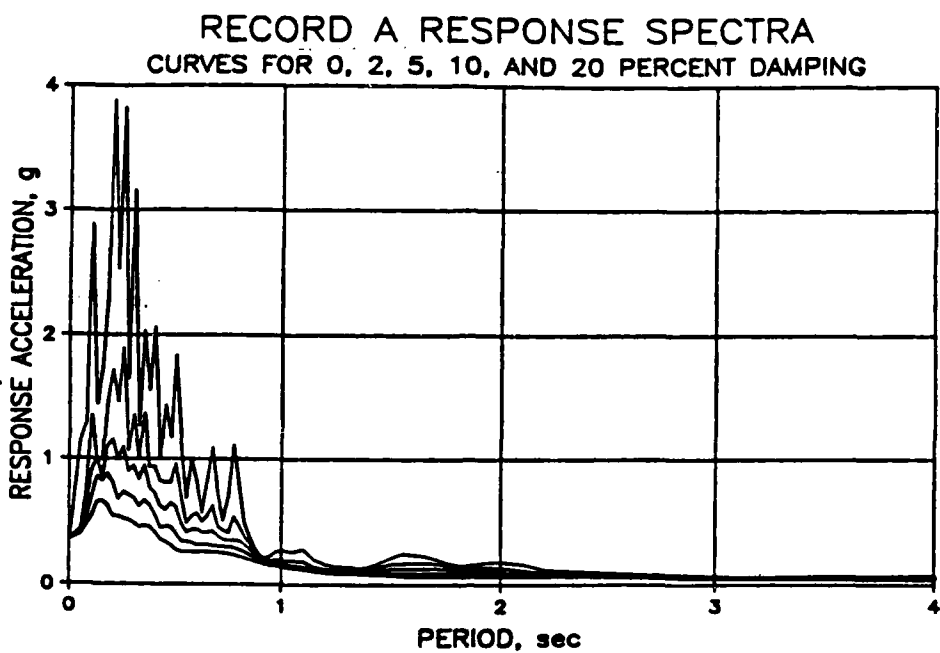
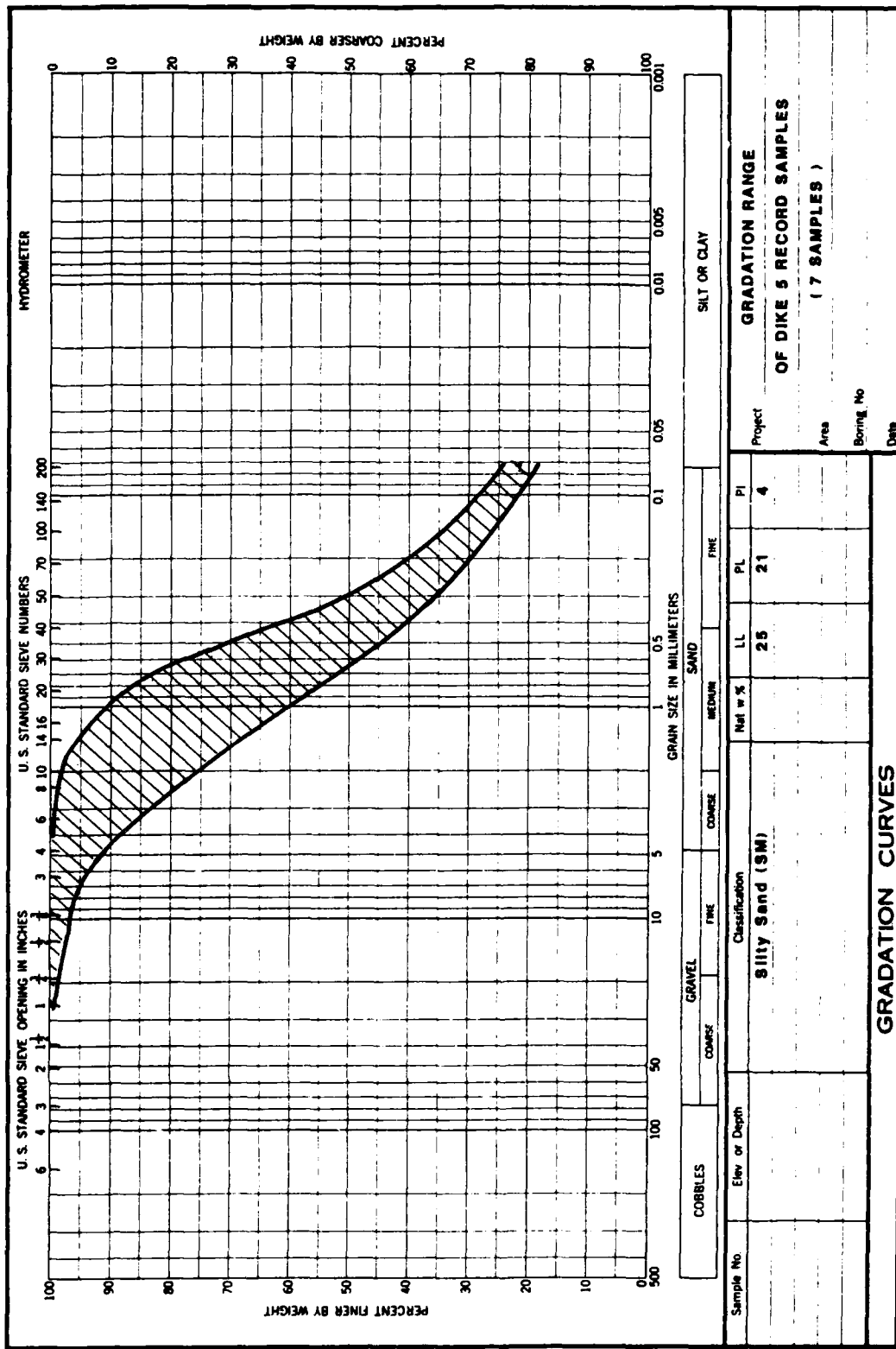


Figure 6. Response Spectra of Records A and B.



ENG FORM 2087  
1 MAY 63

Figure 7. Gradation Ranges of decomposed granite obtained during construction from record samples.

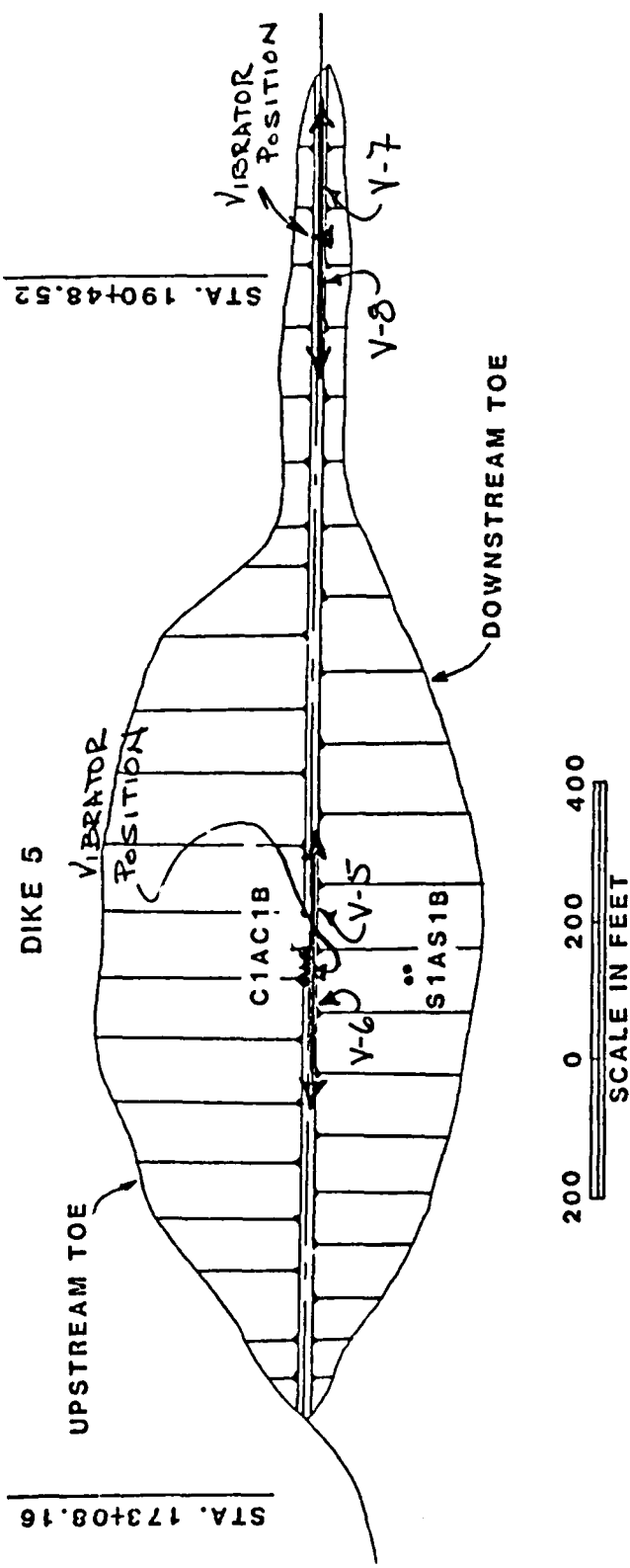


Figure 8. Plan view of Dike 5 showing the locations of the geophysical tests.

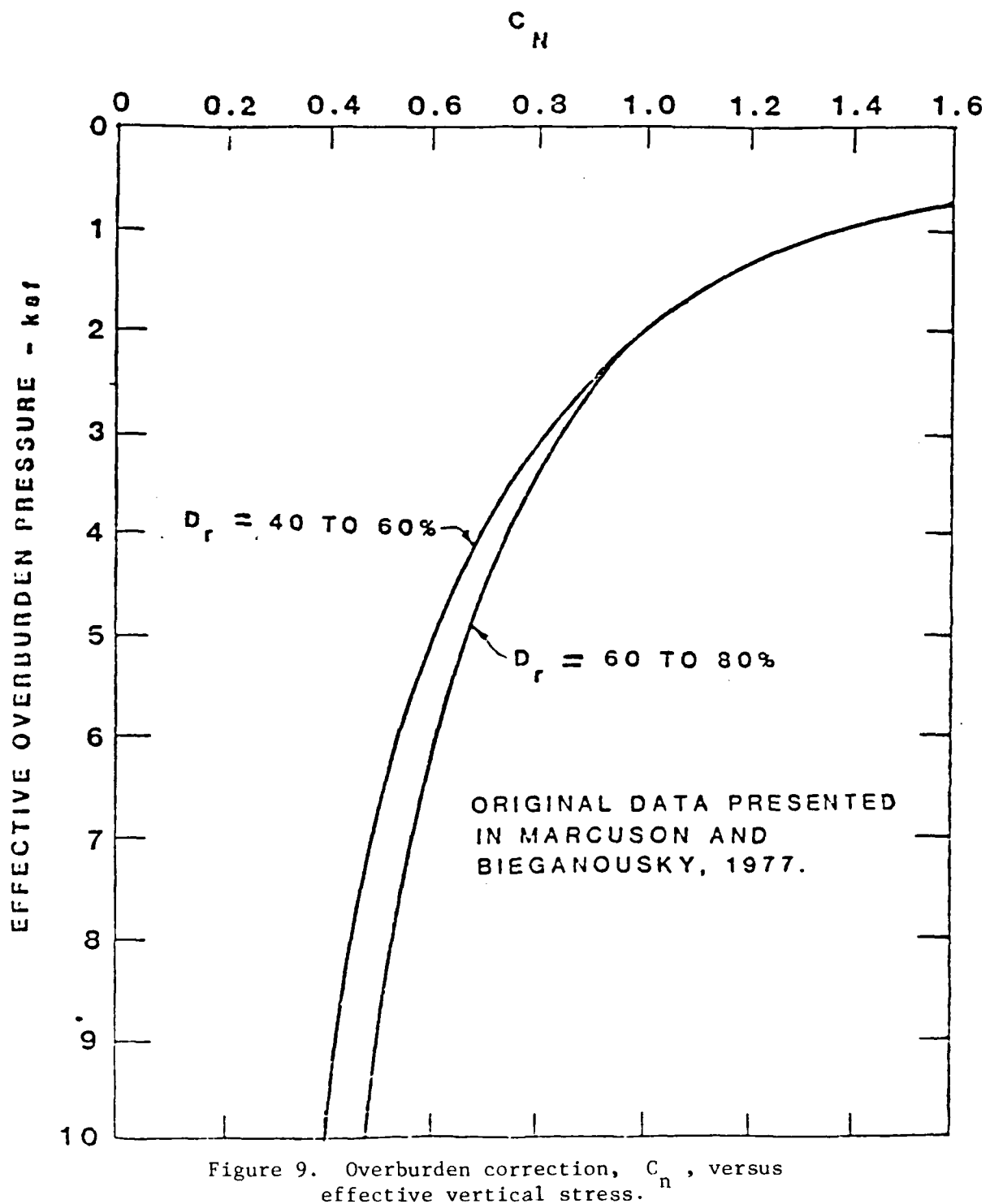


Figure 9. Overburden correction,  $C_n$ , versus effective vertical stress.

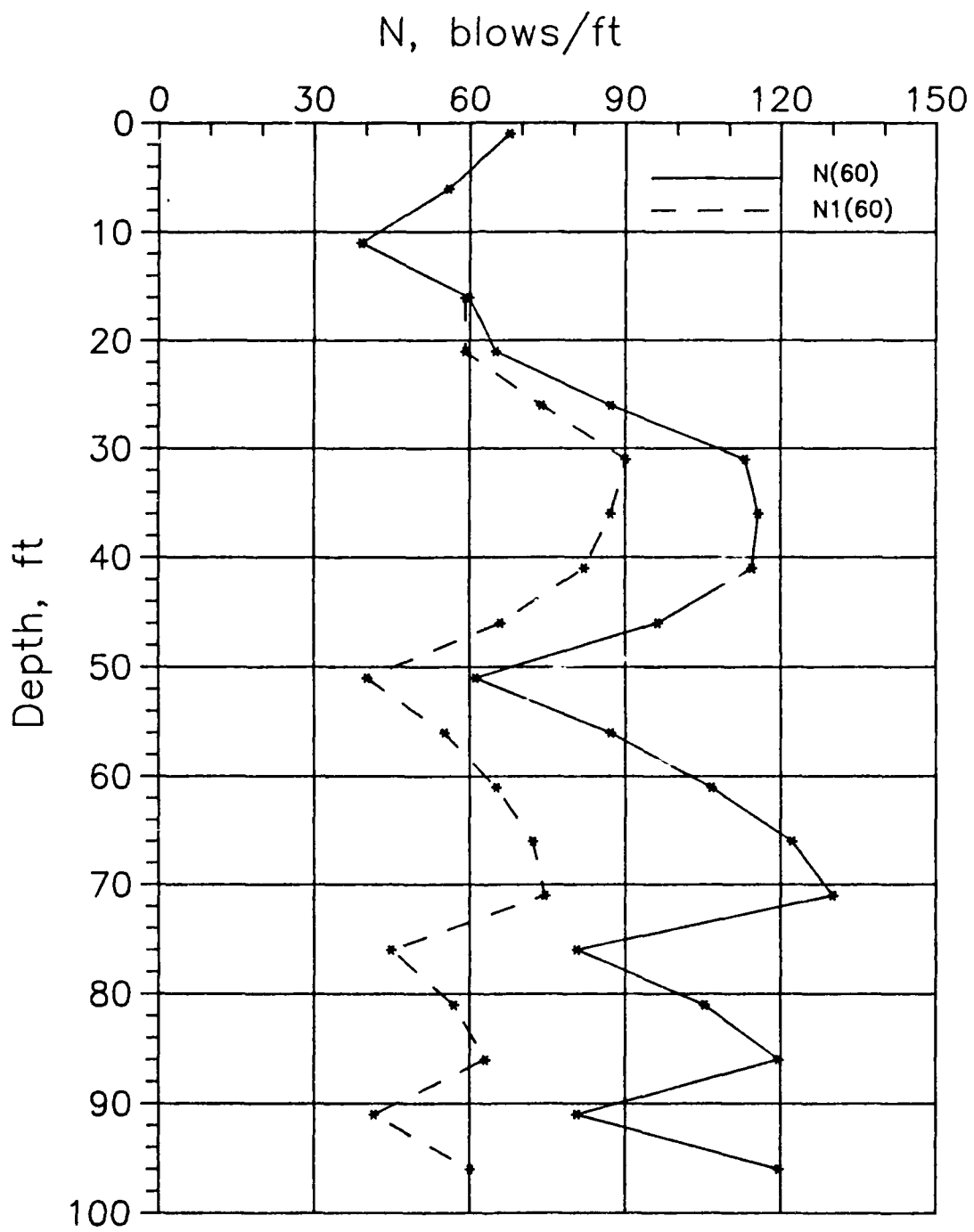


Figure 10.  $N_{60}$  and  $(N_1)_{60}$  blowcounts from boring SS-1.

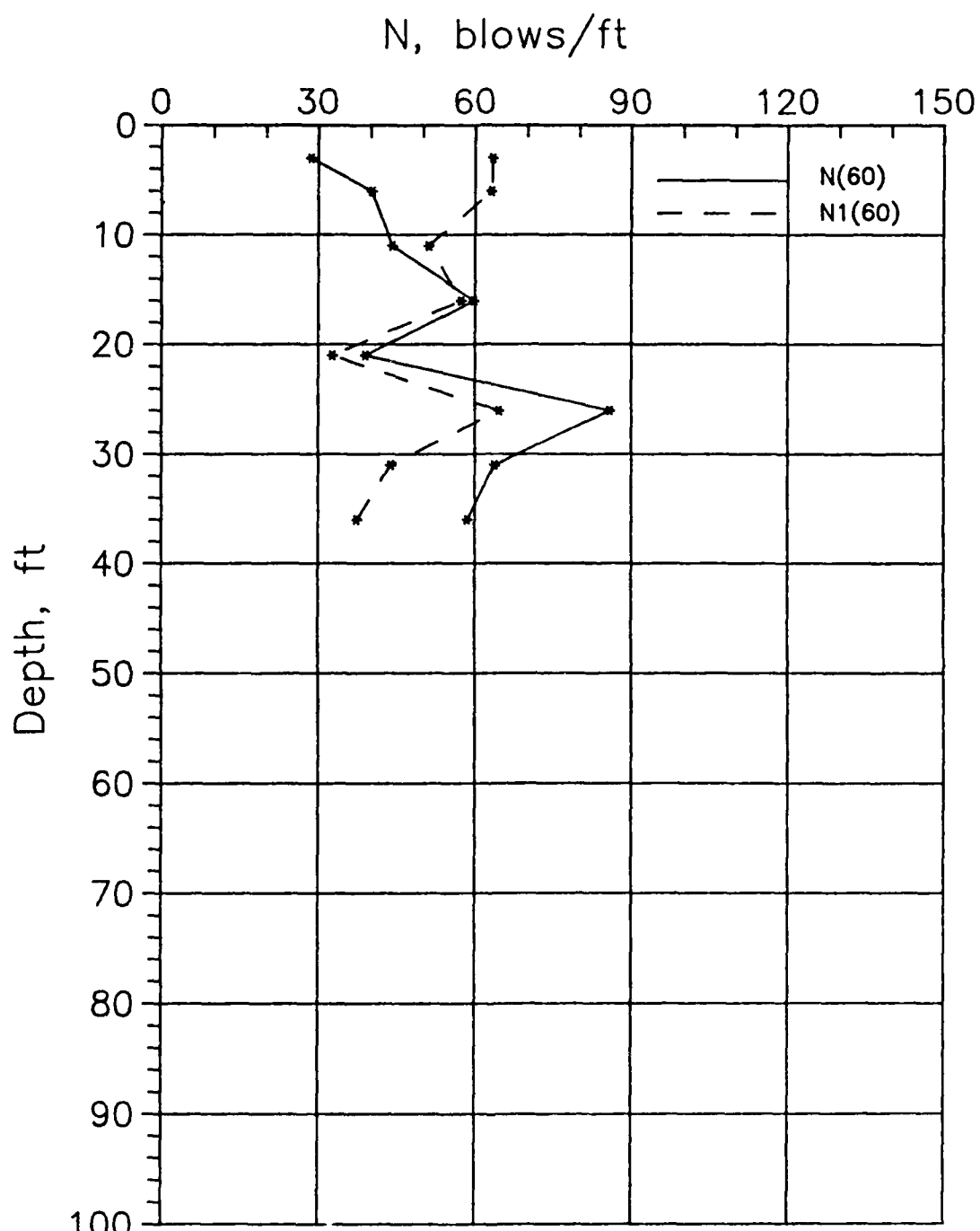


Figure 11.  $N_{60}$  and  $(N_1)_{60}$  blowcounts from boring SS-10.

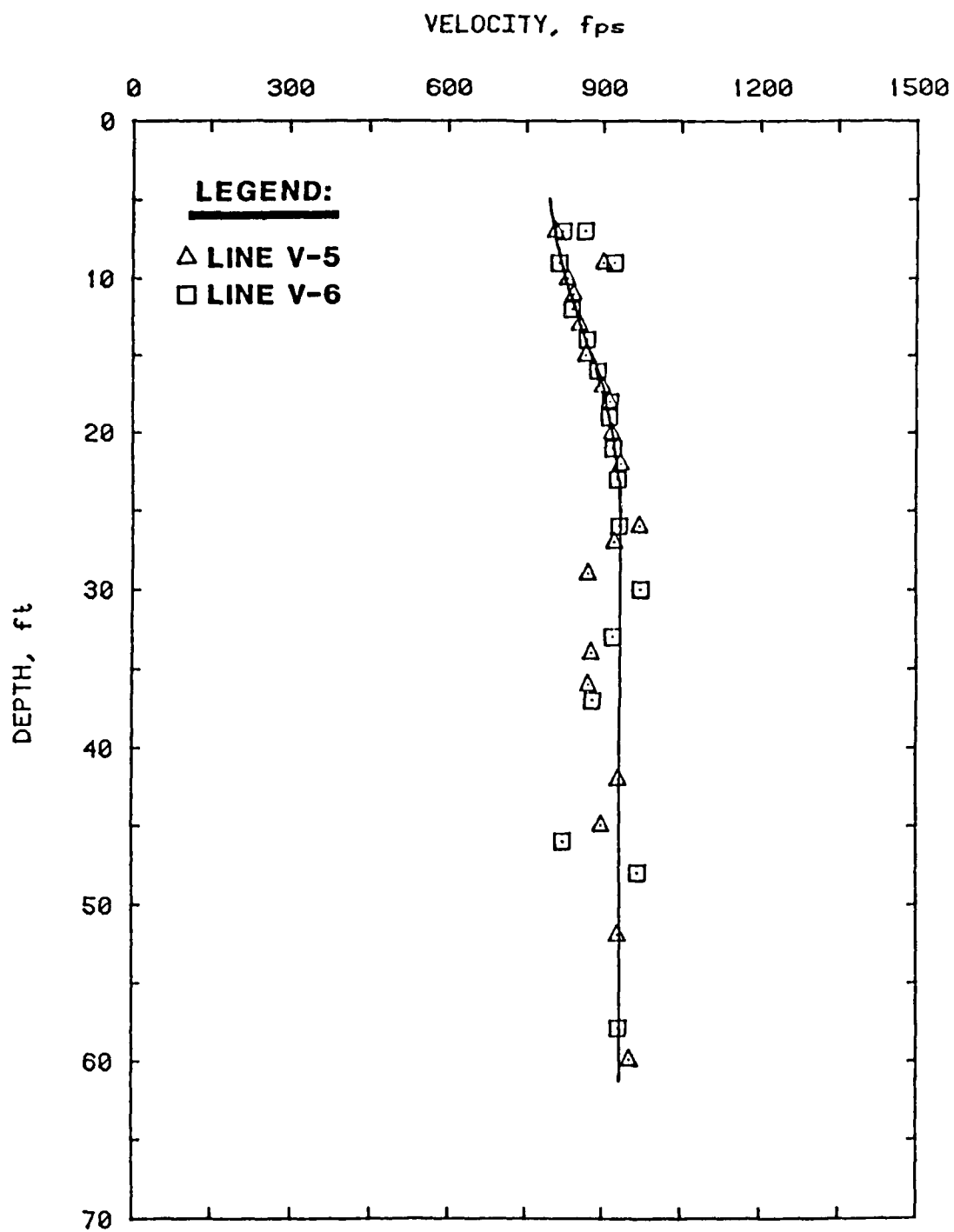


Figure 12. R-wave velocity versus depth for lines V-5 and V-6, on crest of Dike 5.

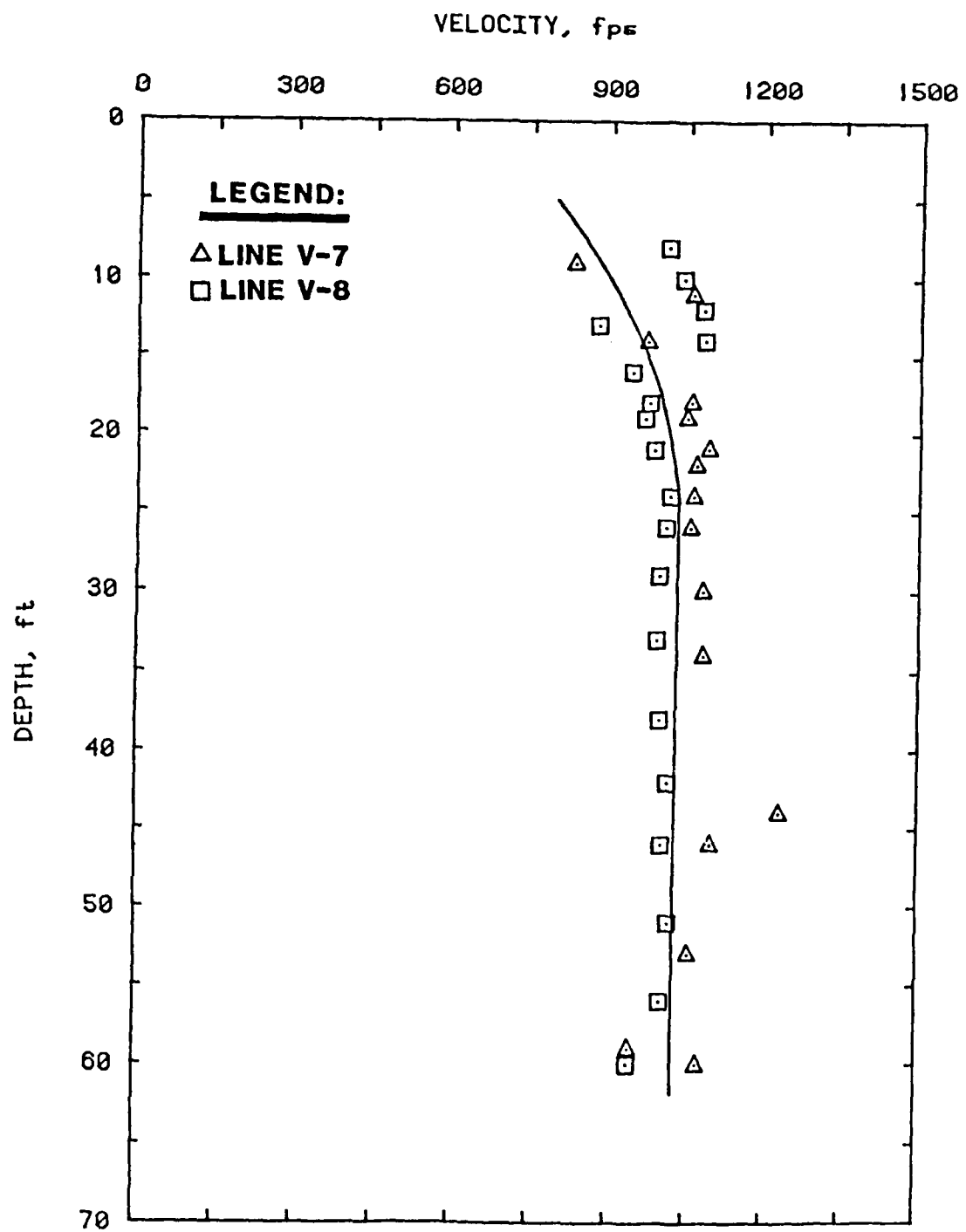


Figure 13. R-wave velocity versus depth for lines V-7 and V-8, on crest on crest of Dike 5.

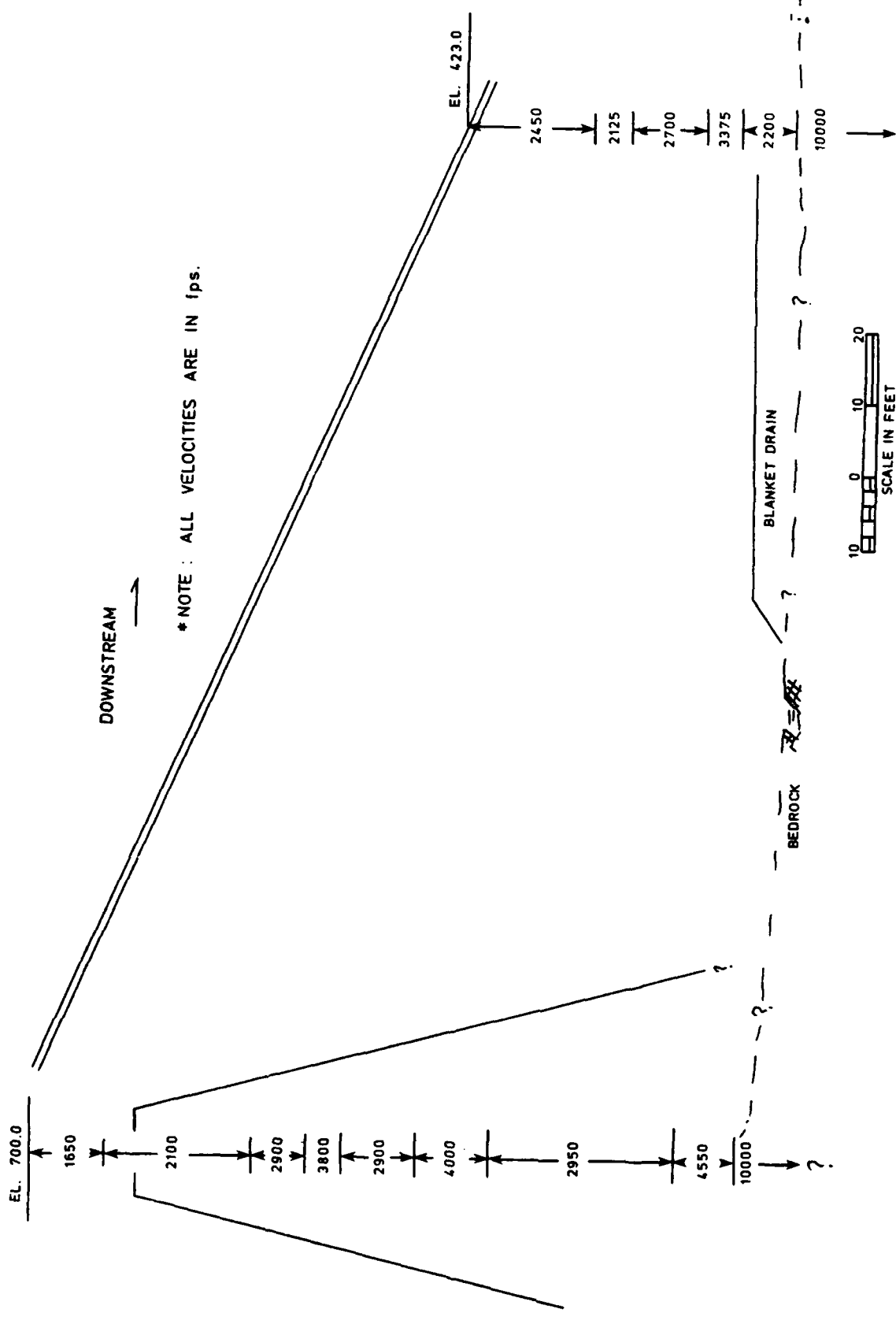


Figure 14. P-wave zones interpreted from crosshole tests at Sta 180+50 at Dike 5.

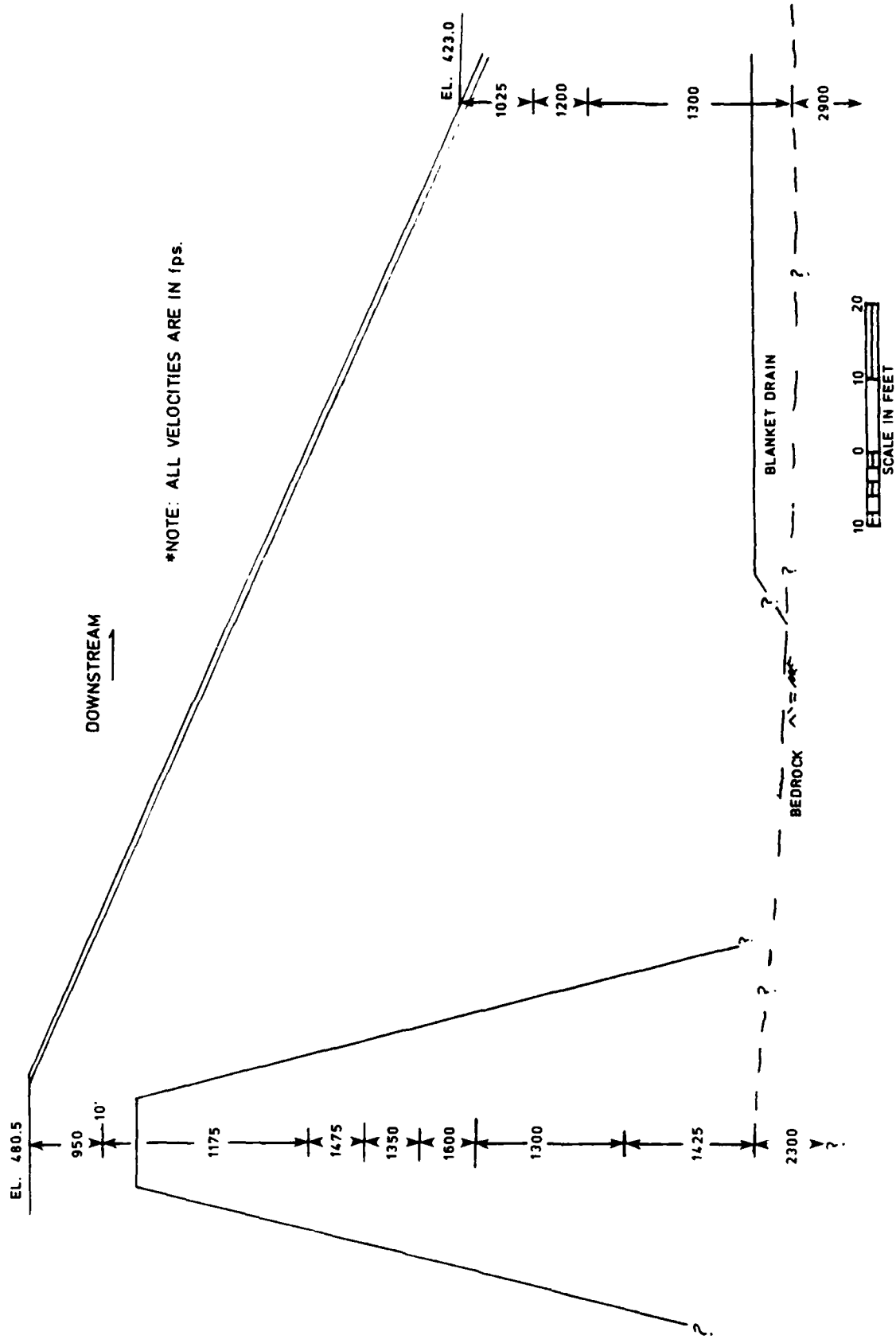
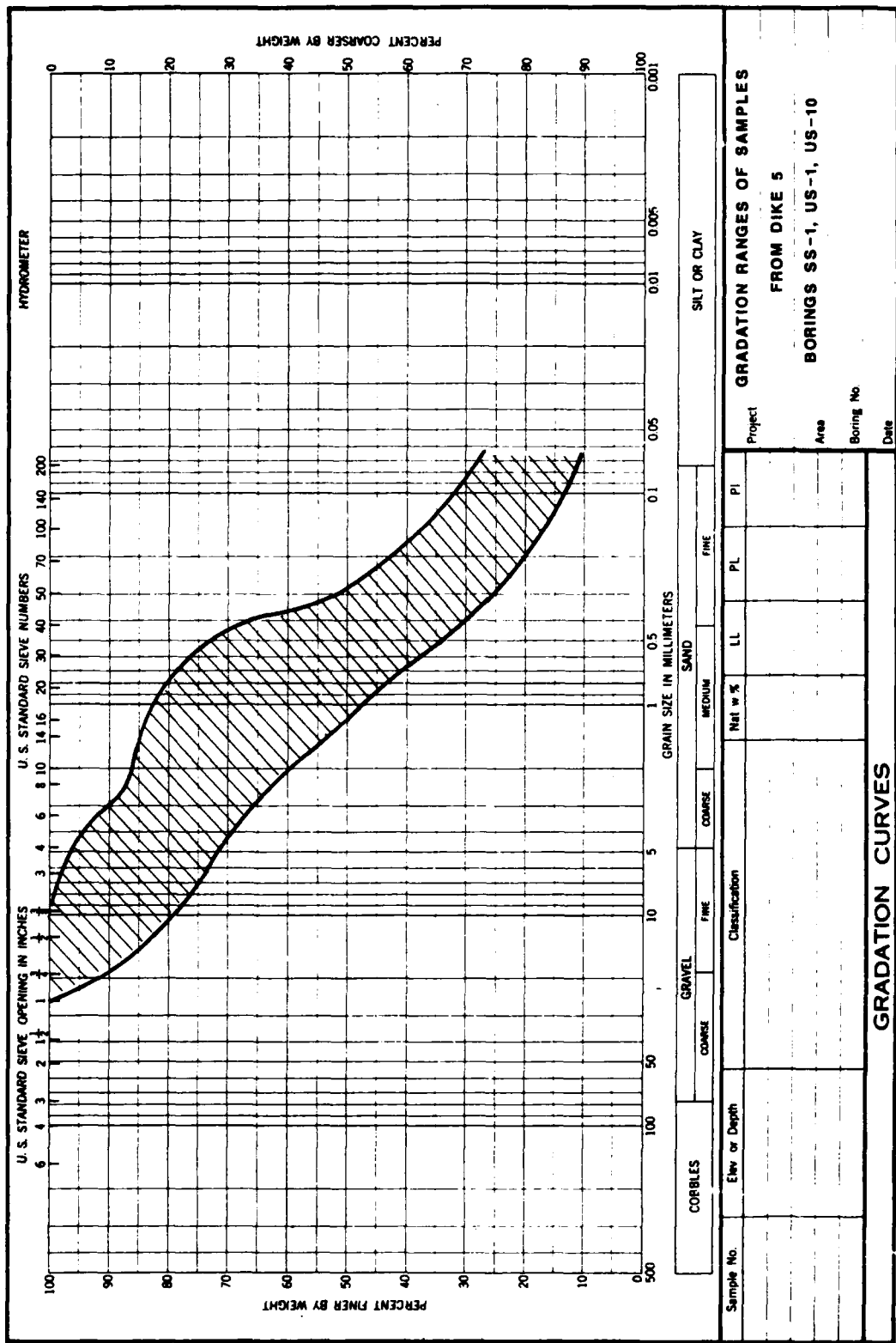


Figure 15. S-wave zones interpreted from crosshole tests at Sta 180+50 at Dike 5.



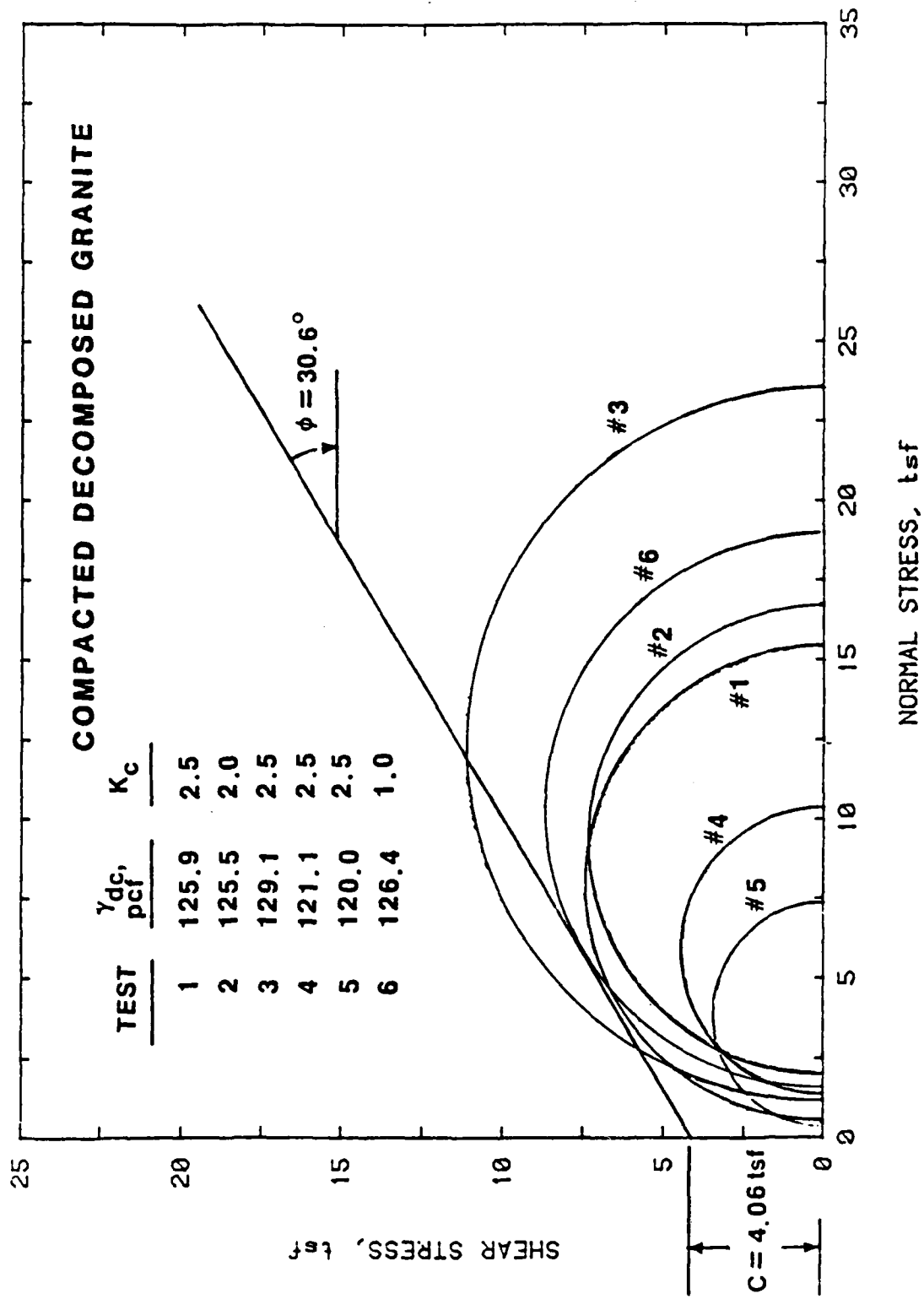


Figure 17. Failure envelope of compacted decomposed granite for total stress (undrained) conditions (R envelope).

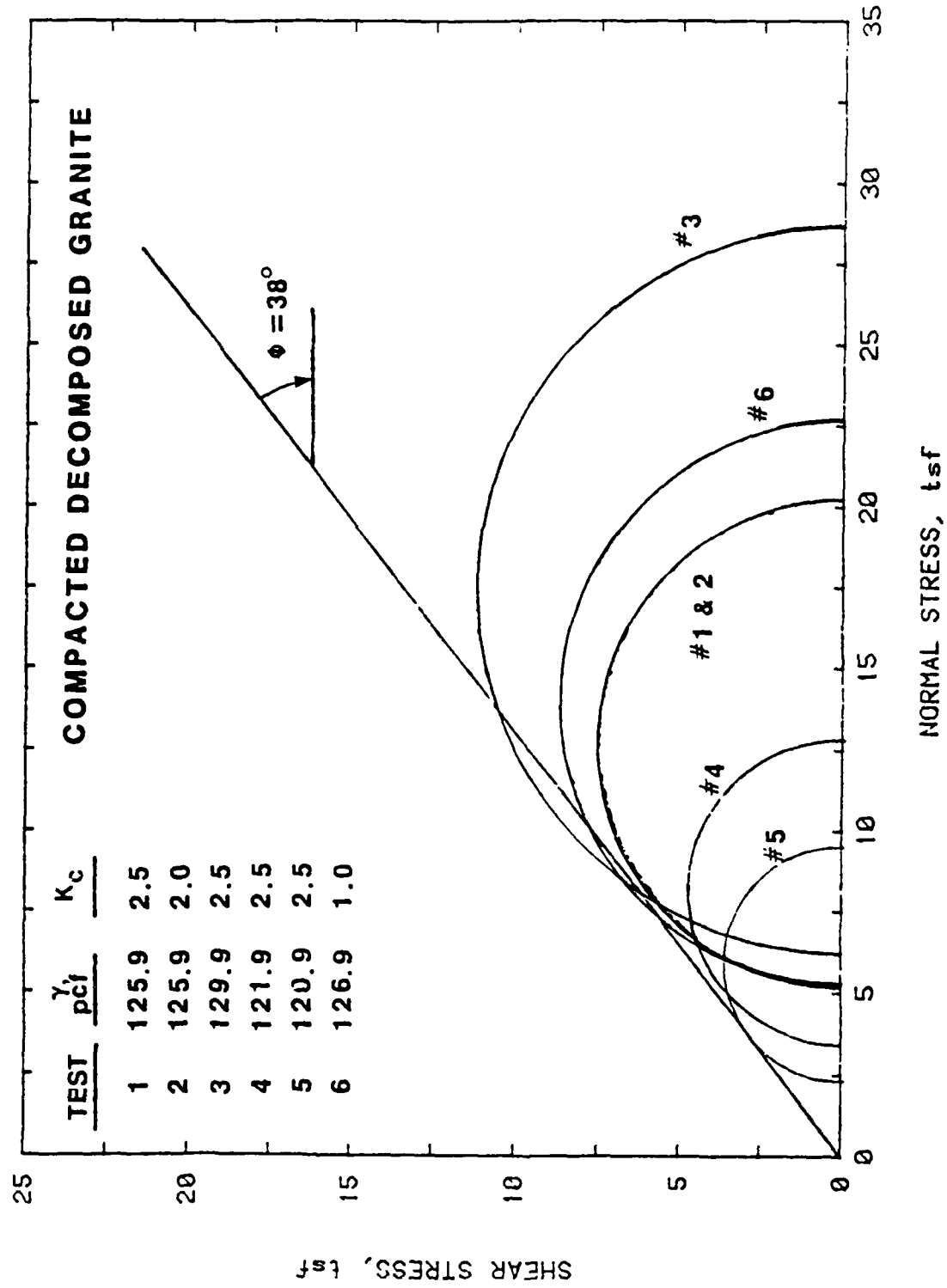
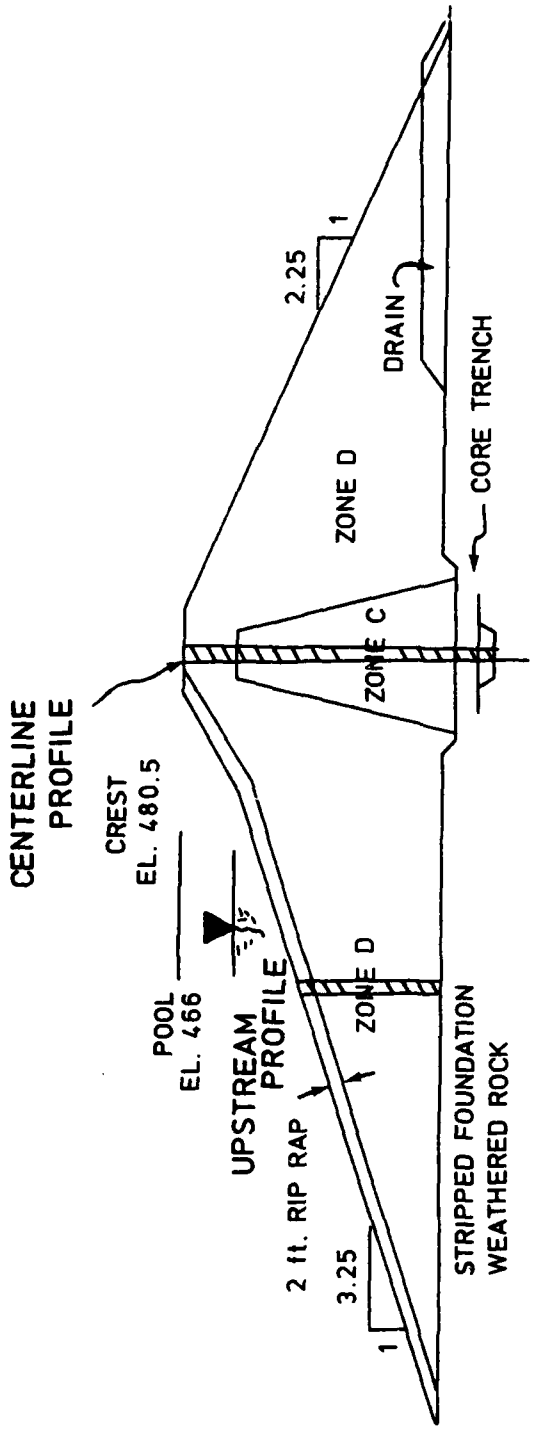


Figure 18. Failure envelope of compacted decomposed granite for effective stress (drained) conditions (R-bar envelope).



DIKE 5 - TYPICAL SECTION

Material Descriptions

**Zone C** - Decomposed granite from Borrow Area No. 2 and suitable fine-grained material from American River channel.

**Zone D** - Decomposed granite from Borrow Area No. 2 - practically the same as material in Zone C.

Figure 19. Cross section of Dike 5 showing locations of centerline and upstream slope SHAKE profiles.

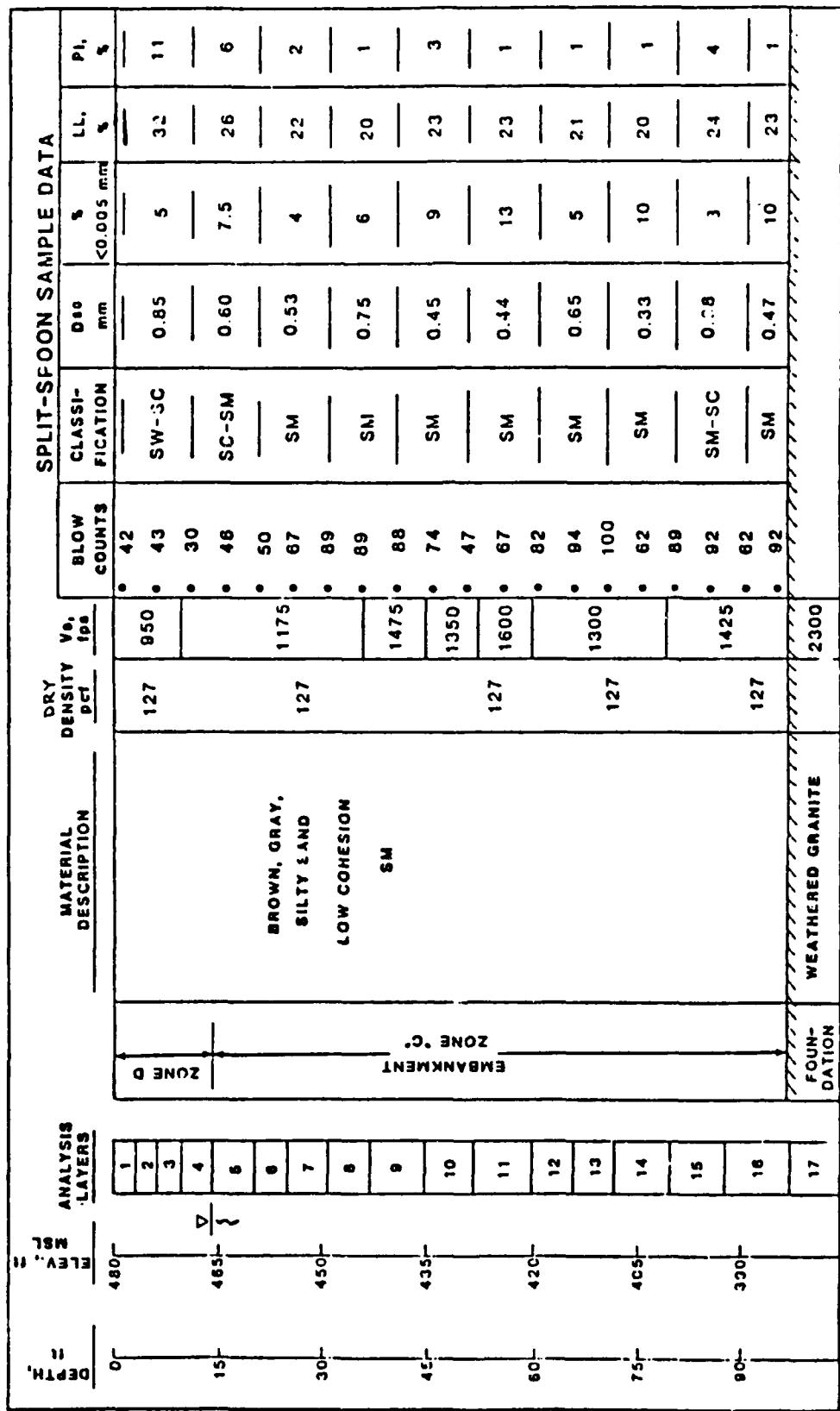


Figure 20. Centerline profile used in SHAKE analysis.

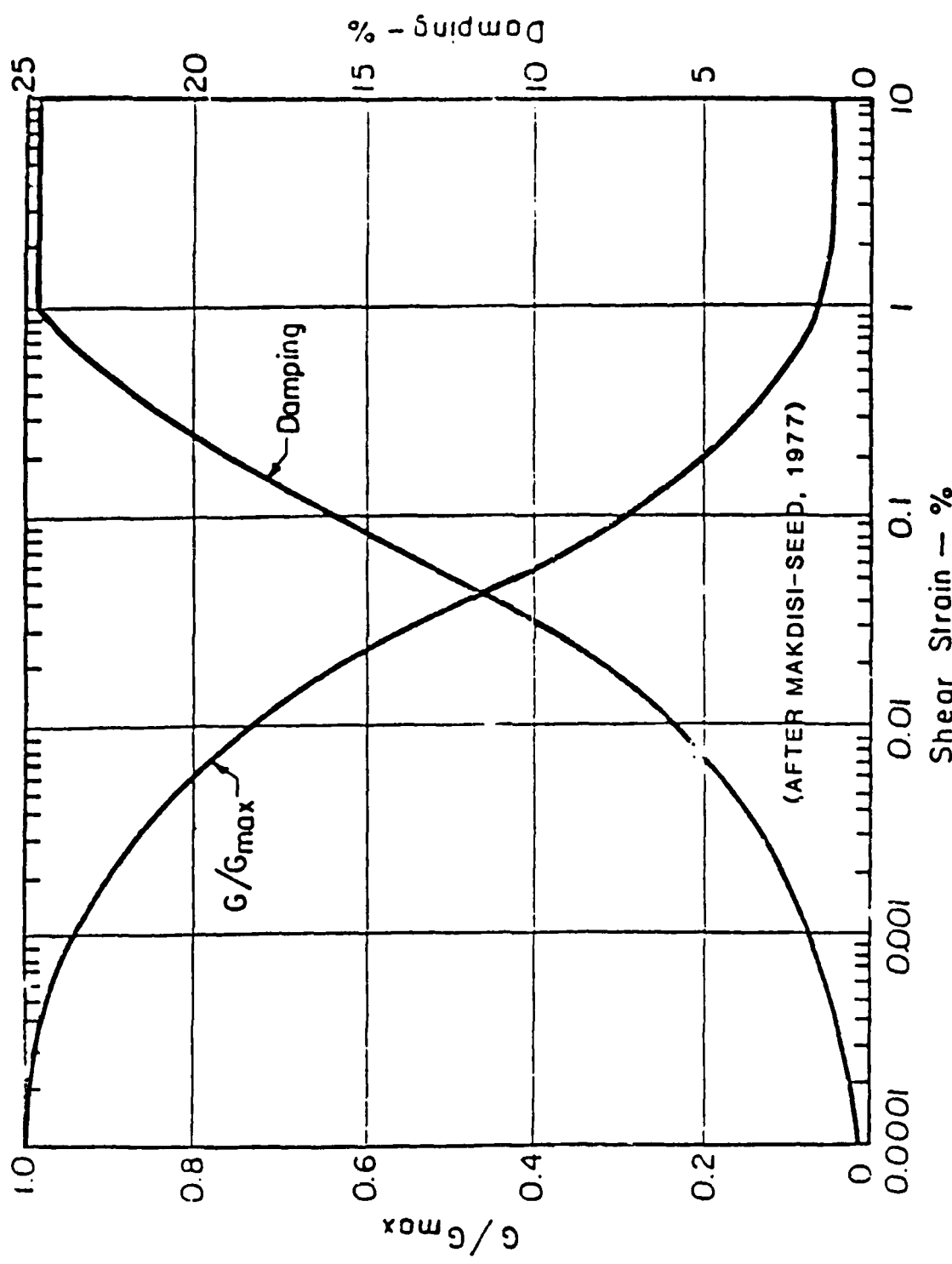


Figure 21. Strain dependent modulus degradation and damping curves used by SHAKE.

# RECORD A

## MAXIMUM ACCELERATION, g's

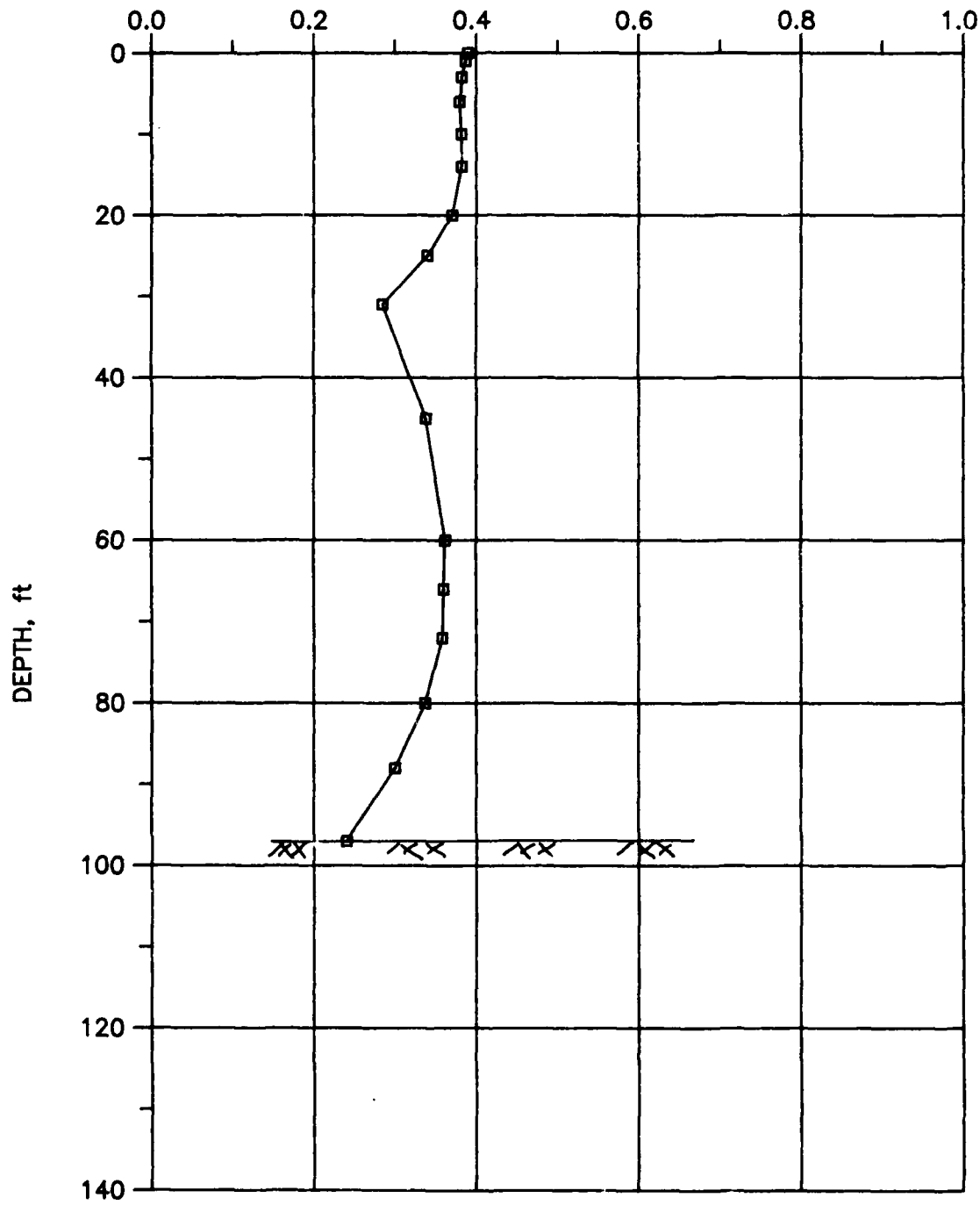


Figure 22. Peak accelerations in the centerline profile due to Accelerogram A.

## RECORD B

MAXIMUM ACCELERATION, g's

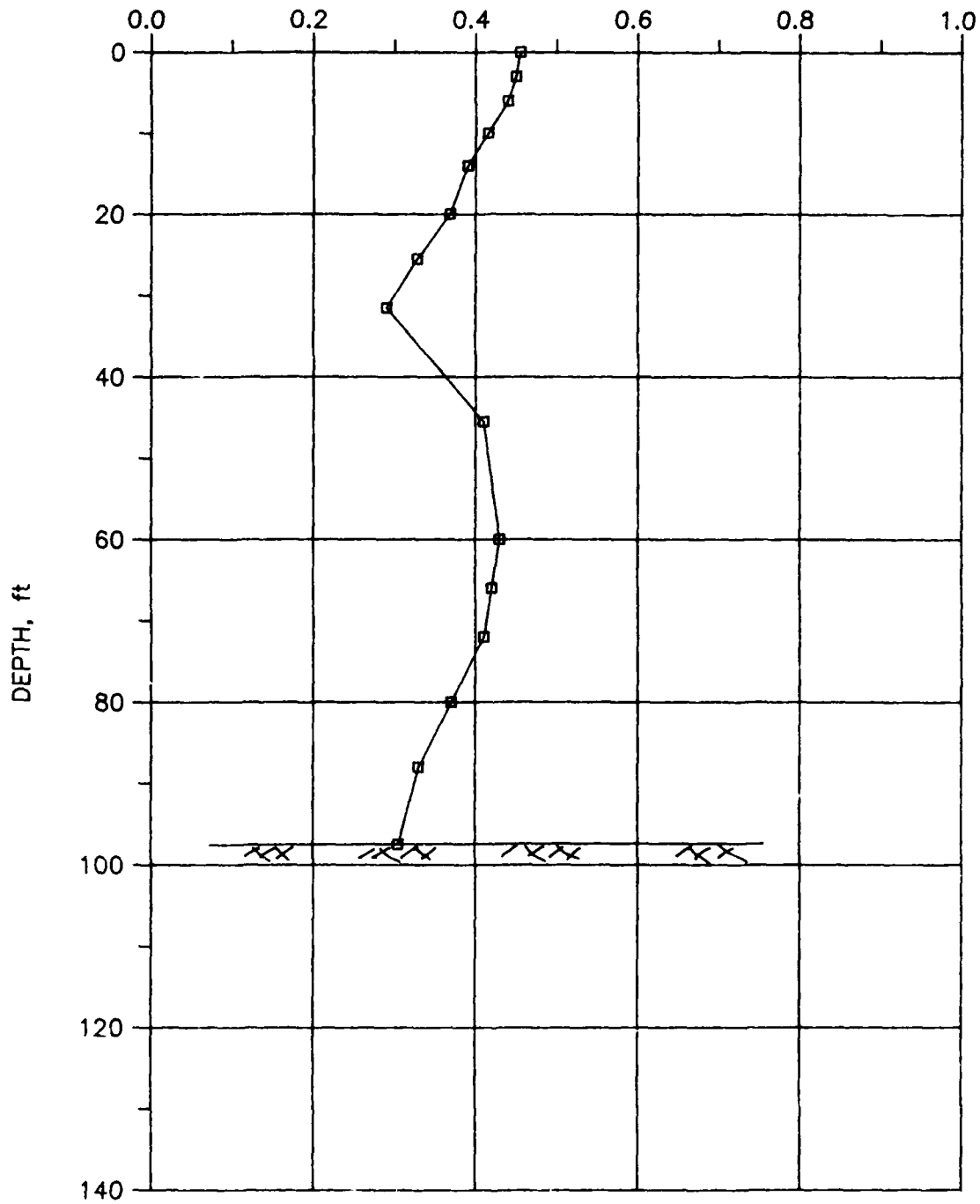


Figure 23. Peak accelerations in the centerline profile due to Accelerogram B.

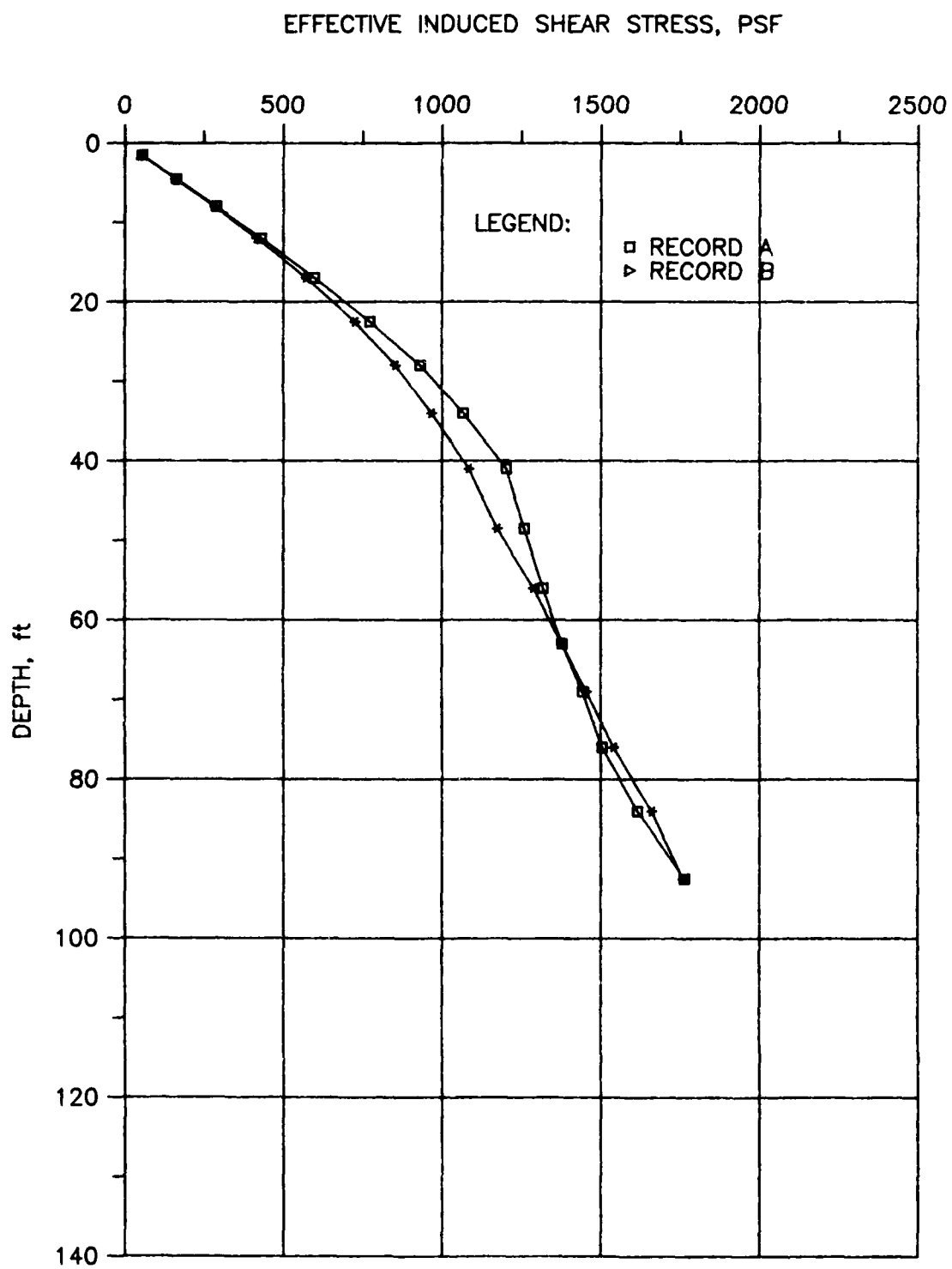


Figure 24. Effective dynamic shear stresses in the centerline profile induced by Records A and B.

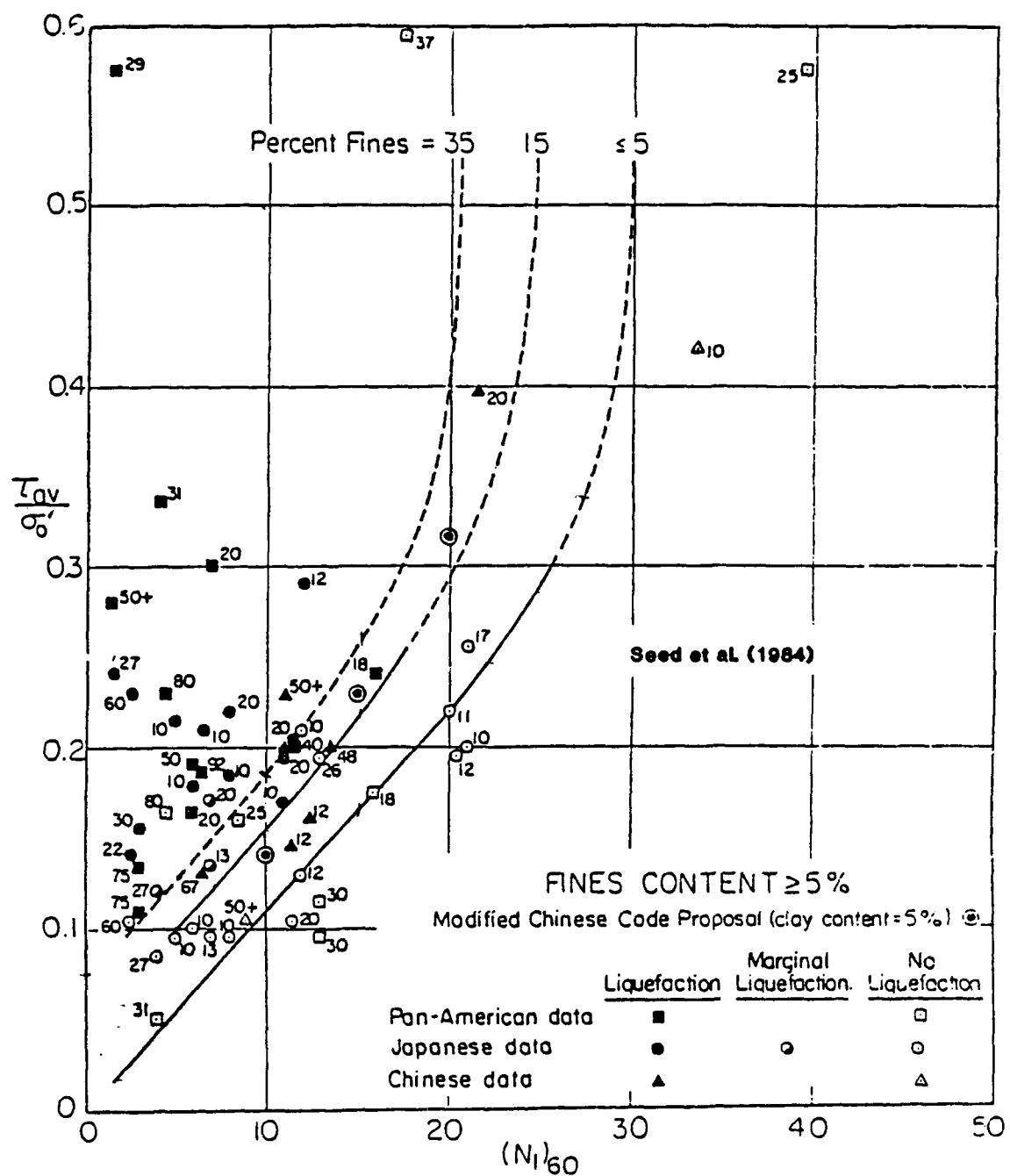


Figure 25. Relationships between stress ratio causing liquefaction and  $(N_1)_{60}$  - values for silty sand for  $M = 7.5$  earthquakes (from Seed, Tokimatsu, Harder, and Chung, 1984).

## Cyclic Strength Versus (N1)60

Magnitude = 6.5

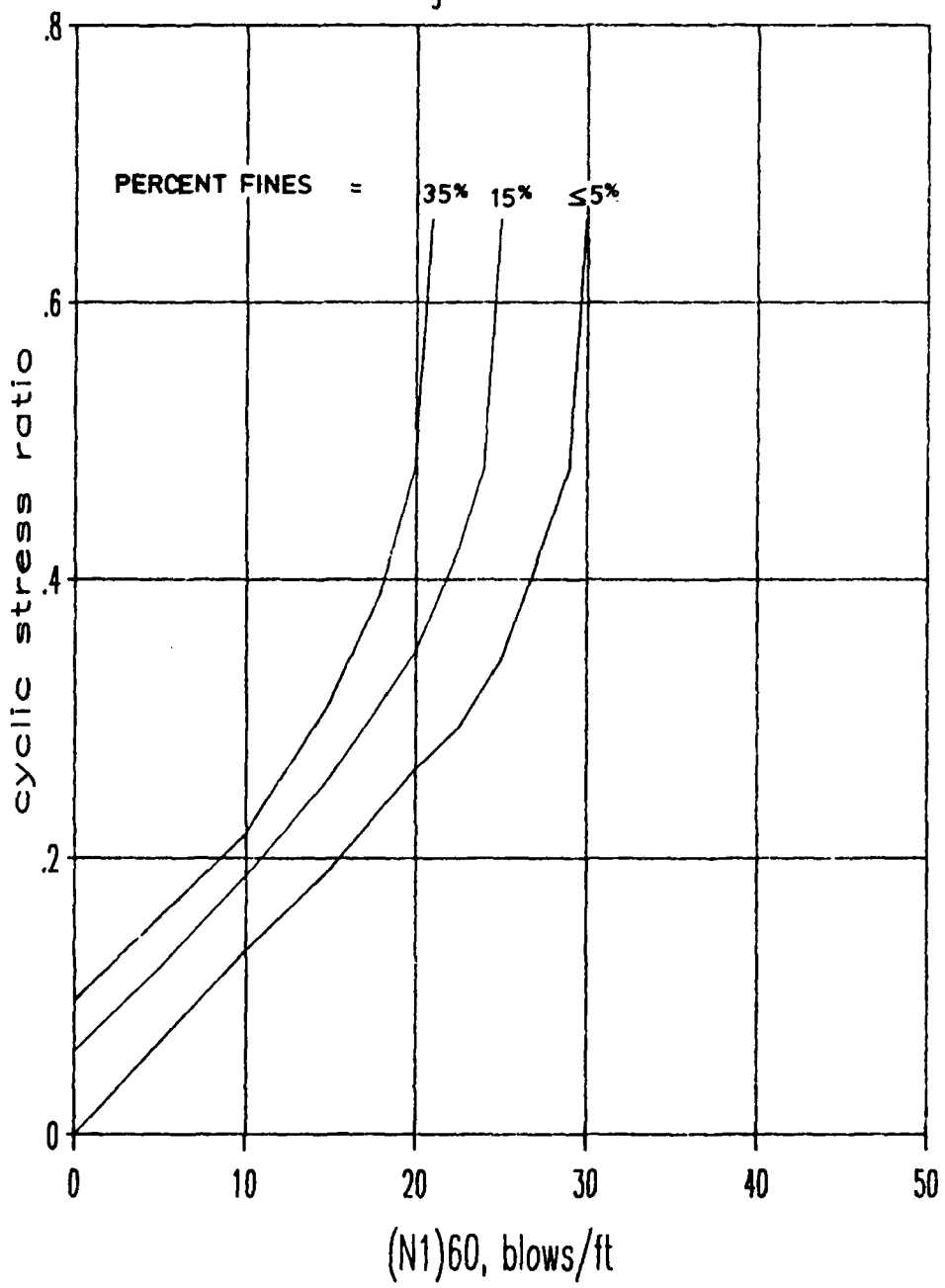


Figure 26. Relationships between stress ratio causing liquefaction and  $(N_1)_{60}$  - values for silty sand for  $M = 6.5$  earthquakes  
(developed from Seed, Tokimatsu, Harder, and Chung, 1984.)

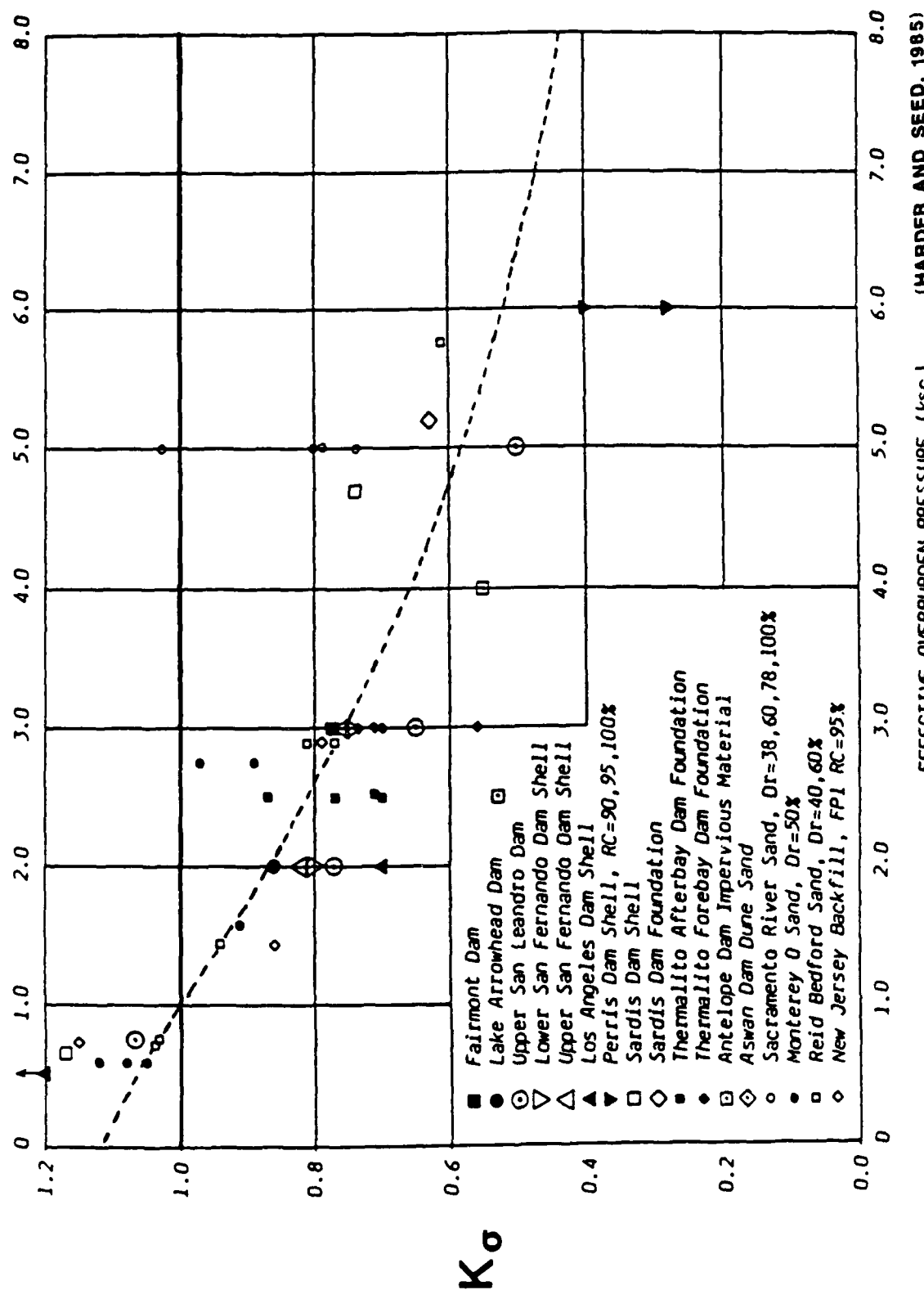


Figure 27.  $K_{\sigma}$  versus effective vertical stress.

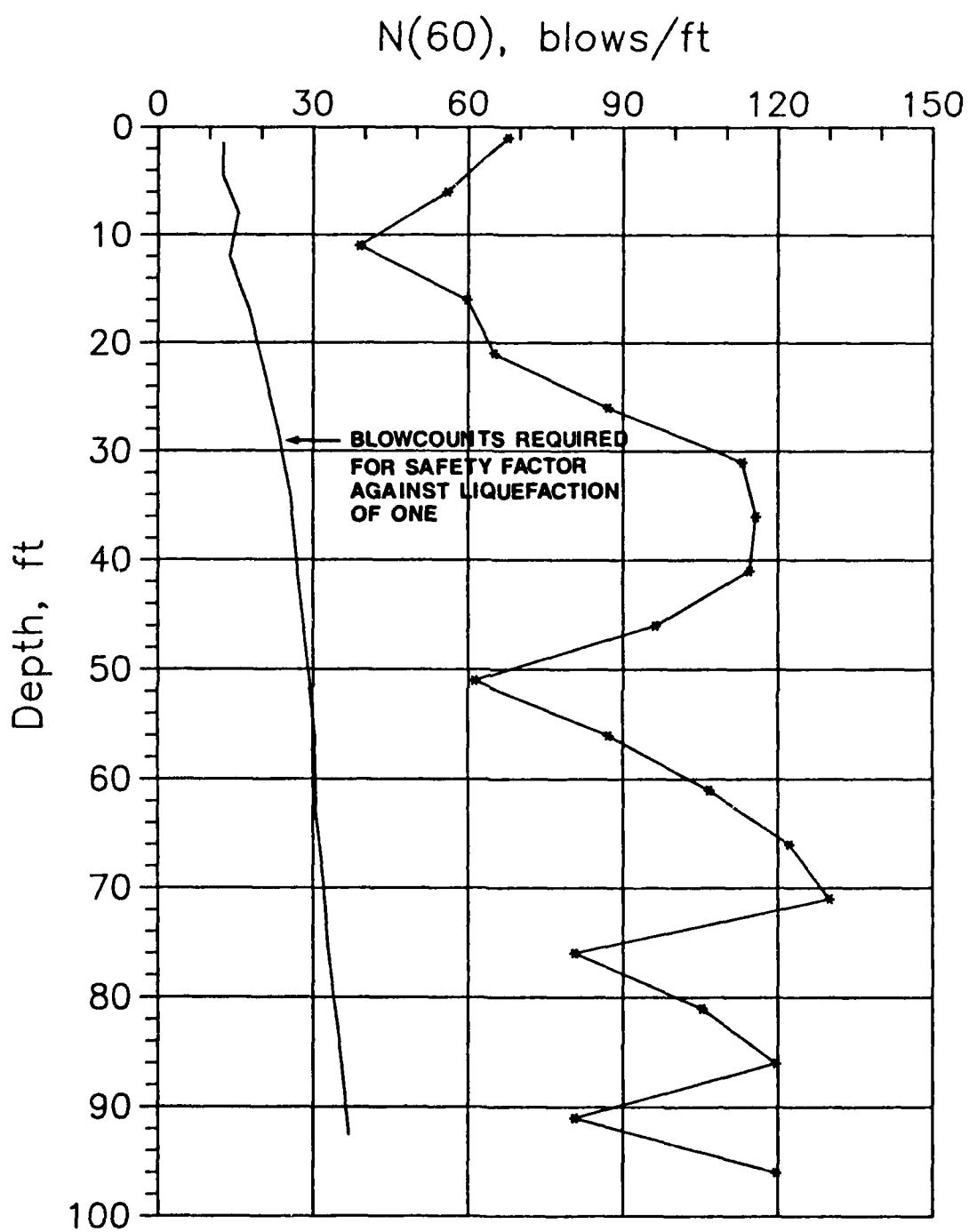


Figure 28. Comparison of  $N_{60}$  blowcounts from boring SS-1 on centerline which calculated blowcounts required to give safety factor against liquefaction of one.

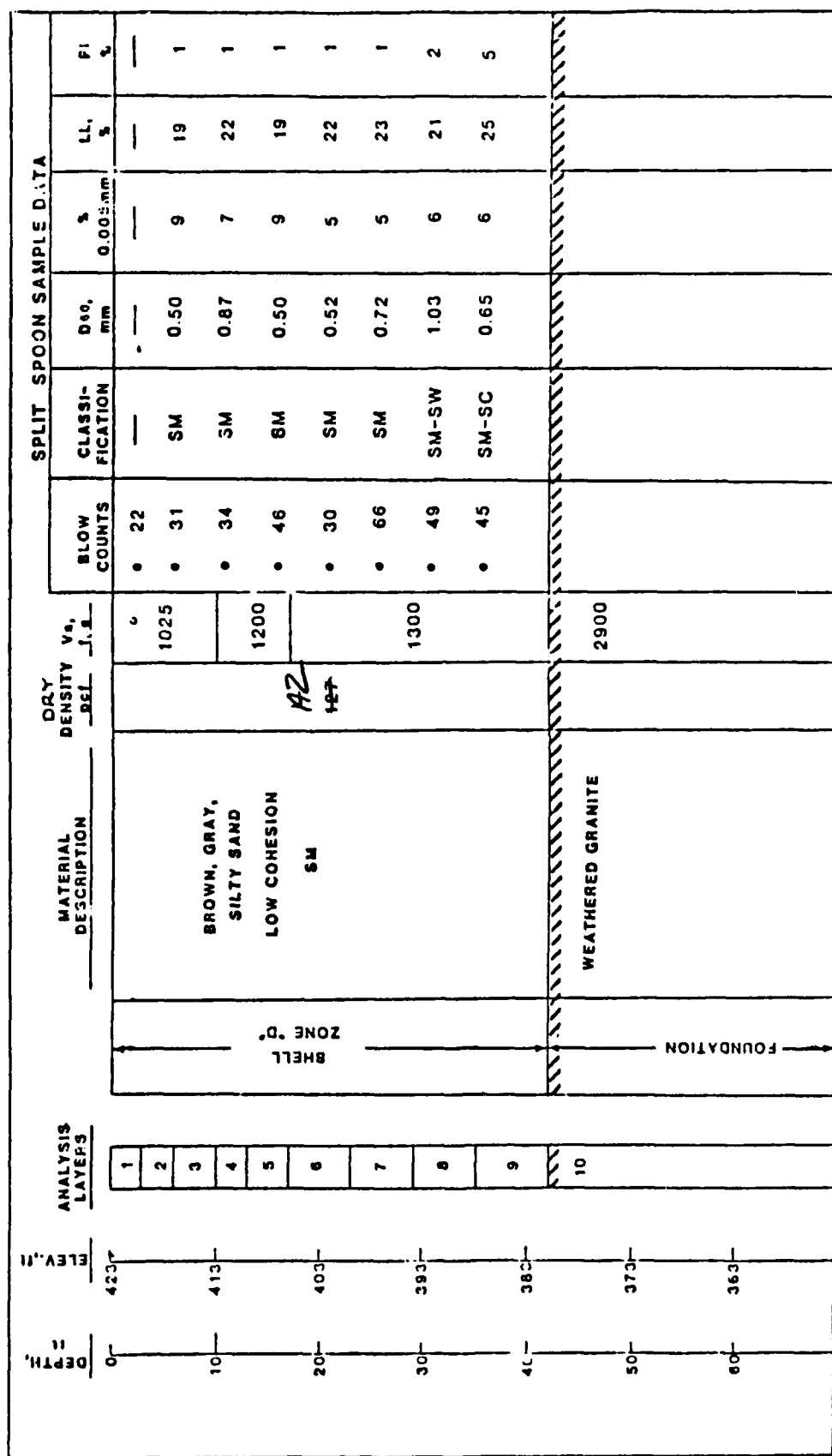


Figure 29. Upstream Slope profile used in SHAKE analysis.

## RECORD A

MAXIMUM ACCELERATION, g's

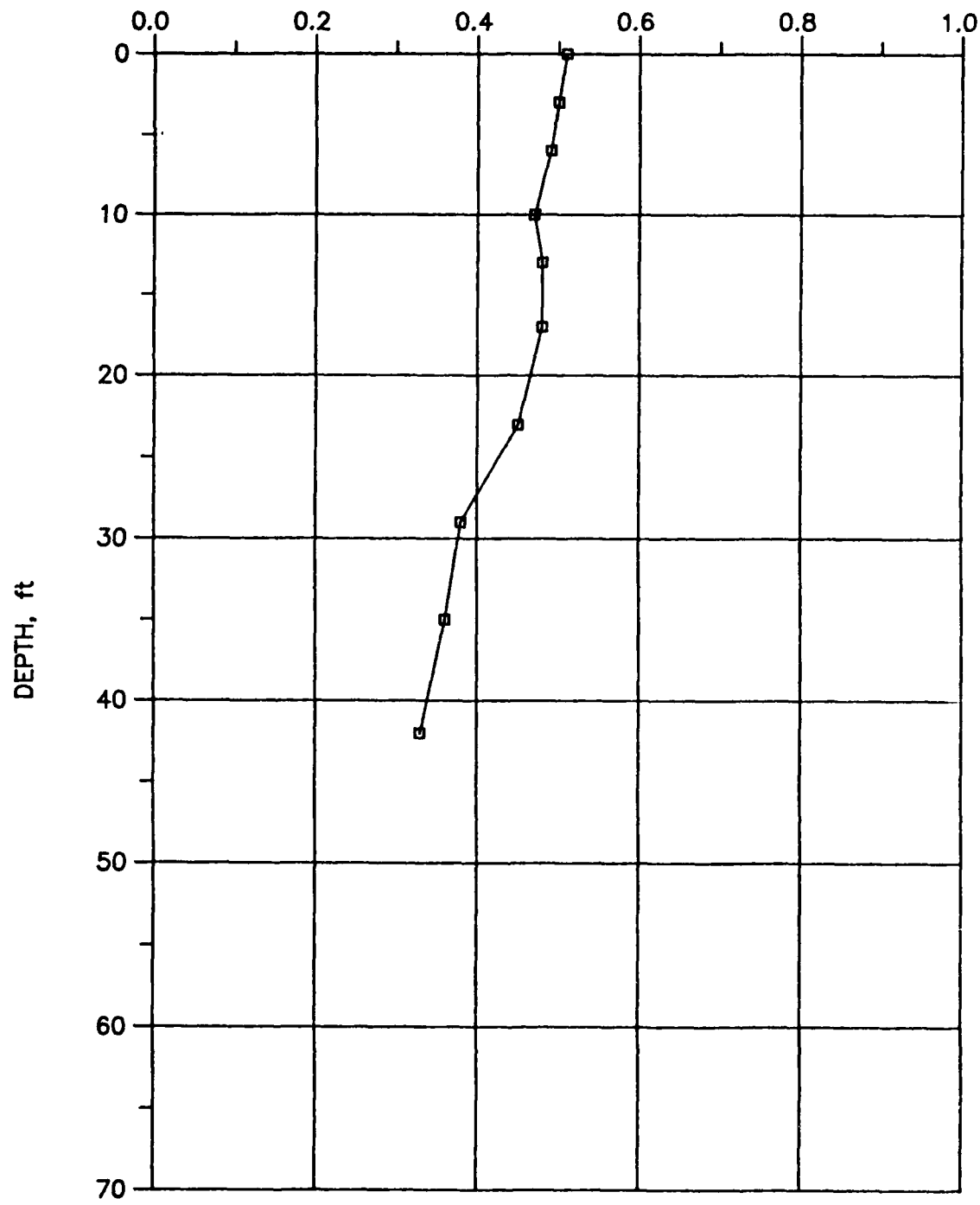


Figure 30. Peak accelerations in the upstream slope profile due to Record A.

## RECORD B

MAXIMUM ACCELERATION, g's

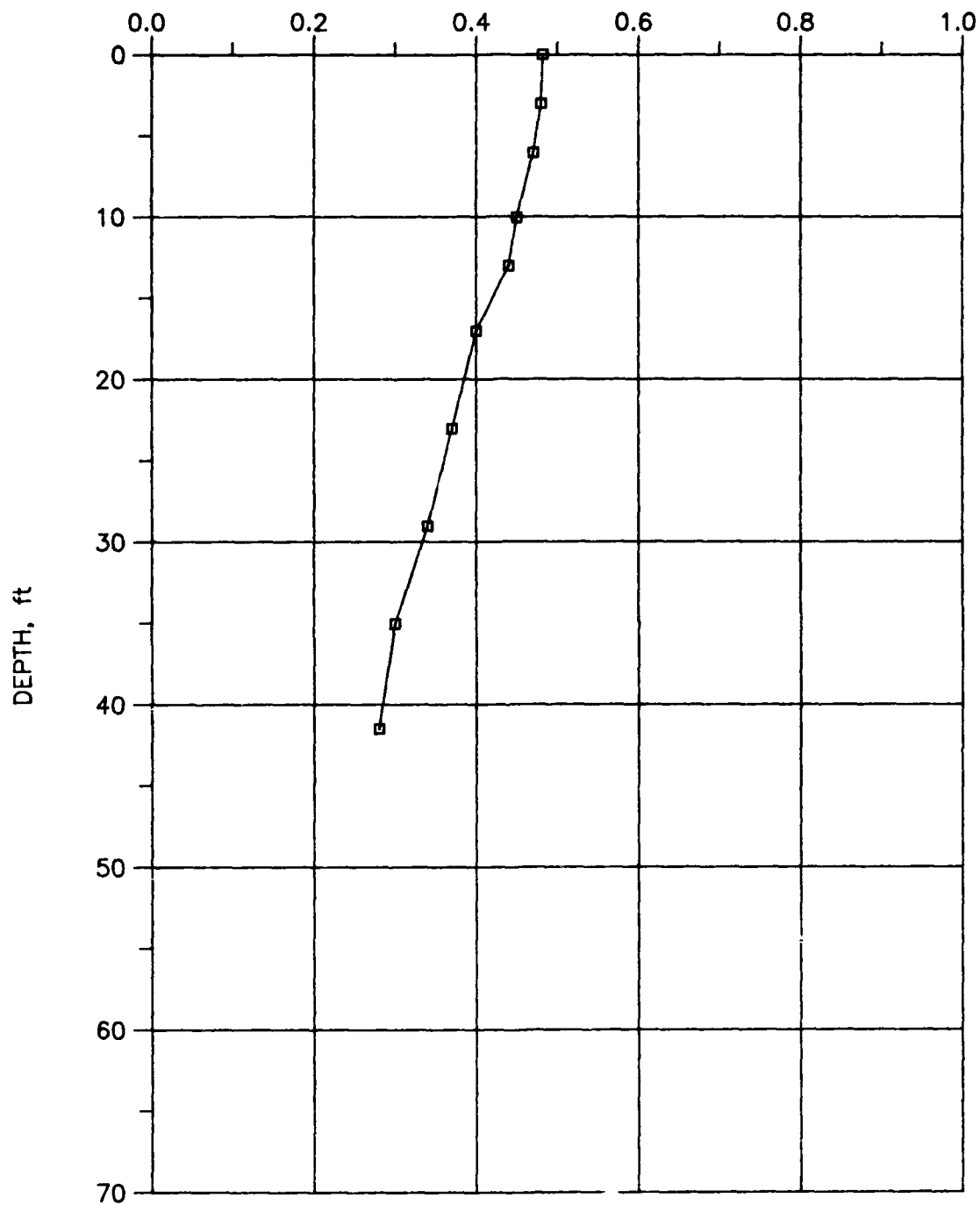


Figure 31. Peak accelerations in the upstream slope profile due to Record B.

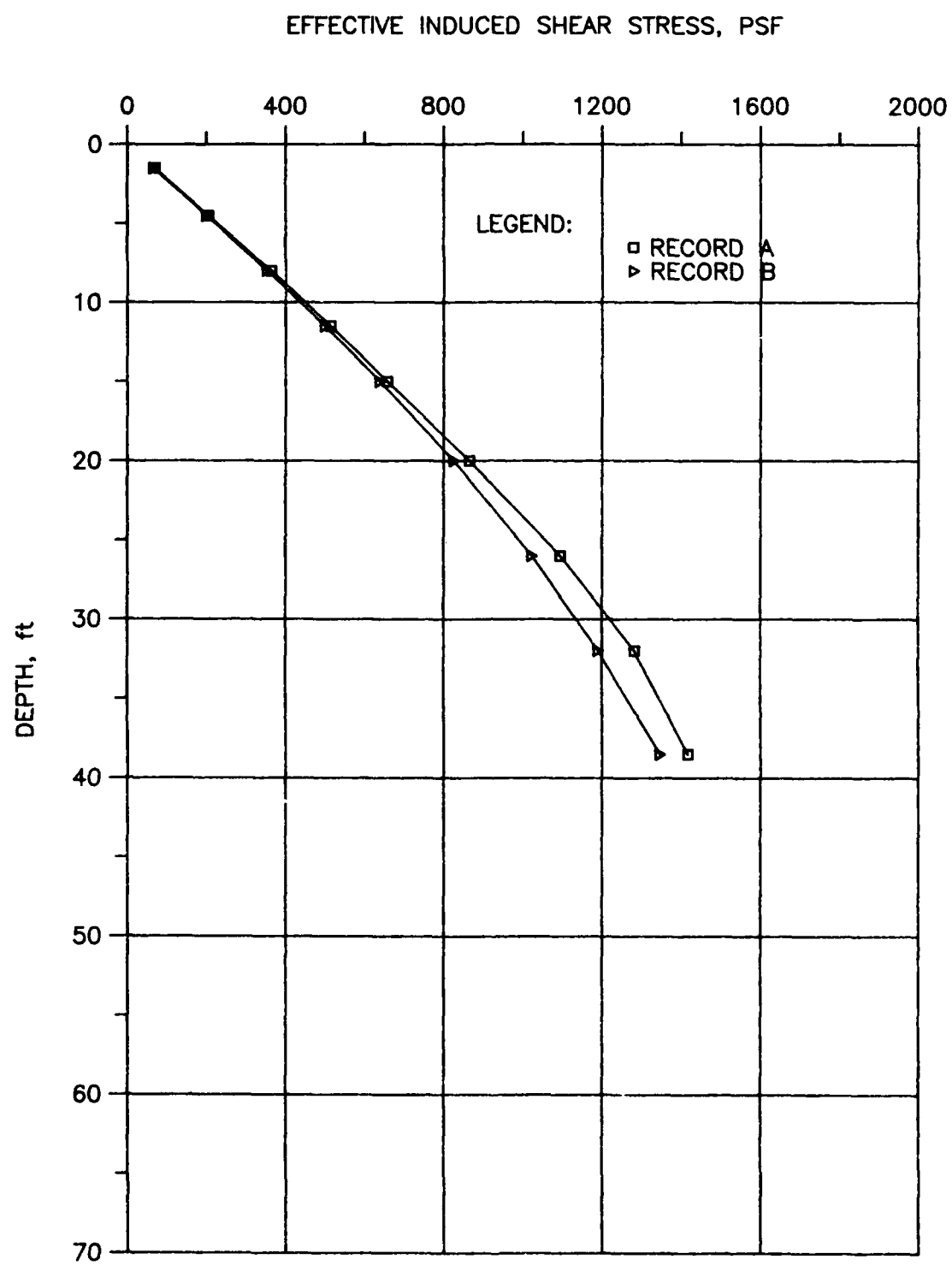


Figure 32. Effective dynamic shear stresses in the upstream slope profile induced by Records A and B.

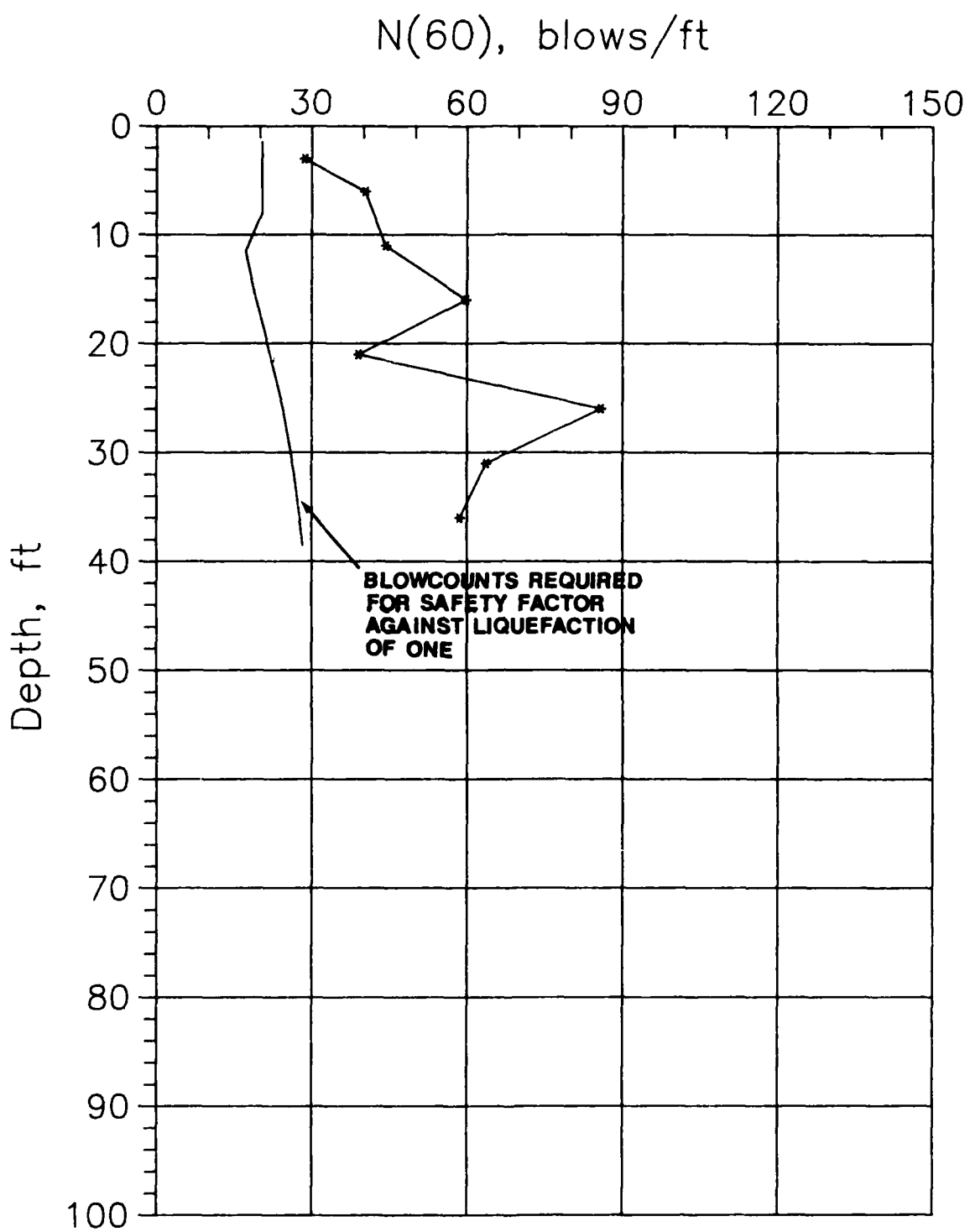


Figure 33. Comparison of  $N_{60}$  blowcounts from boring SS-10 on slope with calculated blowcounts required to give safety factor against liquefaction of one.

HOMOGENEOUS CROSS-SECTION

STRENGTH PARAMETERS USED

IN STABILITY CALCULATIONS:

$$C = 0$$

$$\phi = 32^\circ$$

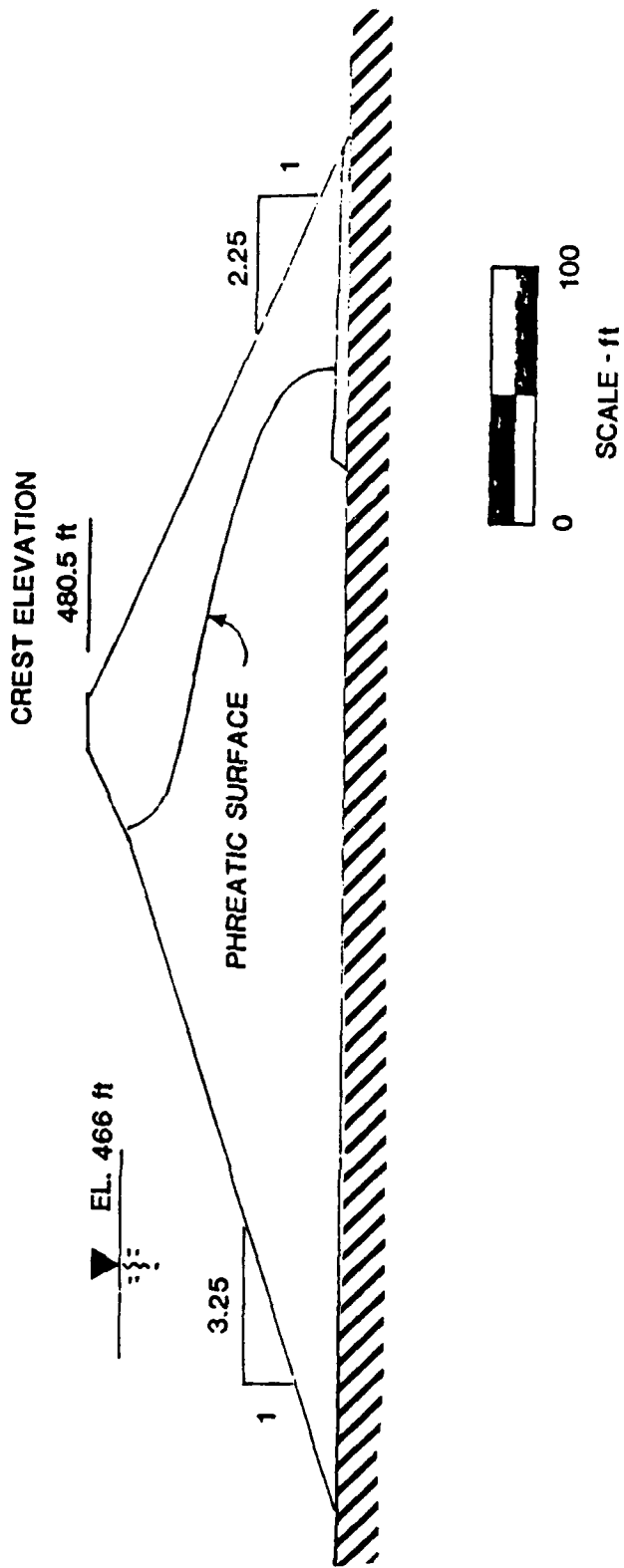


Figure 34. ARCEQS model of Dike 5 used to compute yield accelerations.

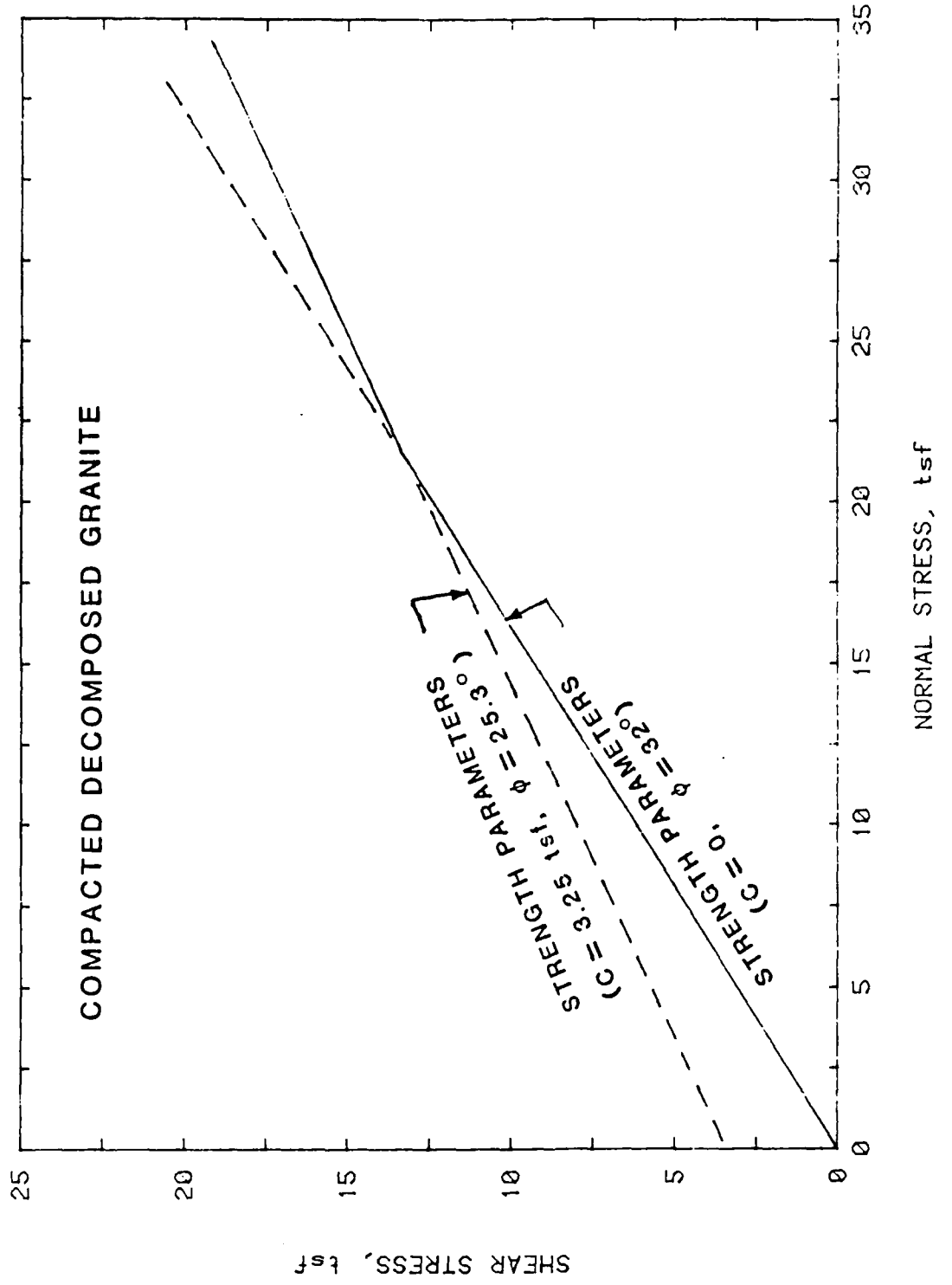
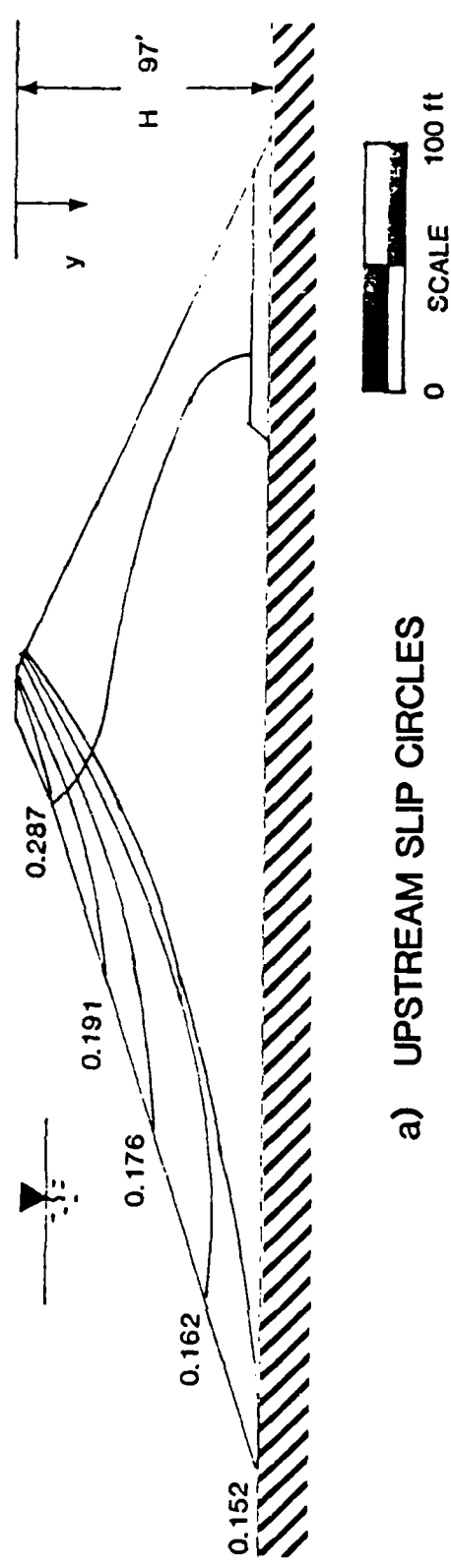
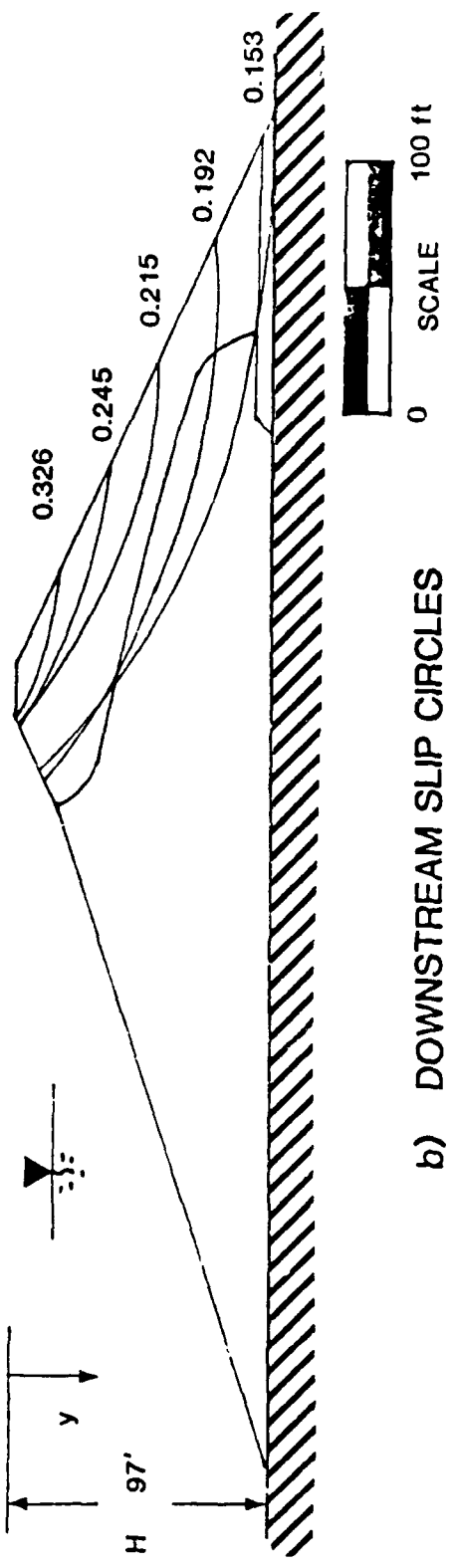


Figure 35. Failure envelope used in ARCEQS stability calculations.

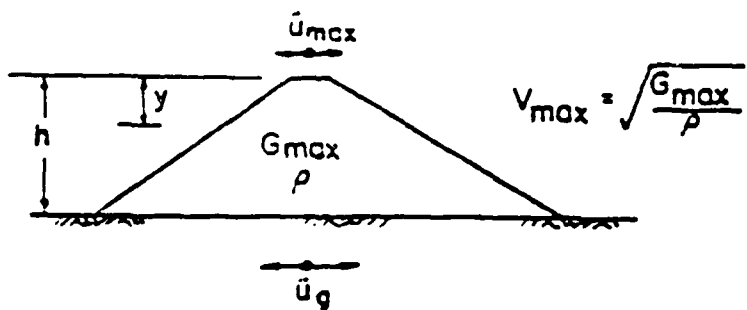


a) UPSTREAM SLIP CIRCLES

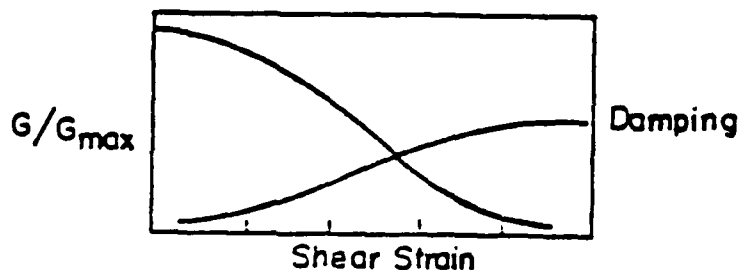


b) DOWNSTREAM SLIP CIRCLES

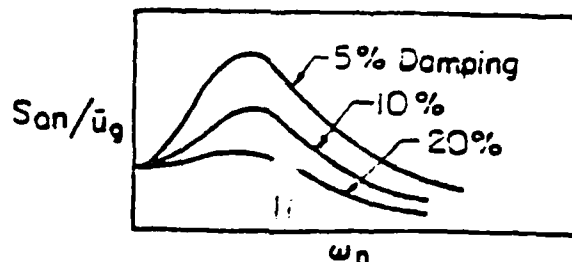
Figure 36. Cross sections of Dike 5 showing yield accelerations and slip circles determined by ARCEQS.



(a) Homogeneous Dam Section



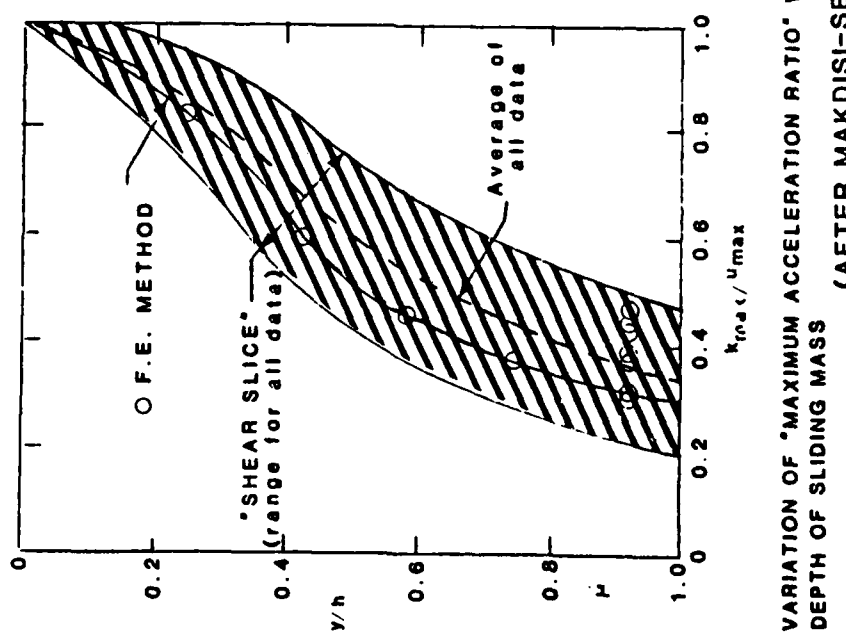
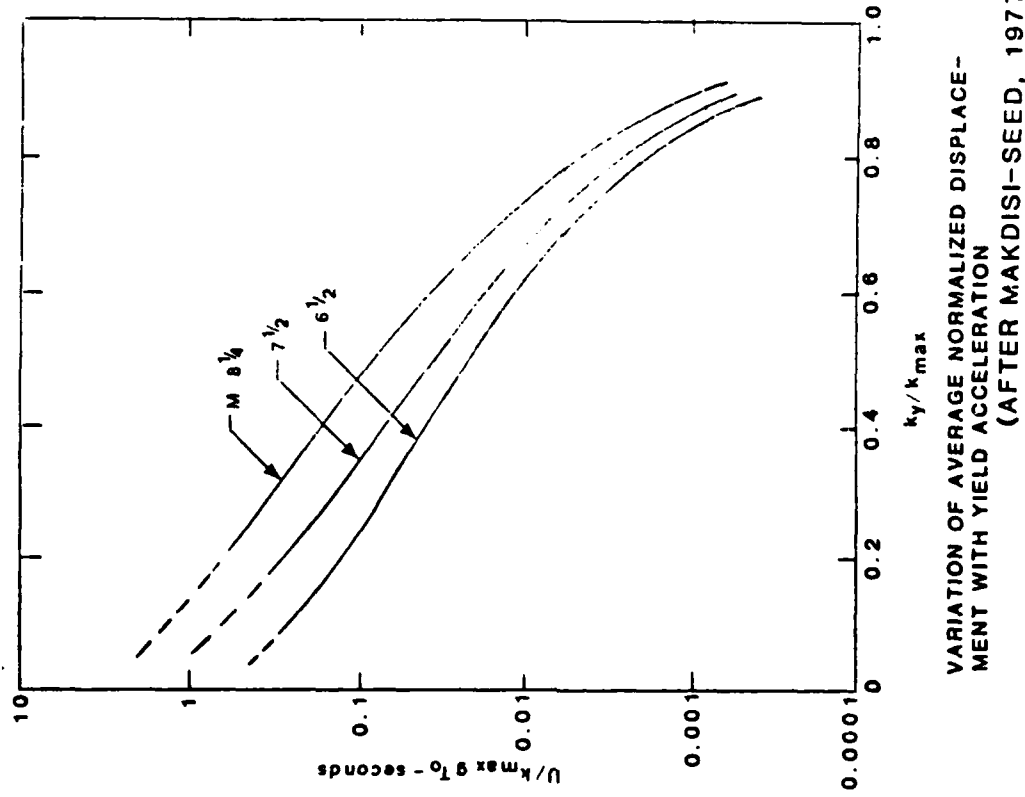
(b) Strain Dependant Soil Properties



(c) Earthquake Acceleration Response Spectra

(AFTER MAKDISI-SEED, 1977)

Figure 37. Primary components involved in the Makdisi-Seed approximate procedure for computing fundamental period and peak crest acceleration.



VARIATION OF AVERAGE NORMALIZED DISPLACEMENT WITH YIELD ACCELERATION (AFTER MAKDISI-SEED, 1977)

Figure 38. Makdisi-Seed charts.

# MAKDISI-SEED DISPLACEMENT ANALYSIS

## DIKE 5 - UPSTREAM SLIP CIRCLES

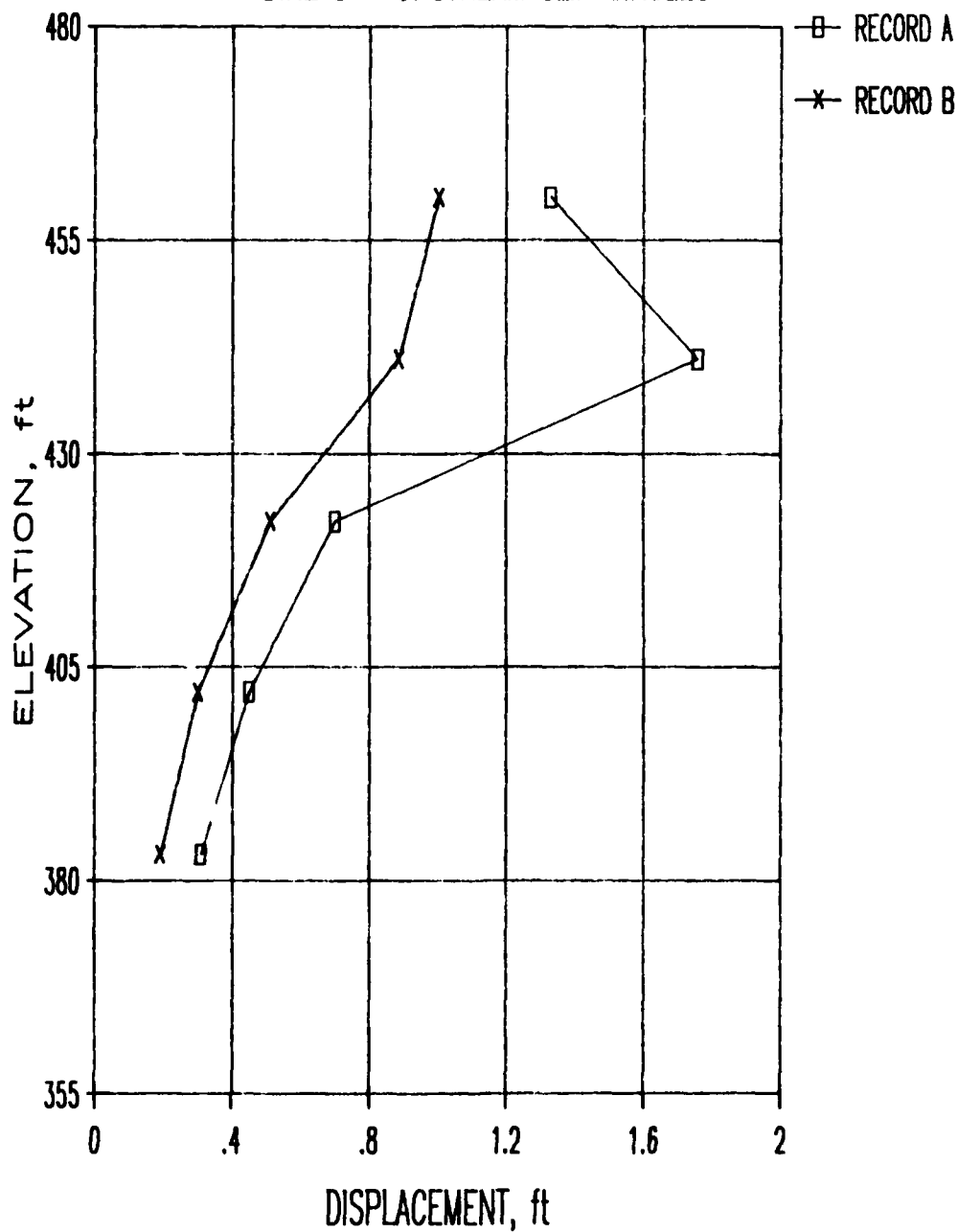


Figure 39. Potential Displacements for upstream slip circles calculated using the Makdisi-Seed technique.

# MAKDISI-SEED DISPLACEMENT ANALYSIS

## DIKE 5 - DOWNSTREAM SLIP CIRCLES

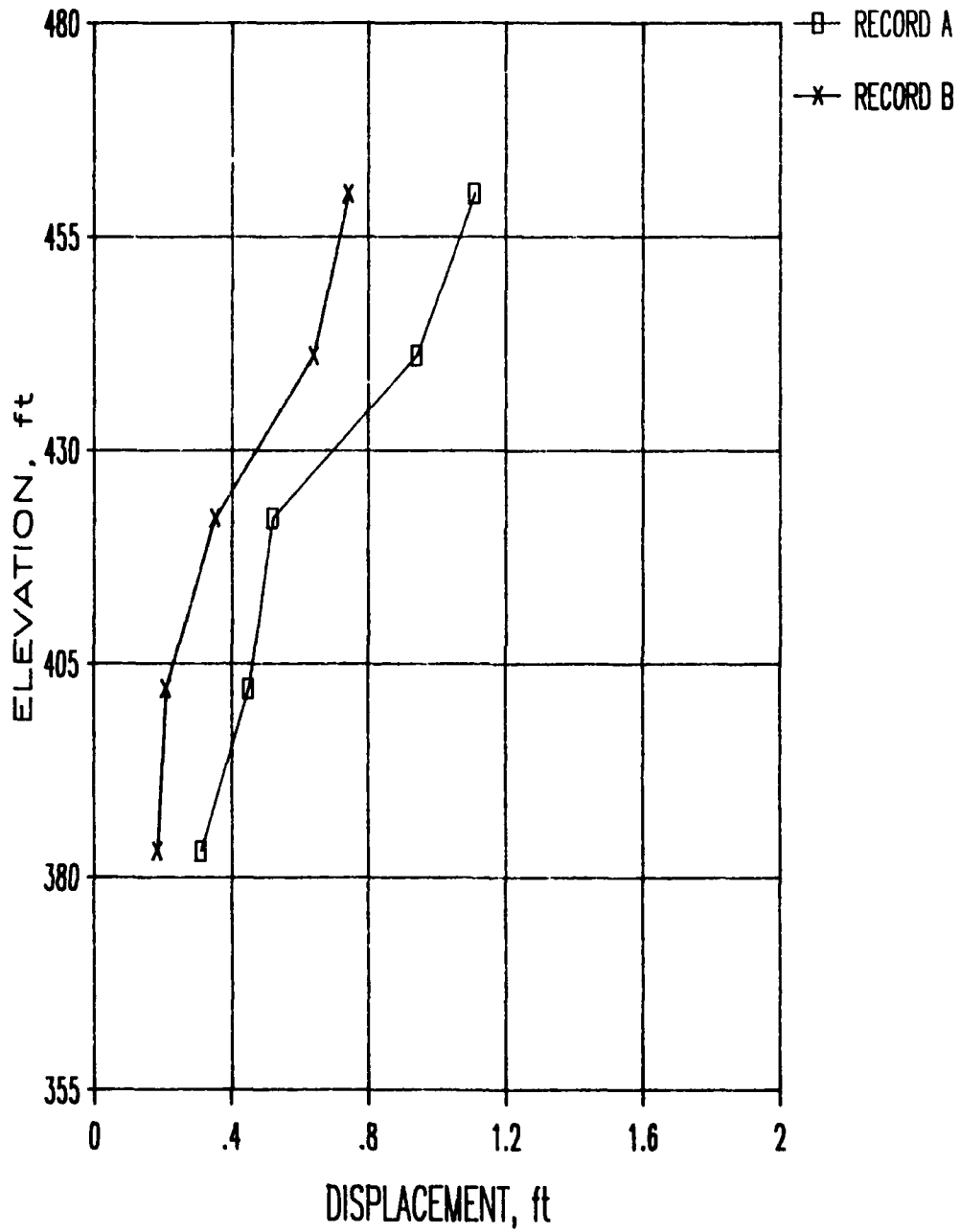
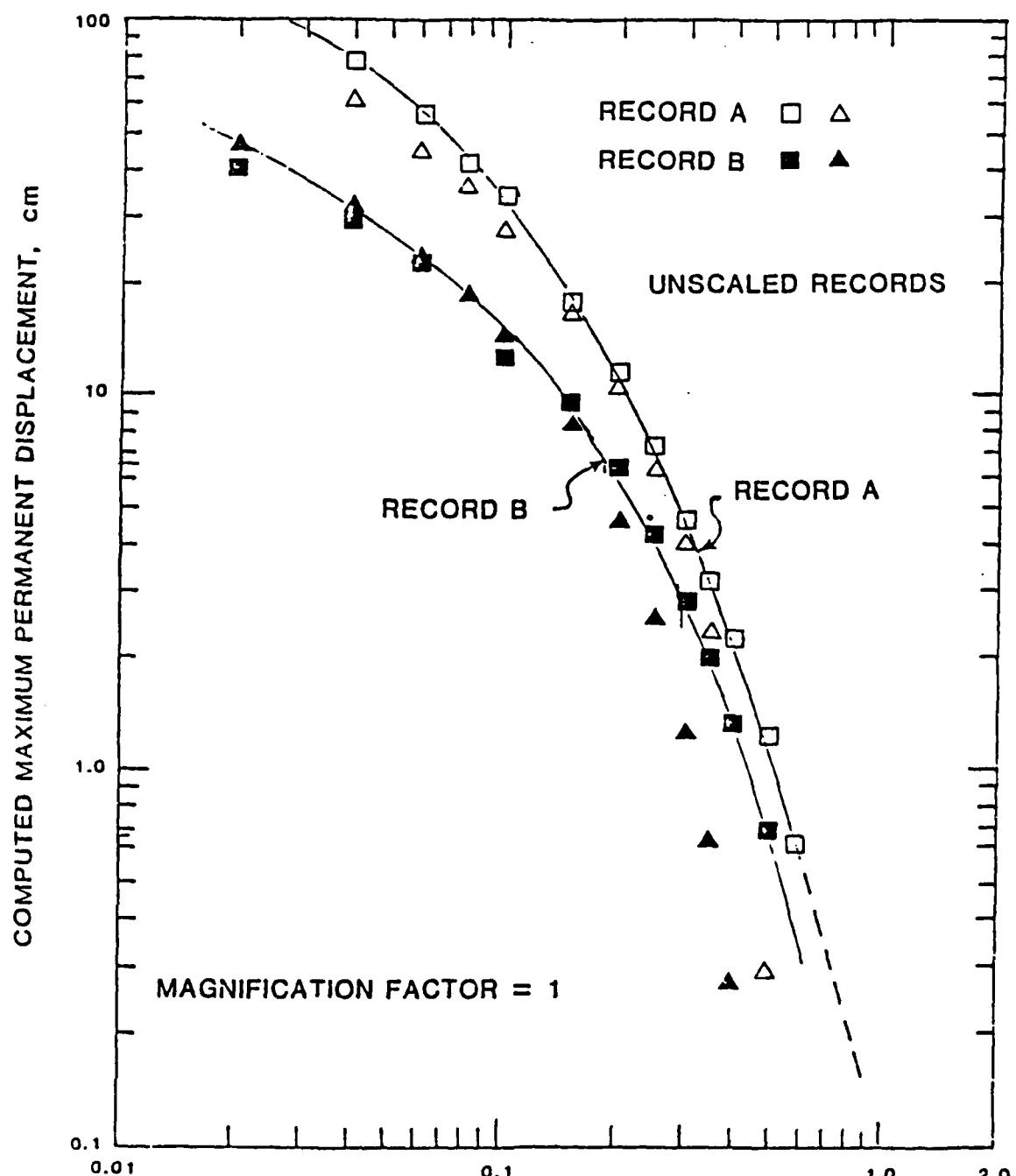


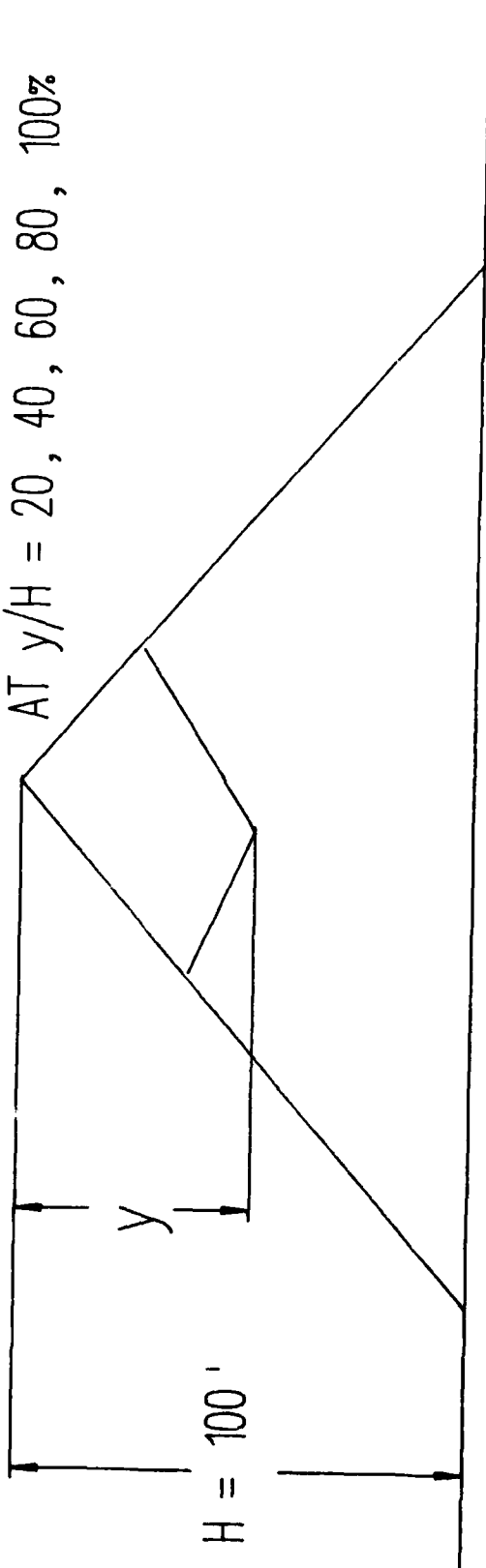
Figure 40. Potential Displacements for downstream slip circles calculated using the Makdisi-Seed technique.



$$\frac{N}{A} = \frac{\text{MAXIMUM EARTHQUAKE COEFFICIENT}}{\text{MAXIMUM EARTHQUAKE ACCELERATION}}$$

Figure 41. Results of Newmark Sliding Block Analysis - computed displacements for Accelerograms A and B.

AMPLIFICATION FACTORS  
COMPUTED FOR WEDGES  
AT  $y/H = 20, 40, 60, 80, 100\%$ .



EMBANKMENT PROPERTIES:

$V_s$  = 1225 fps  
DAMPING = 9%  
DENSITY = 127pcf

Figure 42. SEISCOE model of Dike 5.

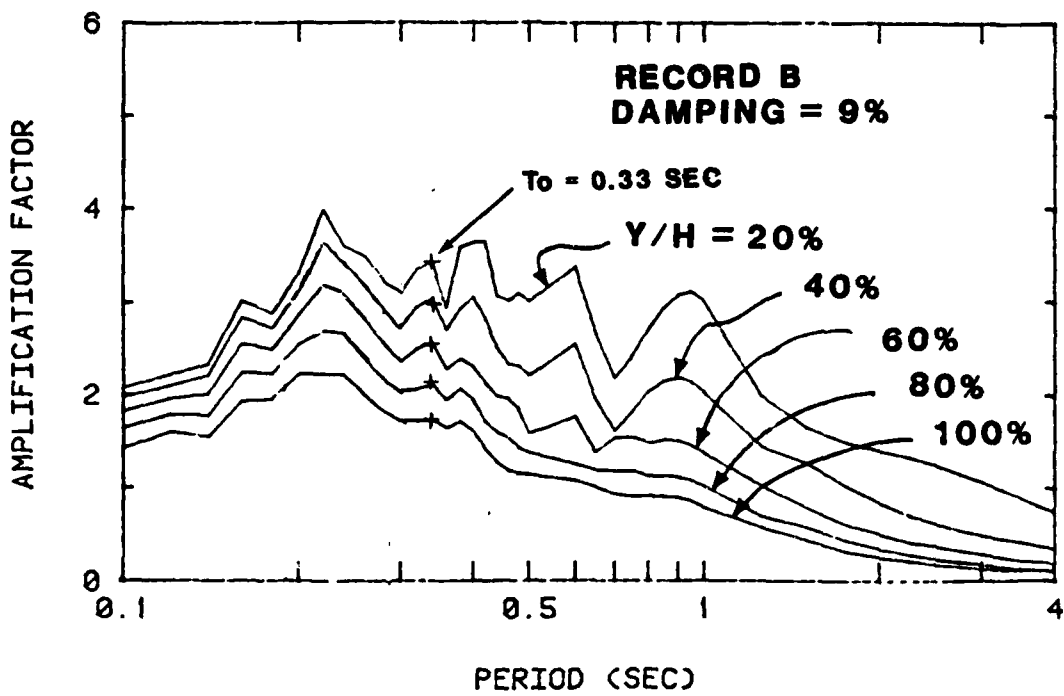
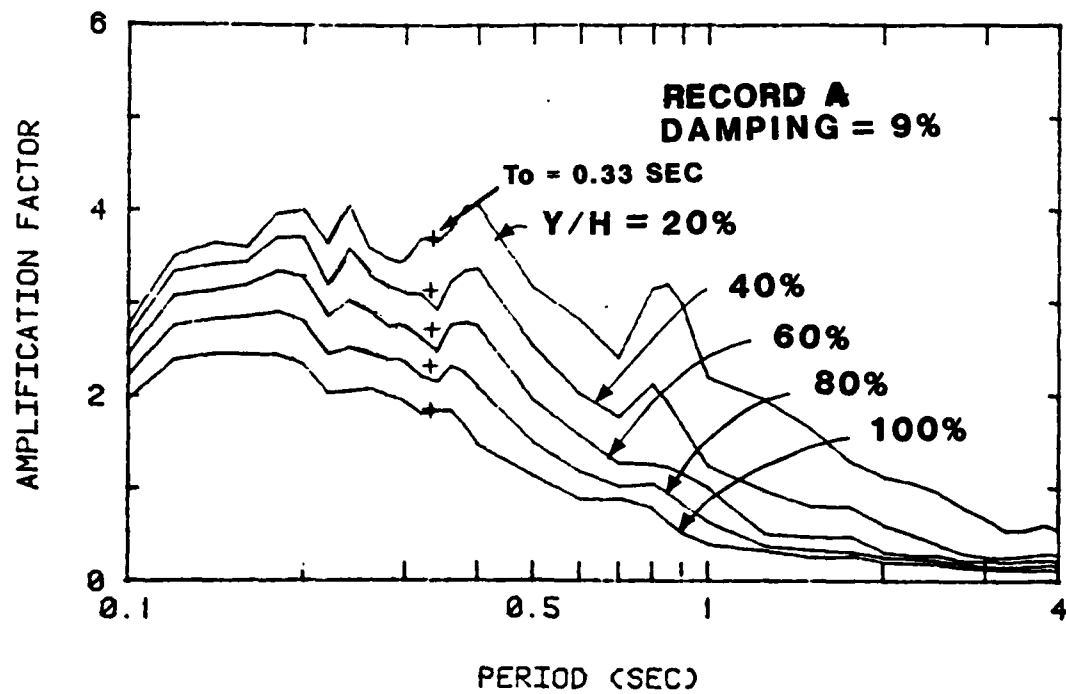


Figure 43. SEISCOE amplification factors for Dike 5.

# SARMA-AMBRAYSEYS PERMANENT DISPLACEMENTS

## DIKE 5 - UPSTREAM SLIP CIRCLES

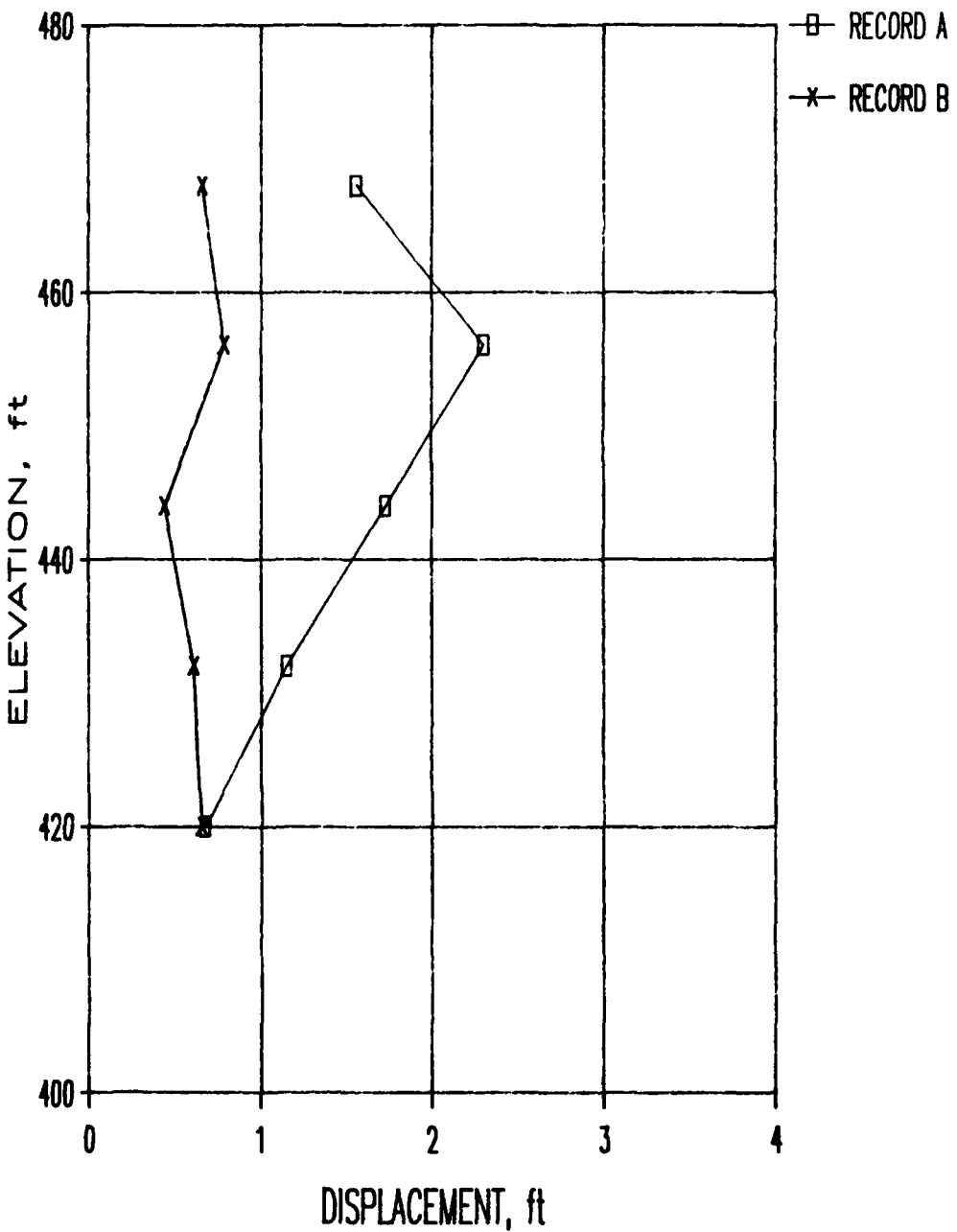


Figure 44. Sarma-Ambrayseys displacements for upstream slip circles.

# SARMA-AMBRAYSEYS PERMANENT DISPLACEMENTS

## DIKE 5 - DOWNSTREAM SLIP CIRCLES

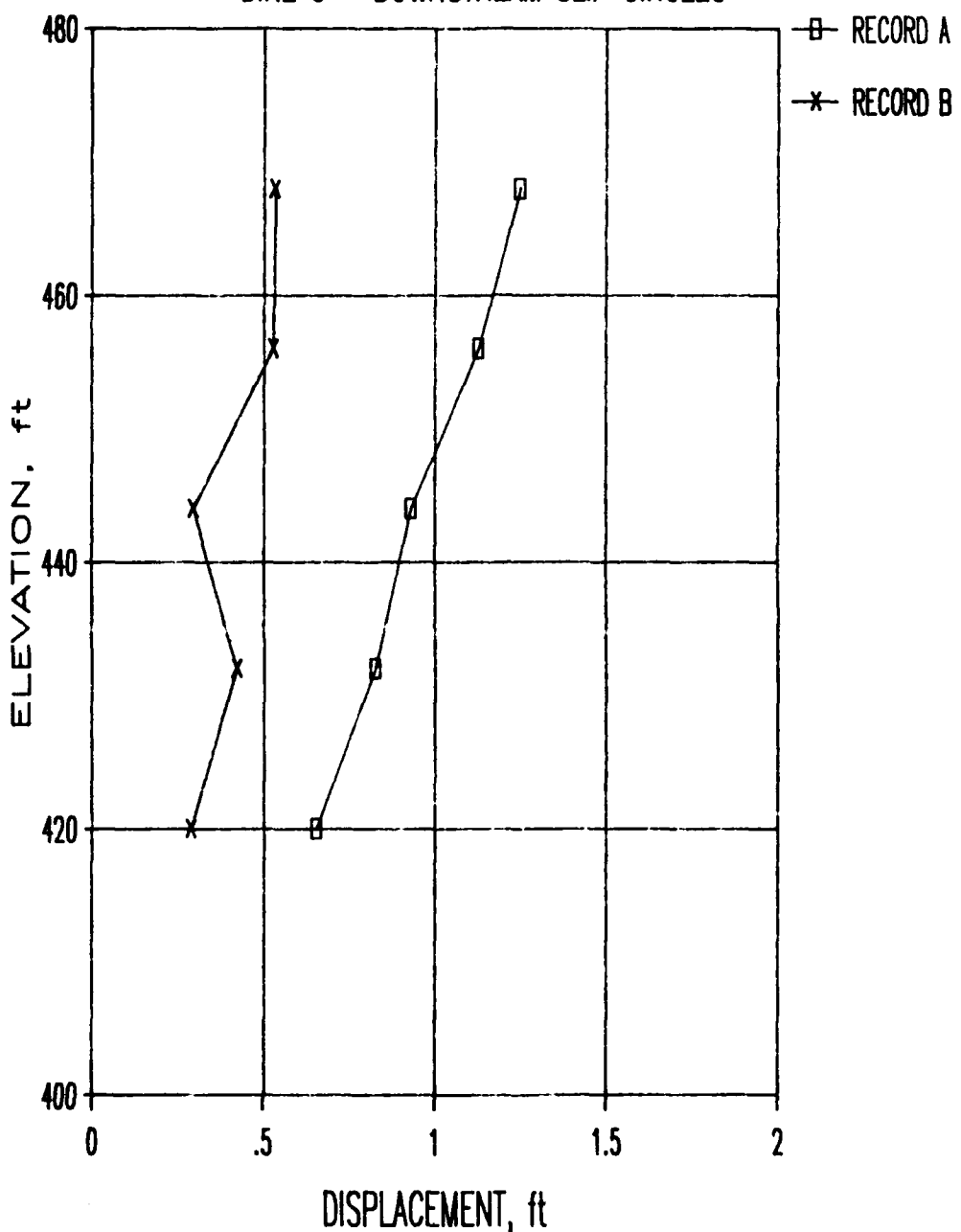


Figure 45. Sarma-Ambrayseys displacements for downstream slip circles.

APPENDIX A: COMPUTATIONS USING THE MAKDISI-SEED SIMPLIFIED  
PROCEDURE FOR ESTIMATING THE CREST ACCELERATION  
AND FUNDAMENTAL PERIOD OF DIKE 5

1. The peak crest acceleration,  $\ddot{u}_{\max}$ , and fundamental period,  $T_o$ , of Dike 5 were estimated using a simplified procedure developed by Makdisi and Seed (Makdisi and Seed 1979a). The technique was developed for homogeneous embankments founded on rock. The solution employs an iterative technique which uses the strain dependent properties of the embankment soils (see Figure 21 in main text) and the acceleration response spectra of the input accelerogram. The response spectra for Records A and B are shown in Figure 6 of the main text. The iterations are carried out until the strain dependent damping and shear modulus are compatible.

2. The properties used to model Dike 5 are listed below.

Height, $h$	97 ft
Unit weight, $\gamma$	127 pcf
Mass density, $\rho$	3.94 slugs/ft
Maximum shear wave velocity, $v_{\max}$	1,225 fps
Maximum shear modulus, $G_{\max}$	5,920 ksf

Estimate  $\ddot{u}_{\max}$  and To Using Record A

Iteration No. 1

3. Initial guess:

$$v_s = 900 \text{ fps}$$

$$(v_s/v_{\max}) = (900 \text{ fps}/1,225 \text{ fps}) = 0.735$$

and

$$(G/G_{\max}) = (v_s/v_{\max})^2 = 0.540$$

4. From Figure 21 for  $(G/G_{\max}) = 0.540$

Effective dynamic shear strain,  $(\gamma_{ave})_{eq} = 0.029 \text{ percent}$

and

Damping,  $\lambda = 9.7 \text{ percent}$

5. The first three natural frequencies are given by:

$$\omega_1 = 2.40 \times v_s/h = 2.40 (900/97) = 22.3 \text{ rad/sec} ; T_1 = 0.282 \text{ sec}$$

$$\omega_2 = 5.24 \times v_s/h = 5.24 (900/97) = 51.2 \text{ rad/sec} ; T_2 = 0.123 \text{ sec}$$

$$\omega_3 = 8.65 \times v_s/h = 8.65 (900/97) = 80.3 \text{ rad/sec} ; T_3 = 0.078 \text{ sec}$$

6. The maximum crest acceleration for the first three modes are given by:

$$u_{1\max} = 1.60 \times s_{a1} = 1.60 (0.70) = 1.12 \text{ g}$$

$$u_{2\max} = 1.06 \times s_{a2} = 1.06 (0.83) = 0.88 \text{ g}$$

$$u_{3\max} = 0.86 \times s_{a3} = 0.86 (0.51) = 0.44 \text{ g}$$

The spectral accelerations,  $s_{a1}$ ,  $s_{a2}$ , and  $s_{a3}$  in the above computations were obtained from the response spectra chart on Figure 6 by entering the abscissa at  $T_1$ ,  $T_2$ , and  $T_3$ , for 12 percent damping. The maximum crest acceleration ( $\ddot{u}_{\max}$ ) is obtained using the following equation:

$$\ddot{u}_{\max} = \left[ \sum_{n=1}^3 (\ddot{u}_{n\max})^2 \right]^{1/2} = \left[ (1.12 \text{ g})^2 + (0.88 \text{ g})^2 + (0.44 \text{ g})^2 \right]^{1/2}$$
$$= 1.49 \text{ g}$$

7. The new shear strain is computed using:

$$(\gamma_{ave})_{eq} = 0.65 \times 0.3 \times \frac{h}{v_s^2} \times s_{a1}$$

$$(\gamma_{ave})_{eq} = 0.65 \times 0.3 \times \left( \frac{97 \text{ ft}}{(900 \text{ fps})^2} \right) \times 0.70 \times 32.2 \text{ ft/sec}$$
$$= 0.053 \text{ percent}$$

8. Another iteration is required since the initial estimate for dynamic shear strain (0.029 percent) is not within 5 percent of the new estimate of 0.053 percent.

Iteration No. 2

9. From Figure 21 for  $(\gamma_{ave})_{eq} = 0.0526$  percent

$$(G/G_{max}) = 0.41$$

$$\lambda = 12.7 \text{ percent}$$

$$v_s/v_{max} = \left( G/G_{max} \right)^{1/2} = 0.64$$

and

$$v_{max} = 0.64 \times 1,225 \text{ fps} = 784 \text{ fps}$$

The first three natural frequencies are:

$$\omega_1 = 2.40 \times \frac{784}{97} = 19.4 \text{ rad/sec} ; T_1 = 0.324 \text{ sec}$$

$$\omega_2 = 5.52 \times \frac{784}{97} = 44.6 \text{ rad/sec} ; T_2 = 0.141 \text{ sec}$$

$$\omega_3 = 8.65 \times \frac{784}{97} = 69.9 \text{ rad/sec} ; T_3 = 0.090 \text{ sec}$$

10. The maximum crest accelerations for the first three modes are determined using the response spectra for Record A and 12.7 percent damping as follows:

$$u_{1 \max} = 1.60 \times 0.61 = 0.98 \text{ g}$$

$$u_{2 \max} = 1.06 \times 0.79 = 0.84 \text{ g}$$

$$u_{3 \max} = 0.86 \times 0.56 = 0.48 \text{ g}$$

The peak crest acceleration is computed as follows:

$$\ddot{u}_{\max} = (0.98^2 + 0.84^2 + 0.48^2)^{1/2} = 1.37 \text{ g}$$

11. The new dynamic shear strain is:

$$(\gamma_{ave})_{eq} = 0.65 \times 0.3 \times \frac{97}{784^2} \times 0.61 \times 32.2 = 0.0604 \text{ percent}$$

Still another iteration is required since the new dynamic shear strain of 0.0604 percent is not within 5 percent of the effective dynamic shear strain (0.0526 percent) used in this iteration.

Iteration No. 3

12. From Figure 21 for  $\gamma = 0.0604$  percent

$$(G/G_{\max}) = 0.38$$

and

$$\lambda = 13.5 \text{ percent}$$

$$v_s/v_{\max} = (0.38)^{1/2} = 0.62$$

Hence,

$$v_s = 0.62 \times 1,225 \text{ fps} = 755 \text{ fps}$$

Repeating the same calculations for iteration No. 3 as for the preceding iterations yields the following results:

$$\ddot{u}_{\max} = 1.27 \text{ g}$$

$$\text{Fundamental period, } T_1 = T_0 = 0.336 \text{ sec}$$

$$(\gamma_{ave})_{eq} = 0.0620 \text{ percent}$$

$$G = 2,249 \text{ ksf}$$

$$\lambda = 13.5 \text{ percent}$$

Estimate  $\ddot{u}_{\max}$  and To Using Record B

13. The peak crest acceleration and effective fundamental period were also computed using Record B. The calculations were performed in the same manner as for Record A. The results are given below:

$$\ddot{u}_{\max} = 1.11 g$$

$$\text{Fundamental Period, } T_0 = T_1 = 0.322 \text{ sec}$$

$$(\gamma_{ave})_{eq} = 0.0528 \text{ percent}$$

$$G = 2,249 \text{ ksf}$$

$$\lambda = 12.6 \text{ percent}$$